FINAL REPORT

Investigation of the Low Enrichment Conversion of the Texas A&M Nuclear Science Center Reactor

By

Jon A. Reuscher
Nuclear Science Center
Texas Engineering Experiment Station
Texas A&M University
College Station, Texas

DOE Contract No.
DE-FG05-87ER75346

DISCLAIMER

DOE/ER/75346--T1

DOE/ER/75346--T1

DE91 005588

FINAL REPORT

Investigation of the Low Enrichment Conversion of the Texas A&M Nuclear Science Center Reactor

By

Jon A. Reuscher
Nuclear Science Center
Texas Engineering Experiment Station
Texas A&M University
College Station, Texas

DOE Contract No.
DE-FG05-87ER75346

Investigation of the Low Enriched Uranium Conversion of the Texas A&M University Nuclear Science Center Reactor

INTRODUCTION

The use of highly enriched uranium as a fuel for research reactors is of concern due to the possibility of diversion for nuclear weapons applications. The Texas A&M TRIGA reactor currently uses 70% enriched uranium in a FLIP (Fuel Life Improvement Program) fuel element manufactured by General Atomics. Thus fuel also contains 1.5 weight percent of erbium as a burnable poison to prolong useful core life. U.S. university reactors that use highly enriched uranium will be required to covert to 20% or less enrichment to satisfy Nuclear Regulatory Commission requirements[1] for the next core loading if the fuel is avalable. This investigation examined the feasibility of a material alternate to uranium-zirconium hydride for LEU conversion of a TRIGA reactor. This material is a beryllium oxide uranium dioxide ($BeO-UO_2$) based fuel. The theoretical aspects of core physics analyses were examined to assess the potential advantages of the alternative fuel.

A basic model was developed for the existing core configuration since it is desired to use the present fuel element grid for the replacement core. The computing approach was calibrated to the present core and then applied to a core of $BeO-UO_2$ fuel elements. Further calculations were performed for the General Atomics TRIGA low-enriched uranium zirconium hydride fuel.

The core physics calculations were performed using SCALE-2[2] and BOLD VENTURE IV[3] which are code systems written by Oak Ridge National Laboratory. SCALE-2 is a reactor licensing code that includes modules for several aspects of reactor analysis. The modules of interest for this work are NITAWL-S and XSDRNPM-S. NITAWL-S reads microscopic cross sections for individual isotopes from a file created by ORNL and performs resonance corrections, if necessary. XSDRNPM-S

approximates the solution to the neutron transport equation using a discrete-orginates method. When given geometric specifications and the cross sections produced by NITAWL-S in the same energy groups as the original cross section file, XSDRNPM-S produces a library of macrospic isotopic cross sections collapsed in energy to the number of energy groups requested with the energy groups requested. This can be done for each separate type of material region within a reactor if the appropriate boundary conditions and approximations are made. The code BOLD VENTURE IV contains several modules for reactor analysis; the main module of interest for this work is VENTURE. A series of processors within BOLD VENTURE IV are used to convert the cross sections produced by XSDRNPM-S to macroscopic material cross sections and to convert the cross section files to a format that VENTURE can use. Another processor reads a complete three-dimensional description of the system. VENTURE then approximates the solution to the three dimensional diffusion equation and produces a multiplication factor for the system and a flux distribution throughout the entire core over the energy groups that XSDRNPM-S produced.

The necessary modules for both SCALE-2 and BOLD VENTURE IV were previously loaded and compiled on the Texas A&M Computing Service Center's AMDAHL 5860/470V8. BOLD VENTURE IV was used to model the NSCR.[4] The primary difference between that work and this research is that the macroscopic cross sections for the previous work were supplied by General Atomics. Since there were no pre-existing macroscopic cross sections for fuels other than FLIP fuel, the procedure from macrosopic isotopic cross section generation to three-dimensional modeling was verified using the current core.

SCALE-2 and BOLD VENTURE IV were transferred to the IBM 3090-200E in 1987 when that system replaced the AMDAHL. SCALE-2 became useable on this system after an

emulator was installed for the IBM 3350 disks that were used by the AMDAHL. Additional system changes required that some of the basic ASSEMBLY routines for each code system, such as clocks and header-writers, be replaced by FORTRAN routines that were later released by the Radiation Shielding Information Center (RSIC) of Oak Ridge National Laboratory. Verification of the use of these codes, both at ORNL and at Texas A&M University and indicate that they are sufficient calculational tools for this study.

Heat transfer effects were simulated at a power of 2 Mw with the code, FIDEP[5]. This code uses multi-dimensional, finite elements and the four-rod fuel element bundle was approximated as a two-dimensional problem with the minimum water spacing between fuel elements. The simplified geometry was used to obtain scoping calculations to simulate a realistic heat transfer situation without excessive computer time. The calculations included the actual pool depth to account for natural convection through the core.

Stress analysis of fuel material under transient conditions was evaluated using the finite element code ANSYS.[6] Steady State conditions were assumed to generate much lower thermal stresses and were not evaluated.

THE CREATION OF THE MICROSCOPIC CROSS SECTION LIBRARY

The neutron microscopic cross section library used for this research is a 27 energy group library created at ORNL called 27SHIELDLIB in the SCALE-2 documentation.[2] This library includes all the data from another library called 27GROUPNDF4 and additional isotopes useful in shielding applications. 27GROUPNDF4 was created by collapsing the cross sections in 218GROUPNDF4, a 218 energy group library. 218GROUPNDF4 was created from the Evaluated Nuclear Data File, Type B, Version IV (ENDF/B-IV). The additional isotopes in 27SHIELDLIB came from ENDF/B-V. This chapter describes the general procedure used to compile the ENDF/B libraries and collapse them to create 27SHIELDLIB.

The Evaluated Nuclear Data File is a cross section library appropriate for a wide range of applications in the nuclear industry. It is an extensive collection of different types of cross sections for different isotopes over the energy range from 10^{-5} eV to 2.0×10^{7} eV.[3,4] It is intended as a source for the creation of both fine and broad group cross section libraries. The data is compiled by the National Nuclear Data Center (NNDC) of Brookhaven National Laboratory (BNL). The data contributions come from members of the Cross Section Evaluation Working Group (CSEWG). Each contribution goes through an approval process involving extensive review and tests. The first libraries released by the NNDC were ENDF/A and ENDF/B. ENDF/B was given recommended complete material evaluations and ENDF/A was given data from

other evaluations and some partial evaluations. Modifications over the years have led to the release of five different versions of ENDF/B. The modifications have included changes such as improvements in existing data to comply with more recent knowledge, descriptions of additional types of reactions for some isotopes, and extensions in the neutron energy range. The differences in ENDF/B-V from ENDF/B-IV are revisions for some materials and the addition of photon production data for some materials. Both of these datasets and other datasets made from them are still in common use.

The neutron cross section library 218GROUPNDF4 was generated from ENDF/B-IV by XLACS, which is a module of the AMPX modular code system from ORNL written for such a purpose.[3,4,7,8] The thermal energy range for this library is from 10^{-5} eV to 3.05 eV and is divided into 78 groups. The remaining 140 groups (from 3.05 eV to 2.0×10^7 eV) are considered epithermal. Selection of the energy ranges for each group was based on the resonance structure of certain prominent nuclei, the thresholds of important types of reactions, and the fission spectra. Among the information included in this library is one-dimensional multigroup cross section data, transfer matrices for elastic and inelastic scattering reactions, transfer matrices for neutron producing reactions (such as (n,2n)) with arbitrary orders of scatter for fast and thermal data, resonance self-shielding parameters for generation of problem-dependent resonance region group cross sections by NITAWL-S, fission spectrum data, and weighting function data. A potential scattering cross section of 5×10^4 barns/atom was used to process unresolved resonance data. Doppler broadening for the resonances was performed at 293 K. The point-to-fine group weighting

functions that were used to generate the data vary with the type of material (resonance, non-resonance, and structural) and the energy range of application. Table 1 shows the weighting functions used for each material and energy range. This library has been sufficiently validated through analyses of existing systems.

All the data in 218GROUPNDF4 was collapsed to 27 groups to make the library 27GROUPNDF4.[2] 27SHIELDLIB came from this library and data on actinide and fission product isotopes from ENDF/B-V. The collapsing of 218GROUPNDF4 was performed with MALOCS, a collapsing module of the AMPX code system. MALOCS used a flux file that contained the original weighting spectrum used to generate the 218-group library from the ENDF/B-IV dataset. The library has 14 fast groups and 13 thermal groups separated at 3.05 eV. This library was designed for shipping cask and thermal neutron system analyses and has been validated against critical experiments, which is further verification of the 218 group library.

Table 1. Point-to-Fine Point Group Weighting Functions

Non Resonance Materials (fission-$1/E\sigma_t$-Maxwellian)

Energy Range	Weighting Spectrum
$20 - 1.4$ MeV	Fission
$1.4 \times 10^6 - 0.1264$ eV	$1/E\sigma_t$
$0.1264 - 1.0 \times 10^{-5}$ eV	Maxwellian (293 K)

Resonance Materials (fission-1/E-Maxwellian)

Energy Range	Weighting Spectrum
$20 - 0.1$ MeV	Fission
$1.0 \times 10^5 - 0.1264$ eV	$1/E$
$0.1264 - 1.0 \times 10^{-5}$ eV	Maxwellian (293 K)

Selected Structural Materials (Fe, Ni, Cr)

Energy Range	Weighting Spectrum
$2.0 \times 10^7 - 0.1264$ eV	$(1/E\Sigma_T)$ inconel or $(1/E\Sigma_T)$ stainless steel 304
$0.1264 - 1.0 \times 10^{-5}$ eV	Maxwellian (293 K)

GENERATION OF THE MACROSCOPIC ISOTOPIC CROSS SECTIONS WITH NITAWL-S and XSDRNPM-S

The cross section library 27SHIELDLIB was supplied on a tape containing SCALE-2 in a binary code decimal (BCD), or card image, format. AIM, a module of AMPX-II written in IBM FORTRAN-H, was used to convert the entire library to a binary format that NITWAL-S is capable of reading.[9] AIM also produced as output a listing of all the isotopes that are represented in the cross section file and all of their corresponding identification numbers. AIM and all other codes used for this project are on account E919GS on the Texas A&M Computing Services Center's IBM 3090-200E. The one exception to this is the subroutine library named "SCALE.-SUBLIB" on account T706tp used by AIM. For this project it was necessary to modify AIM slightly so that it would compile in FORTRAN-66 since there is no FORTRAN-H compiler on the IBM.

NITAWL-S and XSDRNPM-S were used to generate the macroscopic cross sections for each isotope for conversion to macroscopic material cross sections by processors in BOLD VENTURE IV.NITAWL-S read the converted binary file, performed the appropriate resonance corrections, and passed the resulting macroscopic cross sections to XSDRNPM-S. XSDRNPM-S used the microscopic cross sections and a geometric description of the section or cell being modeled to create the macroscopic cross sections.

Most of the input to NITAWL-S and XSDRNPM-S was based on the geometry of the system to be modeled. A top view of the core of the NSCR is shown schematically in Figure 1. This figure also shows some of the different material regions to be modeled and the intervals used by VENTURE. Figure 2 shows the vertical dimensions and intervals with the lengths of the fuel rod sections as a reference. All

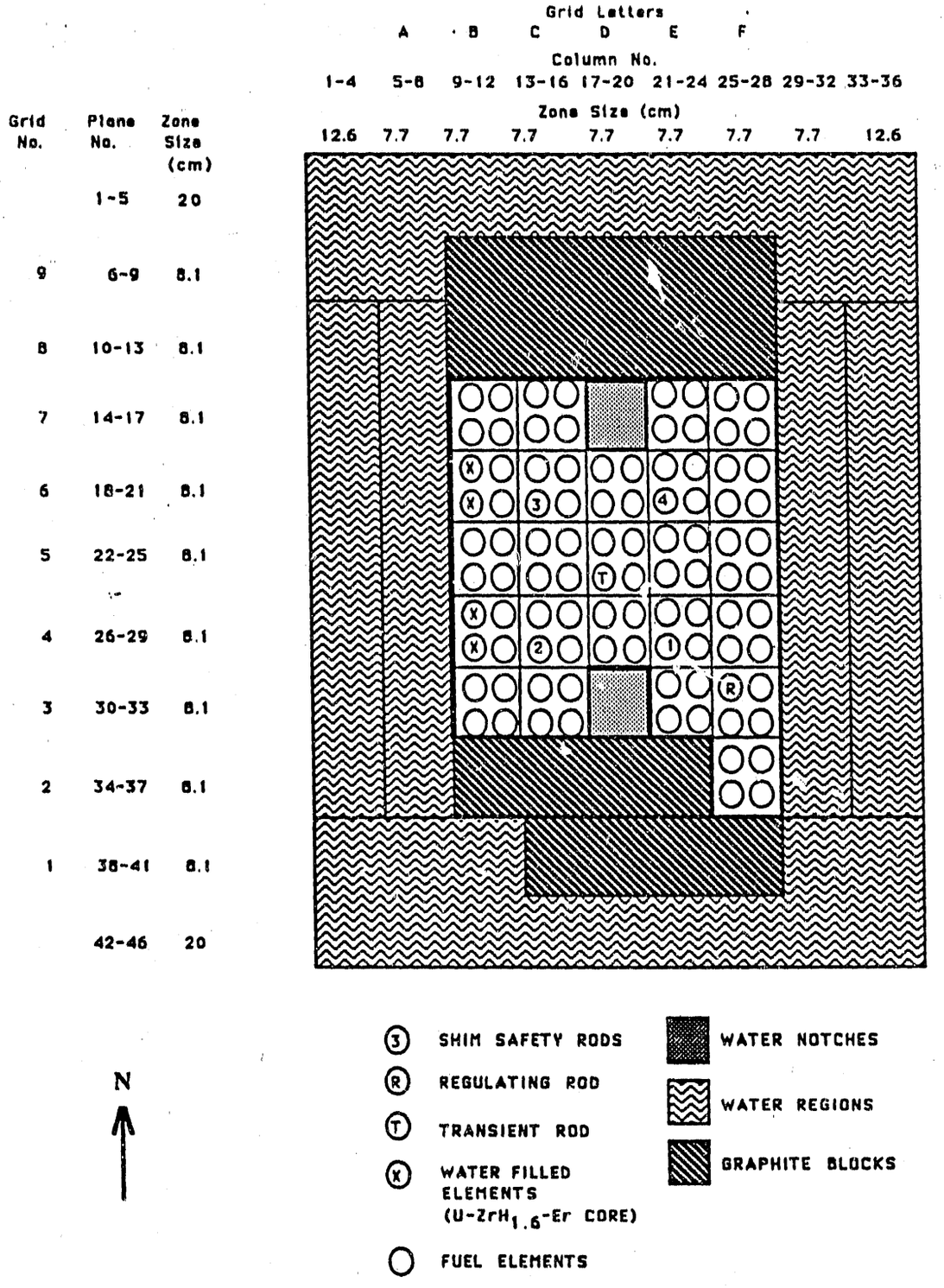

Fig. 1. Schematic Top-View of the Reactor

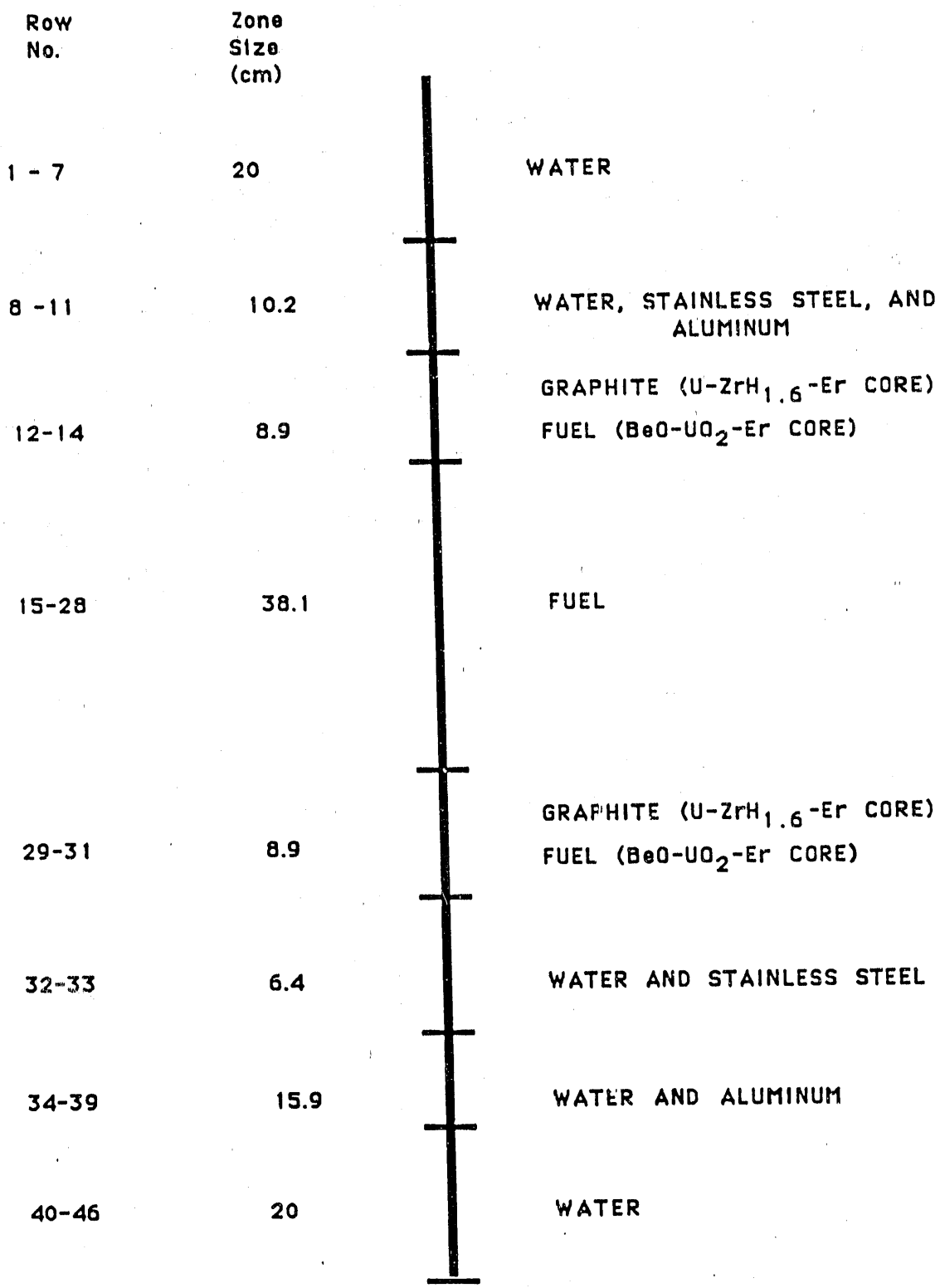

Fig. 2. Side-View Dimensions of the Reactor

vertical specifications used these intervals. Separate executions of NITAWL-S and XSDRNPM-S were used to generate the macroscopic cross sections. All executions were performed for new materials, with no burnup or degradation. Each execution represented a single cell of the system which was modeled as close as possible to its actual shape. Each cell represented more than one material region, although only the cross sections for the regions of interest were passed into the output files for each execution. The material names for each of the material regions and a brief description of those regions are given in Table 2. These material names comprise the latter four characters of the file names mentioned previously. The first two letters identify which fuel is used for the core and the power level of operation "LT" was used for the U-$ZrH_{1.6}$-Er core at low power or temperature. "HT" was used for the U-$ZrH_{1.6}$-Er core at high power. "LP" was used for the BeO-UO_2-Er core at low power. "FP" was used for the BeO-UO_2-Er core at high or full power. The file names were used as the names for every JCL-data file that was unique to that name. The same names were also used for all the alphanumeric material names required by all the BOLD VENTURE IV processors.

The two basic purposes of NITAWL-S for this project include reading the cross section library to pass on to XSDRNPM-S and performing resonance correction calculations on specified cross sections from the library. The resonance corrections are based on the Nordheim integral treatment, which solves for the energy dependence of the neutron flux in a specified material region.[2] The microscopic cross section values used come from both the cross section library and from user-supplied moderator cross

Table 2. Material Names for Different Regions of the Reactor

Name	Description
FUEL	Fuel section of a single fuel rod or shim safety rod, its cladding, and the immediately surrounding water
GPIN	Graphite section of a single U-$ZrH_{1.6}$-Er fuel rod
HSAL	Homogenized mixture of water and structural steel and aluminum immediately above the fuel rods
HSBC	Homogenized mixture of water and structural steel immediately below the fuel rods
WALM	Homogenized mixture of water and structural aluminum below HSBC
WRAC	Water above HSAL
WRBC	Water below WALM
NOCH	Water in experimental notches (also used for water in control rods positions when the rods are out)
ELEM	Water in water filled elements on the west side of the core (eventually removed from the BeO-UO_2-Er core model)
RROD	Homogenized mixture of B_4C powder of regulating rod, its cladding, and the immediately surrounding water
BORG	Borated graphite section of a single control rod or the transient rod, its cladding, and the immediately surrounding water
AIRT	Air section of the transient rod, its cladding, and the immediately surrounding water (also used for the tubes above the transient and regulating rods when in the core)
GREF	Graphite reflectors on the north and south ends of the core
WNSE	Water beyond the graphite reflectors on the north and south ends of the core
NSID	Water nearest the west and east sides of the core
FSID	Water beyond the regions designated as NSID on the west and east sides of the core

section values. The effect of the presence of up to two moderators per absorber can be accounted for when correcting the resonances of the absorbers. The material region can be surrounded by a moderating medium with a spatially flat neutron flux that varies slowly with energy. The presence of other absorber lumps external to the one being modeled is accounted for by the user-supplied Dancoff correction factor (DCF). The equation for the collision density is

$$\phi(E)\Sigma_T(E) = \sum_{i=1}^{3}\left[\frac{1-P_0^*(E)}{\alpha_i}\int_E^{E/(1-\alpha_i)}\phi(E')\Sigma_{si}(E')\frac{dE'}{E'} + P_0^*(E)\Sigma_{Ti}(E)W(E)\right] , \tag{1}$$

where

$\phi(E)$ = neutron flux,

$\Sigma_T(E)$ = macroscopic total cross section in the absorber,

i = nuclide index where 1 = absorber, 2 = first admixed moderator, and 3 = second admixed moderator,

$P_0^*(E)$ = first-flight escape probability from the absorber region as corrected by the DCF,

α_i = maximum fractional energy loss for a neutron that has collided with a nuclide of mass A_i,

Σ_{Ti} and Σ_{si} = macroscopic total and elastic scattering cross sections of nuclide i,

and $W(E)$ = assumed energy variation of the neutron flux in the external moderator region.

The functions used for $W(E)$ depend on the energy range of application. The first of four assumptions that are made for Eq. 1 is that each resonance nuclide may be considered separately from other resonance nuclides in the system. The second is that the neutron flux does not vary spatially in the absorber and moderator regions. The third assumption is that first-flight escape probabilities are sufficient to model neutron transport into and out of the absorber region. The final assumption is that the DCF properly accounts for absorber lumps.

Eq. 1 is converted to the lethargy variable using[2]

$$F(E) = \phi(E)\Sigma_T(E) \tag{2}$$

and

$$u = \ln(\frac{E_1}{E}) \tag{3}$$

where

$F(E)$ = collision density at energy E,

E_1 = maximum neutron energy,

and u = neutron lethargy.

After dividing by the atomic density of the absorber and changing the limits of integration, Eq. 1 becomes

$$F(u) = \sum_{i=1}^{3}\left[\frac{1 - P_0^*(u)}{\alpha_i}\int_{u-\Delta u_i}^{u} F(u')\frac{\sigma_{si}(u')}{\sigma_T(u')}du' + P_0^*(u)\sigma_{Ti}(u)W(u)\right]. \tag{4}$$

The resonance escape probabilities are calculated from various equations that have their own range of application with respect to the neutron mean free path. The

function $F(u')$ comes from the integration of sources due to the asymptotic flux below lethargy $u = 0$, or

$$F(u) = \frac{-\sigma_s}{\alpha E_1} \int_0^{u-\Delta u} e^{u'} du' \tag{5}$$

where

σ_s = microscopic scattering cross section.

The integration of the equations is performed with Simpson's rule for isolated resonances over ranges chosen so that only a small portion of each resonance is not included in the integration region. The portions of the resonance outside the region are called "wings", which get their own corrections. With everything on the right side of Eq. 4 known, $F(u)$ and consequently $\phi(E)$, can be solved for each resonance. Finally, the microscopic cross sections for each energy group over each resonance can be solved using

$$\sigma^{res} = \frac{\int_{E_1}^{E_2} \phi(E)\sigma(E)dE}{\int_{E_1}^{E_2} \phi(E)dE} \tag{6}$$

where

E_1 and E_2 = lower and upper energy bounds of the energy range bracketing the resonance.

Both the corrected and non-corrected microscopic cross sections were passed to XSDRNPM-S.

XSDRNPM-S was used to convert the microscopic isotopic cross sections supplied by NITAWL-S to macroscopic problem-dependent isotopic cross sections. It

does this by calculating fluxes and using them to collapse the input cross sections. The fluxes are calculated from a one-dimensional discrete ordinates solution to the time independent Boltzmann transport equation:[2]

$$\vec{\Omega}\cdot\nabla\psi(\vec{r},E,\vec{\Omega})+\Sigma_t(\vec{r},E)\psi(E,\vec{r},\vec{\Omega})=S(\vec{r},E,\vec{\Omega}) \qquad (7)$$

where the first term represents losses due to leakage, the second term represents losses due to collisions, and the term on the right represents scattering, fission, and fixed neutron sources, although there were no fixed sources used for any of the cells in this work. The code uses a multigroup form of the equation that depends on the geometry of the cell (slab or cylindrical for this work). The discretization of the solid angle $\vec{\Omega}$ is performed using the user-supplied order of angular quadrature. The number of intervals per zone of the cell is also specified by the user. The number of energy groups is the number of groups in the cross section library. The boundary conditions used depend on the cell model. XSDRNPM-S solves the set of equations generated from the multigroup form of Eq. 7 by iterating on the flux values over energy groups, angles, and intervals using two iteration loops, each with their own user-supplied convergence criteria. Once the fluxes have been determined, the code then determines new microscopic isotopic cross sections that are collapsed to the number of energy groups requested. The equations used depend on the weighting scheme specified. Cell weighting was used to obtain macroscopic cross sections homogenized over the entire cell. Zone weighting was used when the the cross sections desired were only for one zone within the cell, as in the frequently used case with a zone that approximates the

surrounding fissionable material around the zone of interest. The equation used for the cell weighting model is

$$\bar{\sigma}_G = \frac{\sum_{j}^{IZM} N^j \sum_{g \in G} \sigma_g^j W_g^j}{\bar{N} \sum_{j}^{IZM} \sum_{g \in G} W_g^j} \tag{9}$$

where

$\bar{\sigma}_G$ = average cross section for collapsed energy group G,

IZM = number of zones in the cell,

N^j = atomic density of the isotope in zone j,

σ_g^j = cross section for fine energy group g and zone j,

W_g^j = flux weighting function for fine energy group g and zone j,

and $\bar{N}$ = volume weighted average of the isotopic atomic density.

The equation used for the zone weighted cross sections is

$$\bar{\sigma}_G^j = \frac{\sum_{g \in G} \sigma_g^j W_g^j}{\sum_{g \in G} W_g^j}. \tag{10}$$

The group-to-group scatter cross sections come from similar weighting equations. The macroscopic cross sections are determined for each weighting scheme by multiplying the microscopic cross sections by the user-supplied isotopic atomic densities. The values of $\bar{\nu}$, the average number of neutrons produced per fission, are determined by

$$\bar{\nu}_G = \frac{(\overline{\nu\sigma_f})_G}{(\overline{\sigma_f})_G} \tag{11}$$

where

$\overline{\sigma_f}$ = average fission cross section.

These values are passed to BOLD VENTURE IV, which uses a processor to convert the individual macroscopic isotopic cross sections for each zone of interest for each cell to macroscopic material cross sections that represent the entire zone.

Some clarification of the data requirements for NITAWL-S and XSDRNPM-S is warranted. The FIDO input system, which requires that all data be input in sets called "arrays", is used to read the values in the input decks.[2] The unformatted version of this system was used for this work to avoid concern over columns. Temperatures are given in Kelvin. Dimensions are given in centimeters. Microscopic cross sections are given in barns. Atomic densities are given in atoms /(cm · barn of zone). For each zone that is actually a homogeneous mixture or is just one compound, the isotopic densities are simply the densities as would ordinarily be calculated for that material. However, if the zone consists of physically separate materials that are modeled as a homogeneous material, the isotopic densities are the actual densities multiplied by the volume fraction of the material the isotope is in. For use with the BeO-UO_2-Er fuel, two programs were written to calculate these densities and various cross sections that come from them, one for the fuel cell and another for the homogeneous zones. These programs (FUEL.FOR and HOMOG.FOR), a dataset for FUEL.FOR, and a dataset modeling the water, steel, and aluminum regions above the core for use with HOMOG.FOR are presented in Appendix C. Atomic masses are given in atomic mass units.

The first line of the input to NITAWL-S requires "=NITAWL" to call the module. In the 0$$ array of NITAWL-S, the logical assignments for files that are actually used must match the unit numbers in the JCL. The default values were used for most of these. (For the remainder of this discussion, input variables that are not discussed are not mentioned either because the values to be input are obvious, the default values are sufficient, or they pertain to calculations that do not need to be performed for this work.) The isotope identification numbers for array 3$$ can be found in the output from AIM. For array 3**, the resonance data array, a set of fifteen values is given for each absorbing isotope for which resonance corrections are desired. There is no character that separates these sets. It should be stated that there is not one exclusive set of correct values for this array for any given cell model. Several approximations must be made based on the judgment of the user. The first quantity required for each absorbing isotope is its temperature, which may be taken as the temperature of its medium. This and all other temperatures come from operational data on the NSCR and the ACRR.[10] For the fuel cell, which is cylindrical, the absorber lump dimension is the radius of the fuel zone. For the remaining cells, for which no cross sections are being passed from the absorbing medium, it is desired to keep this value relatively small to avoid exaggeration of the effects of the absorbing medium on the zone of interest. The value chosen to meet this criterion is 0.01 cm. The DCF for the fuel cell model is determined from the pitch and radius of the fuel rods and the transport mean free path. The pitch is an average of the north-to-south

pitch and the east-to-west pitch. The radius is the radius of the fuel zone only. The equation for the transport mean free path λ_{tr}, is calculated from

$$\lambda_{tr} = \left[\sum_{1}^{I} \sigma_{tr_i} N_i\right]^{-1} \tag{11}$$

where

I = number of isotopes in the non-fuel zones,

σ_{tr_i} = microscopic thermal transport cross section for non-fuel isotope i,

and N_i = atomic density of isotope i averaged over all non-fuel zones.

σ_{tr} is determined for each isotope from

$$\sigma_{tr} = \sigma_t - \frac{2\sigma_s}{3A} \tag{12}$$

where

σ_t = total microscopic cross section

and A = atomic mass number.

The DCF is then linearly interpolated from a table of values depending on the ratio of the pitch to the radius and on the ratio of the radius to λ_{tr}.[11] For the remaining cell models, this value was kept at 0, which corresponds to a single absorber lump isolated in an infinite moderating medium.[2] This approximation was chosen because the remaining cells model relatively isolated regions, although not necessarily absorbing. The NITAWL-S input description gives the effective moderator cross section, $(\sigma_m)_{eff}$, as

$$(\sigma_m)_{eff} = \sigma_{p_o} + \sigma_m + \sigma_e \tag{13}$$

where

σ_{p_o} = absorber potential scattering cross section,

σ_m = moderator cross section per absorber atom,

and σ_e = effective escape cross section.

σ_{p_o} is given by

$$\sigma_{p_o} = 4\pi R^2, \tag{14}$$

where

R = approximate radius of the absorbing isotope,

which is given in centimeters by the following empirical relation:[15]

$$R = 1.25 \times 10^{-13} A^{\frac{1}{3}}. \tag{15}$$

σ_m was determined from

$$\sigma_m = \frac{\sum_{i=1}^{I} \sigma_{s_i} N_i}{N_a} \tag{16}$$

where

σ_{s_i} = average microscopic scattering cross section of moderator i over the resonance absorption energy range of the absorber,

N_i = atomic density of moderator i averaged over the absorbing zone,

and N_a = atomic density of the absorber averaged over the absorbing zone.

σ_e is given in the NITAWL-S input specifications by

$$\sigma_e = \frac{1}{\bar{\ell} N_a} \tag{17}$$

where

$\bar{\ell}$ = mean chord length in the lump.

For the fuel cell models, this is given by

$$\bar{\ell} = \frac{4V}{S} \tag{18}$$

where

V = volume of the absorbing region

and S = surface of the absorbing zone.

Simplification of this equation for a cylinder shows that $\bar{\ell}$ is simply the diameter. As with the absorber lump dimension, this quantity should be kept relatively small for the remaining cells and is set at 0.01 cm. Setting this parameter so small effectively makes the absorbing regions infinitely dilute and inhibits their resonance corrections, which is desirable for a fission source. The treatment of all the absorbers' and moderators' contribution to the collision density is specified as the Nordheim integral method. The moderators used in entries 9 through 14 of array 3** are in the absorbing zone. Since NITAWL-S limits these moderators to two per absorber atom, chemical combinations or mixtures were taken to be single moderators. The calculation of σ_{s1} and σ_{s2}, the first and second moderator scattering cross section per absorber atom, is therefore performed as in Eq. 16 for σ_m, except that only the isotopes making up the moderator combination are used. The volume fraction of the absorber lump in the cell is specified as 1.0 for every cell model even though the value is lower than 1.0. For the fuel

cell model for which cell weighting is performed, this is recommended by the input specification because the cell weighting will be performed by XSDRNPM-S. For the remaining cells, this value is not even used. The last array input to NITAWL-S is 4**, which requires temperatures for every isotope. These values are given at the operating temperature of the medium for every isotope. In the case of an isotope within two or more mediums at different temperatures, a volume weighted calculation is required.

The data for XSDRNPM-S is included in the same file as the NITAWL-S data. The "=XSDRN" label is placed on the line immediately after the "END" for the NITAWL-S data. The line after the label is a title for the case. In array 1$$, the number of zones (IZM) is the number of separate, but not necessarily unique, material regions. The boundary conditions used depend on the individual cell models. The number of compositions (MXX) refers to the number of unique material regions. One zone is composed of just one material, however more than one zone can be composed of the same material. MS is the total of the number of isotopes that make up each individual zone. An isotope that is present in more than one zone would be counted more than once. The order of angular quadrature is used to discretize the solid angle $\vec{\Omega}$. It must be an even number. It should be also be kept fairly small since this is generally adequate and large orders require considerable computer time. For this project, 8 was used due to the requirements of another project that used the cross sections generated in this project.[16] For ISCT, the order of scattering, a value of 3 was specified to meet the requirements of the same project. A value of 1 would have been sufficient for the diffusion theory calculations of BOLD VENTURE IV. For IEVT, 1 was specified for multiplication factor calculations for every cell model. S_n

theory and the forward Boltzmann equation were specified as the desired method of solution. A specification of -1 for the number of flux rebalance bands (NBANDS) in array 2$$ means that within-group scattering in the thermal groups is treated as one band to speed up convergence. In array 3$$, a value of 1 for IFG was used to specify cross section collapsing. For the BeO-UO_2-Er fuel cell model, a value of 2 was given for IPN. This spatially averages the transport cross section over all zones to avoid generating a very large diffusion coefficient for the low-density helium zone, which can lead to non-physical behavior. In array 4$$, ICON was specified as -1 (cell weighting) for the fuel cell model and 0 (zone weighting) for the remaining models. The number of energy groups in the collapsed sets (IGMF) was set to 7 for every model. For ITP, a value of 20 was used to produce the output in the CCCC ISOTXS format for the BOLD VENTURE IV processors. This value also corresponds to the unit number used for the output file in the JCL. For IPP, a 3 was specified to have the P_3 cross sections printed. IHTF is the number of isotopes being passed to BOLD VENTURE IV. For the fuel cell model, this is all the isotopes in the model. For the remaining cell models, this is only the number of isotopes in the zone of interest. It should be mentioned that the current version of XSDRNPM-S operating from "SCALE6" prints the default value of 3 for this variable when reproducing the input, regardless of the value that is given. However, this variable does work as it should. In array 5**, a calculation is required for the normalization factor XNF. For the flux values that XSDRNPM-S produces to be in units of n /(cm^2·s), XNF needs to

be the number of fission neutrons produced by the system per second. The following equation with the appropriate unit conversions is used to produce this value:

$$\text{XNF} = \frac{P\bar{\nu}}{E_R} \tag{19}$$

where

P = reactor power

and E_R = recoverable energy per fission.

For the buckling factor (BF), the value used is 0 because geometric buckling calculations do not need to be performed when producing cross sections for a three-dimensional diffusion program. There is a one-to-one correspondence between the values given in arrays 13$$, 14$$, and 15**. Array 14$$ is a listing of every isotope in every zone, starting with zone number 1. Array 13$$ is the material numbers (from 1 to MXX) for each of the isotopes listed, in array 14$$. The "R" multiplier may be used to avoid repeatedly typing numbers. Array 15** is atomic densities of each of the isotopes in array 14$$. Array 16$$ is numeric labels for each of the isotopes whose cross sections are to be passed to BOLD VENTURE IV. If cell weighting is used, this array would match array 2$$ of NITAWL-S exactly. If zone weighting is used, the isotope identifiers from the zone of interest are listed in the same order as is in array 14$$ with one change: the zone number is added as an additional digit on the left for each identifier. Array 18 is specified as 18## because the Hollerith field option was chosen. Alphanumeric labels for every isotope in array 16$$ are given in this array. For this work, fields of six characters were specified for each entry by putting

"6H" before each label as a multiplier. This multiplier value does not include the space that is always left between entries on the same line of input. For array 33##, the flux guess is specified with an "F" immediately preceding the values. The "F" fills the array with the guess so that it is used for every energy group in every interval. The value of the guess only effects the number of iterations necessary to converge on the fluxes. Arrays 35** and 36** specify the zone dimensions along a cylinder radius or slab thickness and the number of intervals in each of those zones. The first zone is specified in array 35** as

$$\text{"}(n_1 - 1)\text{I}0.0\ x_1\text{"}$$

where

n_1 = number of intervals in zone 1

and x_1 = radius or thickness of zone 1.

The parentheses in this expression are not actually included. Single numerical values are printed for both the variable x_1 and the expression within the parentheses. The "I" is actually printed and is telling XSDRNPM-S to create the individual interval dimensions by means of interpolation. The second and all subsequent zones are specified in array 35** as

$$\text{"}(n_z - 2)\text{I}(\frac{x_z - x_{z-1}}{n} + x_{z-1})\ x_z\text{"}$$

where

x_z = radius or thickness to the outer edge of zone z starting from the zero of the axis.

Array 36$$ assigns zones numbers to each spatial interval specified in array 35**. Array 39$$ requires a list of the material numbers for each zone. Array 51$$ requires the number of fine energy groups to be collapsed into each broad energy group. The energy ranges of the broad groups were chosen to match as close as possible the energy group ranges of General Atomic's seven-group cross sections used for the previous modeling of the TRIGA.[4] A perfect match was not possible due to the energy ranges of the groups in the original 27-group library. The broad groups used for this work and those used for the previous modeling with the General Atomic (G. A.) cross sections are presented in Table 3.

The main cell of interest for this project is the fuel cell, which includes just one fuel rod and the surrounding water. The input to NITAWL-S and XSDRNPM-S for the BeO-UO_2-Er fuel cell at 2 MW is presented in Appendix D along with all the input files to these modules for the other cells. The cross sections generated were used for every fuel cell in the system. The model used is a cylinder with a height equal to the length of the fuel section of a rod. The fuel length in the current FLIP fuel rods is 38.1 cm. If the graphite sections of the rods are not used, the fuel length would be 55.88 cm. For the FLIP fuel rods there were three zones: fuel, cladding, and water. For the proposed BeO-UO_2-Er fuel there were four zones: fuel, helium gap, cladding, and water. The true cell model would have a rectangular water region around a rod with boundaries that are centered between the adjacent rods. However, this region cannot be modeled as a rectangular region when the rod is modeled as a cylinder due to the limitations of a one-dimensional analysis. Therefore this water

Table 3. Broad-Group Energy Ranges (eV) for Both NSCR Models

Group No.	Groups for this Work	Groups for G. A. Cross Sections
1	$2.000 \times 10^{7} - 4.000 \times 10^{5}$	$1.500 \times 10^{7} - 6.080 \times 10^{5}$
2	$4.000 \times 10^{5} - 3.000 \times 10^{3}$	$6.080 \times 10^{5} - 9.120 \times 10^{3}$
3	$3.000 \times 10^{3} - 1.130$	$9.120 \times 10^{3} - 1.125$
4	$1.130 - 4.000 \times 10^{-1}$	$1.125 - 4.200 \times 10^{-1}$
5	$4.000 \times 10^{-1} - 2.250 \times 10^{-1}$	$4.200 \times 10^{-1} - 1.400 \times 10^{-1}$
6	$2.250 \times 10^{-1} - 5.000 \times 10^{-2}$	$1.400 \times 10^{-1} - 5.000 \times 10^{-2}$
7	$5.000 \times 10^{-2} - 1.000 \times 10^{-5}$	$5.000 \times 10^{-2} - 2.000 \times 10^{-3}$

region was modeled as a cylindrical region with the radius set so that its volume equals that of the true rectangular region. The outer radius of this water region is 2.2291 cm. The outer radius of the cladding is 1.7958 cm. The inner radius of the cladding is 1.7450 cm. For the FLIP fuel, the inner radius of the cladding corresponds to the radius of the fuel. However, for the BeO-UO_2-Er fuel, this boundary is the outer radius of the helium gap. The radius of the fuel zone for the BeO-UO_2-Er fuel is 1.6550 cm. Since the BeO-UO_2-Er fuel is in pieces with helium between them, this zone was treated as a homogenized region of fuel and helium.

The isotopic temperatures that were used in arrays 3** and 4** of NITAWL-S for this and every other cell model depend on the medium of the isotopes. The temperatures used for the different mediums at both high and low power and for both U-$ZrH_{1.6}$-Er and BeO-UO_2-Er fueled cores are presented in Table 4. Some of the temperatures in Table 4 came from approximations based on the other temperatures. The temperatures of isotopes that are in more than one medium were approximated by volume weighting of these values. The microscopic transport cross sections used to calculate the DCF were determined from Eq. 12. The thermal total and scattering cross section values for hydrogen, oxygen, chromium, manganese-55, iron, and nickel and also helium for the BeO-UO_2-Er model came from tables.[17,18] λ_{tr} was calculated from Eq. 11. The average pitch between the rods is 3.9522 cm. The radius used is the radius of the fuel zone, which is dependent on the fuel cell being modeled. With these parameters, the DCF was linearly interpolated from a table.[14] The DCF obtained for the FLIP fuel element is 5.6579×10^{-2} and for the BeO-UO_2-Er design, the value is

Table 4. Operating Temperatures of Different Mediums (K)

Medium	$U\text{-}ZrH_{1.6}$-Er Core (300 W)	BeO-UO_2-Er Core (300 W)	$U\text{-}ZrH_{1.6}$-Er Core (1 MW)	BeO-UO_2-Er Core (2 MW)
fuel	305.37	305.37	573.15	1673.15
helium gap	-	305.37	-	1023.15
cladding	305.37	305.37	305.37	373.15
water	305.37	305.37	305.37	373.15
fuel rod graphite	305.37	-	323.15	-
graphite blocks	305.37	305.37	305.37	305.37
support materials	305.37	305.37	305.37	305.37
control rods	305.37	305.37	305.37	305.37

5.4886×10^{-2}. The various microscopic cross sections used in array 3** of NITAWL-S for this and all other cell models were obtained using Eqs. 13 – 17. The σ_s values in these equations came from approximations of their averages over the resonance absorption energy range of the absorbers and are presented in Table 5. Both the resonance absorption energy ranges and the σ_s values over these ranges came directly from cross section curves or from extrapolations of these curves.[19] An exception to this is the resonance absorption range of ^{166}Er, which has no resonances in the small energy range shown (0.01 – 0.11 eV). Since this range is below that of the resonance absorption range for ^{167}Er (0.3 – 0.7 eV) and the scattering cross sections of most of the moderators were fairly constant over several orders of magnitude, the resonance absorption ranges of the erbium isotopes were assumed equal.

For XSDRNPM-S, the left-hand boundary condition was specified as a reflected boundary (option 1) because the center of the rod was taken to be the "left" and symmetric conditions apply. The outer edge of the cell was taken to be the "right" and the white/albedo boundary (option 3) was applied here. A "white" boundary condition sets the net flow across the boundary to zero, as is appropriate for cells that occur in lattice geometries.[2] For both the FLIP and BeO-UO_2-Er fuel systems, XNF (Eq. 19) was calculated using 2.47 neutrons per fission and 200 MeV per fission as given for ^{235}U.[15] For the low power runs, 300 W, XNF is 2.3125×10^{13}n/s. At 1 MW and 2 MW, XNF is 7.7082×10^{16}n/s and 1.5416×10^{17}n/s, respectively. The number of intervals / cm is higher for the fuel cell model than for the remaining models because of the need for a fine mesh with so many boundaries in a small cell.

Table 5. Microscopic Scattering Cross Sections (barns) from Curves

	Absorbers (with Resonance Ranges)		
Moderators	^{166}Er & ^{167}Er (0.3 eV – 0.7 eV)	^{235}U (1 eV – 10 keV)	^{238}U (5 eV – 13 keV)
H	21	21	21
Be	6.1	6.0	6.0
O	3.8	3.8	3.7
Zr	6.2	8.0	8.0
^{235}U	13.9	-	20
^{238}U	9.	15	-

The mesh ranges from 11 intervals/cm for the fuel zone of the FLIP fuel rods to 111 intervals/cm for the helium gap of the BeO-UO_2-Er fuel rods. Another reason for the very fine mesh in the helium gap is the difficulty experienced by XSDRNPM-S in modeling a near void region. Although a void correction was applied, this mesh was used to further improve the accuracy.

The other cylindrical cells modled for this work include the experimental water notches, the water filled elements on the west side of the core, the regulating rod, the borated graphite section of the transient and shim safety rods, and the air section of the transient rod. Each of these cells were modeled with two regions. The center region (zone 1) is the region for which cross sections were produced. The center zone for the experimental notches and the water filled elements includes only water. The aluminum tube with holes that comprises each of the water filled elements was neglected because of the small volume percentage of the aluminum in those cells and the slight effect of aluminum on the neutron flux. The center of the regulating rod model contains a homogeneous mixture of B_4C powder, aluminum cladding, and water. The boron is represented by both ^{10}B and ^{11}B. The model of the borated graphite section of the transient rod includes water, the four main isotopes of stainless steel for the cladding (iron, chromium, manganese-55, and nickel), and the borated graphite itself, which is a mixture of 25 mass percent B_4C and 75 mass percent carbon. The air section of the transient rod was modeled as water, stainless steel cladding, and air (approximated as nitrogen, oxygen, and carbon with the actual percentages). The outer region is a homogeneous mixture of fuel, cladding, and water that simulates the surrounding

medium. The homogeneous zone for the experimental notch cell also includes graphite since the notches are adjacent to the graphite blocks. The purpose of these homogeneous zones is to simulate the fission sources for the regions of interest. The dimensions of each of these cells are presented in Table 6. The dimensions of the homogeneous zones were chosen to provide an adequate fission source.

The microscopic scattering cross sections used in Eqs. 13 – 17 for the cylindrical cells are the same values presented in Table 5. The left-hand (center) boundary condition is specified as reflective (option 1) because symmetry about the center also applies for this case. The right-hand (outer) boundary condition is specified as reflective because more of the surrounding homogeneous absorber region is assumed to exist on the other side of the boundary. The number of compositions used for the problem mock-up (MXX) is 2 because each of the two homogenized zones are assumed to be only one material. The mesh for these cells ranges from 5.6 to 8.6 intervals / cm. This mesh is more coarse than that used for the fuel cell because there is not as much of a need for a very fine mesh with a larger cell that has more space between the boundaries and also because there was a need to conserve computer time.

Another set of similar models includes the one for the two water regions on the east and west sides of the core and the one for the graphite blocks and water regions on the north and south ends of the core. The NITAWL-S and XSDRNPM-S input files for these geometries of the BeO-UO_2-Er fueled core are also presented in Appendix D. Each of these two models are in slab geometry and were used to produce

Table 6. Dimensions of Cylindrical Non-Fuel Cells

	Radii (cm)	
Models	Inner Zone	Outer Zone
experimental notch	4.4583 cm	13.151 cm
water filled element	2.2291 cm	9.7609 cm
regulating rod, transient rod, and poison section of control rod	2.2291 cm	10.943 cm

cross sections for two different zones. The only difference between the input files to get two different cross section sets from the same model are the specifications for the output cross section set in arrays 4$$, 16$$, and 18## of XSDRNPM-S. The model for the east and west side water regions has three zones: the homogeneous absorbing zone with a thickness of half the total width of the assemblies or 19.157 cm, the water from the side of the core out a distance of 7.7089 cm (the width of one assembly and its immediately surrounding water), and another water region going out an additional 12.611 cm. This makes the total water distance from the side of the core represented by the model equal to 20.32 cm (8 in), which was used to put the vacuum boundary (at which the flux is set to zero) far enough away from the core to get a natural neutron flux shape. The water was separated into two different zones to give a rough approximation to the cross sections' dependence on distance from the core due to the neutron flux. The other two dimensions given for the model are the entire north-to-south distance across the fuel assemblies (39.878 cm) and the length of the fuel section of a fuel rod (38.10 cm for the U-$ZrH_{1.6}$-Er core and 55.88 cm for the BeO-UO_2-Er core). The model of the north and south ends also has three zones: the homogeneous absorbing zone with a thickness of 20.414 cm corresponding to half the total distance across the assemblies in that direction, the graphite block zone (16.2 cm), and the water zone with a thickness set equal to the homogeneous zone. The graphite block zone was approximated as pure carbon. The other dimensions for this model are the fuel section length and the west-to-east fuel assembly width (38.313 cm). The slight discrepancies between the half and total widths given across the assemblies are due

to the method of treating water dimensions on the outside edge of these regions. Any differences were assumed negligible and ignored.

The temperatures, microscopic scatter cross sections, and densities used in the NITAWL-S input for the side-of-core water models and the north and south end graphite block and water models were all obtained in the same manner as the previously described models. The boundary conditions specified in the XSDRNPM-S input for these models are 0 for a vacuum boundary at the outer water edge (left-hand boundary) and 1 for a reflected boundary on the other side of the homogeneous zone (right-hand boundary). The mesh for these models ranges from 1.9 to 6 intervals / cm. This mesh spacing is generally more coarse than that used in the cylindrical models because these zones are larger than the cylindrical model zones.

The last models to be described are the two that produced the cross sections for the regions above and below the core. These geometries of the BeO-UO_2-Er fueled core also have NITAWL-S and XSDRNPM-S input files represented in Appendix D. Each model is a slab that spans the dimensions of the system in the north-to-south and west-to-east directions (40.500 cm $\times$ 35.545 cm). The above-core model has four zones: the homogeneous fuel zone (19.05 cm thick); a homogeneous mixture of fuel rod graphite, cladding, and water (8.89 cm); a homogeneous mixture of water, structural stainless steel, and structural aluminum (10.16 cm); and water that is above all these zones (20 cm). The below-core model has five zones: the homogeneous fuel zone (19.05 cm); the homogeneous fuel rod graphite zone (8.89 cm); a homogeneous mixture of water and structural stainless steel (6.35 cm); a homogeneous mixture of water and structural aluminum representing the grid plate (15.875 cm); and the water that

is below all these zones (20 cm). Since the BeO-UO_2-Er core was modeled without the graphite sections of the fuel rods, the homogeneous fuel section was lengthened by 8.89 cm to 27.94 cm for this model. As with the other slab models, each individual input file was used to produce cross sections for only one zone. The below-core model was chosen to pass the cross sections generated for the fuel rod graphite zone. The volume percentages within the three zones that represent structural material and water are presented in Table 7. These percentages were approximated from geometric descriptions of the actual regions. The only unique feature of the NITAWL-S and XSDRNPM-S input file for these models that requires any discussion is the mesh spacing used. In this case the mesh ranges from 1.36 to 2.02 intervals / cm. The dominant reason for choosing such a coarse mesh is due to computer time.

Table 7. Volume Percentages Within Structural Zones

	Models		
Materials	H_2O, Al, & Steel Above Core	H_2O & Steel Below Core	H_2O & Al Below Core
H_2O	57.5	67.5	31.5
Al	17.5	-	68.5
steel	25	32.5	-

GENERATION OF THE MACROSCOPIC MATERIAL CROSS SECTIONS WITH THE BOLD VENTURE IV PROCESSORS

Each of the cross section files produced by NITAWL-S and XSDRNPM-S include macroscopic cross sections for each isotope requested in a binary, nuclide-ordered, or ISOTXS, format. For use by the VENTURE neutronics module, these cross sections were converted to material cross sections and combined into just one file that is in a binary, group-ordered format. This involved both running various processing modules of BOLD VENTURE IV and combining and modifying cross section files.

The first step in the cross section processing involves the execution of a JCL file that calls the modules CONTROL1 and DCRSPR directly.[3] CONTROL1 was used for every execution of all BOLD VENTURE IV modules to perform initializations and direct the driver. DCRSPR was used to process data for the cross section processor code. The JCL-data files for two cases (the fuel section of the fuel rods and the water, steel and aluminum region above the core, each for the BeO-UO_2-Er core at 2 MW) were written. Single executions of the CONTROL1-DCRSPR JCL file were used to convert each of the macroscopic material cross sections for just one material. The files produced for each execution are in a binary nuclide-ordered format. The

input files for the executions of these modules for this work have a suffix of "OUT" corresponding to the output file names from the XSDRNPM-S executions. The output files have suffixes of "ISX". The JCL for this and all other BOLD VENTURE IV processors requires assignments of values to memory allocation variables that are used for individual unit numbers. These variables (NB1, NB2, B1, B2, NX, NS, N1, N2, ... N16) are assigned twice in the JCL. The first assignment of these variables is in the same location as given by ORNL and assigns the recommended values. The second assignment overrides the values given in the first assignment and is used to increase the allocations when necessary. The user knows that increases are necessary when the system produces an error message for a particular unit number. The line in the JCL that allocates the memory to that particular unit number uses one of the variables in the "SPACE" parameter. Therefore it can be seen from that line which variable needs to be increased. In case it is necessary to increase the allocations, there are equations that can be used, but seven of the variables must still come from guesses. Therefore for this project, when it became necessary to increase the unit allocations, values assigned to individual variables were increased using a trial-and-error method until the job executed.

A discussion of the some of the input variables to CONTROL1 and DCRSPR follows, but as with the NITAWL-S and XSDRNPM-S discussion, not all variables will be mentioned. It should be noted that the input to both CONTROL1 and DCR-SPR is column-dependent, unlike the NITAWL-S and XSDRNPM-S input.[3] This means that any displacement of data could cause any sort of error in interpretation

of the data — including the order of magnitude of a number. Any variable with a specification that is left blank will either be assigned a default value or 0. The input follows immediately after the line "//GO.SYSIN DD *" of the JCL. The first line calls CONTROL1 with "=CONTROL1" in columns 1 – 9. The second line is an alphanumeric problem identification label. In the third line, for the memory allocation variable (IP1), a value of 190000 was used because the default of 40000 was insufficient for the job for which the JCL was originally being created. It is possible that this could have been decreased. The option 1 was specified for IP7 to specify that interface data file information was included. The option 1 was specified for IP12 to create an initial interface data file table. In the fourth line, the first value of the calculational path array (IM) was set to 2 to specify that a "special processor", a category which includes DCRSPR, was to be executed first. The second value was set to 6 to call the cross section processing module. "ISOTXS" was placed in the fifth line to specify that the input cross section section file is a binary, nuclide-ordered file. "END" was placed in columns 1 – 3 of the last line to terminate the execution of CONTROL1. The initialization "DCRSPR" was placed in columns 1 – 6 in the line immediately following the "END" of the CONTROL1 data. In the second line (card 1) of the DCRSPR data, a 1 was specified for ICD3 to have a new nuclide-ordered file generated. No specification was given for ICD5, however option 2 was attempted to merge two nuclide-ordered files. This would have allowed a series of combinations of cross section files that would have simplified the creation of one macroscopic material cross section file including all the materials of the reactor. However, after several

attempts to use it, it was verified that this option is not working.[21] For ICD11, a 1 was specified to create isotope mixtures, or materials. In the third line (card 2), the number of mixtures (NOP6) was 1 for every case. NOP7 is the number of isotopes in each mixture and must equal the value specified for IIITF in the corresponding XSDRNPM-S runs. In the fourth line (card 7), M1 and M2 were both specified as 1 to indicate that both the first and last mixture are mixture number 1. The next several lines (cards 8) have alphanumeric isotope labels and the corresponding atomic concentrations. The concentrations are in units of atoms /(cm · barn of material), where "material" refers to the physical region for which cross sections were processed by NITAWL-S and XSDRNPM-S. For the fuel model, these concentrations are the product of the concentrations used in array 15** of XSDRNPM-S and the appropriate zone volume fractions. For the remaining cell models, these concentrations are the same as the XSDRNPM-S values. If the last concentration value fell in the last (fourth) column of a line, then a 0 was specified for the concentration in the next line without an alphanumeric label to provide a terminator for the concentration data. A 0 was placed in column 3 of the next line to indicate that there were no more mixtures. The next line (card 9) requires three six-character alphanumeric mixture labels in columns 1 – 18. For convenience, the same label was used for each of these in all cases. The values used for AMASS, EFISS, and ECAPT were set to 0 because these values are no longer needed since the isotopic cross sections had already been processed. For the isotope classification variable (KBR), 1 was specified for the fuel cell to indicate that the material is fissile. For the other cells, a 0 was used to specify

that no classification is needed. An "END" was placed in the last line to terminate the execution of DCRSPR.

The next type of file executed calls CONTROL1 and FPRINT. It was used to convert the files from binary to card-image.[3] The input files for these runs have the suffix "ISX" and the output files have the suffix "CARD". The input specifications were the same for every material. For the CONTROL1 input all the specifications were the same as when using it with DCRSPR except for IM, the calculational path array. The values specified were 1 for the input processor and 3 for the file editor, FPRINT. As with DCRSPR, the data for FPRINT must begin in the line immediately after the "END" statement of CONTROL1. "INPUT PROCESSOR" was placed in the first column of the first line. "OV FPRINT" was placed in the second column of the second line. The data for FPRINT is represented in "records" that do not have many format restrictions. Each data record is labeled at its beginning with its identifier, such as "1D", "2D", ..., etc. In record 1D, the third line, the number of files to be processed (NSPECS) was set to 1. NBCD, the unit number of the output card-image file, was set to 13 to match the number used in the JCL file. 0 was specified for NSTOP to put a "STOP" at tne end of every output file. 1 was specified for NDUM to retain the file. In record 2D, the fourth line, the label "ISOTXS" was used to specify a Hollerith file name. Once again, the data set was terminated with an "END" in the last line.

The final processing job executed calls CONTROL1, ISOTXS, and DCRSPR. It was used to convert a card-image file that represents all the macroscopic material

cross sections to a binary, group-ordered format for the final reactor modeling. The single card-image file that represents all the material cross sections was obtained by combining the output card-image files from the FPRINT runs and modifying the resulting file to meet the specifications of the processor ISOTXS. There is no external input file for these runs. The output file has the suffix "XSECTS". The only input variables to CONTROL1 that were changed for this run are IP1, IP7, and the array IM. IP1 was set to 90000 because it was found to be a sufficient memory allocation. IP7 was set to 0 because no additional data was supplied. The IM array values were set to 1, 2, and 6 to set the calculational path to the input data processor, the special processors, and finally the cross section processor. "INPUT PROCESSOR" was placed in column 1 of the line immediately following the "END" for the CONTROL1 data to start the execution of the processor ISOTXS. The remaining data for ISOTXS came from the card-image cross section files. The data in these files was already in a format that meets the input specifications for ISOTXS, which used data records as used by the module FPRINT. Each individual data file was created with an identification line and records 1D, 2D, 4D, 5D, and four 7D records, one for each scattering order. The identification line and records 1D and 2D were only needed once for the entire ISOTXS data set because the data included in these records is universal to the system, therefore it was easiest to keep these lines from the file representing the first material listed and delete them from the remaining materials. The data in records 4D, 5D, and 7D from each file was retained. The sequence for the resulting ISOTXS data is therefore the identification line first and then records 1D, 2D, 4D, 5D, 7D, 7D, 7D, 7D, 4D, 5D, 7D,... etc. up through the last material. Once the identification line was taken from the first output card-image cross section file, it was not changed. In record 1D, the number of isotopes in the file (NISO) was changed from 1 to the number of materials in the combined file. The maximum number

of upscatter groups (MAXUP) was set to the highest value seen for any of the material cross section sets included in the file. For this work, MAXUP was usually 3, but for the U-ZrH-Er core at 1 MW it was necessary to set it to 4. The first line of record 2D had "2D/" in a line by itself. This was retained. An alpha-numeric problem label was placed in the next line with an "*" in both columns 3 and 72 with the character string in between. It was necessary to change this label from the one supplied by the first data set since its label pertained only to that material. Labels for each material were placed in the next lines. The line that was kept for this label was also changed since it only included the label for the first material. Each material label was created with six characters plus an "*" placed on either side. Up to eight labels with one space between each one were included in each line with the first "*" appearing in column 2 and the last in column 72. Any additional space at the end of the last line of these labels was left blank. It was not necessary to change the fission spectrum (X) values for each energy group, however after the last fission spectrum values are the mean neutron velocities for each energy group, which were not required for this work. Therefore, all of these values were deleted and "0.0 7R/" was put in a separate line to replace them. The "7R" was included to repeat the "0.0" seven times. The next values are the energy group boundaries in electron volts. They were moved so that the upper limit began in column 2 and the lower limit was given a "/" after it. The line after the energy group boundaries that contained only a "0" was modified to have a series of numbers separated by one space that count in multiples equal to three greater than the order of scattering, or 6. The number of integers (including the "0") equals the number of materials. A "/" was put after the last integer. These integers are used to indicate the number of records between materials. The individual material descriptions begin with record 4D. It is started with "4D/" on a line by itself that did not indeed need to be modified.

Since all material labels were being kept the same, the next line needed to have the same material label three times. This was accomplished by modifying each material label line from each file to read "(*name*) 3R", where name is the material name. The rest of record 4D includes data about the material and the energy groups. It was not necessary to change any of these values except for one case: the material that represents the fuel cell. The two-dimensional JBAND array is used to indicate the number of groups that scatter into each group, including self-scatter, for each scattering block. However, for the fuel cell, the number of groups that scatter into group 5 was given as 8, which is an erroneous value since only seven energy groups were used. Since this values was given as 7 for some of the other materials; it was changed to 7 to allow the maximum number of groups. Record 5D requires all necessary macroscopic cross sections other than the scattering matrix. No changes to this record were necessary. The group-to-group cross sections for each scattering block are represented by consecutive entries of record 7D. Once again, no changes were necessary to these blocks with the exception of the fuel material. Since record 4D had one too many groups scattering into group 5 there was also one too many macroscopic scattering cross sections given for scatter into group 5 for each scattering block. The extra value was easily recognized since it was much smaller than the others by several orders of magnitude and was often 0. After removing the extra value, the line was shifted so that no column was entirely blank to keep a blank column from being interpreted as a data terminator. Each consecutive set of material values must have its "4D/" initializer immediately after the last line of scattering cross sections for the previous material. This made it necessary to delete the "STOP" at the end of each material cross section file except for the last one. The "STOP" for the last set must have an "END" statement put after it in the next line. This "END" is immediately followed by the call the DCRSPR. ICD4, in the one line (card 1) of

input to DCRSPR, was set to 1 so that a new group-ordered file would be generated. ICD8 was also set to 1 so that a new group-ordered file would be generated. ICD8 was also set to 1 so that only the scattering cross sections for order 0 were retained for the diffusion theory calculation to come. ICD10 was kept at 0 to keep the total scattering matrix from being computed since total scattering data was already present. An "END" was placed in the last line to conclude the DCRSPR data.

THE APPROXIMATION OF THE SOLUTION TO THE DIFFUSION EQUATION WITH VENTURE

Once the ISOTXS-DCRSPR run producing the binary, group-ordered macroscopic cross section file was completed for a particular core model, the VENTURE neutronics model was ready to be executed. The JCL-data file calls the modules CONTROL1 and DVENTR directly for the case of the BeO-UO_2-Er fueled core at 2 MW. The neutronics module VENTURE is called by CONTROL1. For each case, the binary data file has a suffix of "XSECTS". The multiplication factor (k_{eff}) and the seven-group energy fluxes at each interval location are produced in the standard output file associated with the IBM job number. The fluxes are also produced in a binary file with an "FLX" suffix.

As mentioned previously, VENTURE is based on diffusion theory, which is in turn based on transport theory with approximations to the transport equation. The form of the diffusion equation used by VENTURE is [3]

$$-\nabla D_{r,E}\nabla\phi_{r,E} + (\Sigma_{a,r,E} + \Sigma_{s,r,E} + D_{r,E}B^2_{\perp E})\phi_{r,E} = \int_{E'}(\Sigma_{r,E'\to E} + \frac{1}{k_{eff}}\chi_{r,E}(\nu\Sigma)_{f,r,E'})\phi_{r,E'}dE' \tag{20}$$

where

$D_{r,E}$ = diffusion coefficient at position r and energy E,

$\Sigma_{a,r,E}$ = macroscopic absorption cross section at position r and energy E,

$\Sigma_{s,r,E}$ = macroscopic scatter cross section at position r and energy E,

$B^2_{\perp E}$ = geometric buckling at energy E,

$\Sigma_{r,E'\to E}$ = macroscopic scatter cross section at position r from energy E' to E,

$\chi_{r,E}$ = fission spectrum at position r and energy E,

and $\Sigma_{f,r,E'}$ = macroscopic fission cross section at position r and energy E'.

Discretizing the energy range into groups and simplifying the transport term gives

$$-D_{r,g}\nabla^2\phi_{r,g} + (\Sigma_{a,r,g} + \sum_n \Sigma_{s,r,g\to n} + D_{r,g}B^2_{\perp g},\phi_{r,g} = \sum_n (\Sigma_{s,r,n\to g} + \frac{1}{k_{eff}}\chi_{r,g}(\nu\Sigma)_{f,r,n})\phi_{r,n}. \tag{21}$$

The Laplacian operator used for this project is the Cartesian form

$$\nabla^2 = \frac{\partial^2}{\partial x^2} + \frac{\partial^2}{\partial y^2} + \frac{\partial^2}{\partial z^2}. \tag{22}$$

The set of equations generated by Eq. 21 are solved using an iteration procedure. The initial k_{eff} used is 1.0 and the initial set of fluxes are provided by a solution to a one-dimensional problem. Inner iterations are used to successively recalculate the flux values for each mesh element in an ordered sweep through the space mesh at one energy. The calculations are performed with the neutron balance equations represented in matrix form by

$$\phi_{t,n} = T\phi_{t-1,n} + US_n \tag{23}$$

where

$\phi_{t,n}$ = point flux values for inner iteration t and outer iteration n,

T & U = operators or coupling terms,

and S_n = point source terms.

The inner iterations continue until a fixed number of iterations have been executed. The outer iterations are performed using a matrix simplification of the equations generated from Eq. 21,

$$[D - J - L - U]\phi = [S + T + \frac{1}{k_{eff}}\chi F]\phi \qquad (24)$$

where

ϕ = neutron flux vector,

D = main diagonal term representing loss due to absorption, buckling, and outscatter,

J = coupling terms for a block of points along individual rows at one energy for which the flux values are simultaneously determined,

L = lower triangular matrix with coupling terms in space,

U = upper triangular matrix with coupling terms in space,

S = downscattering source matrix at a point,

T = upscattering source matrix at a point,

F = fission source component, a row matrix operator,

and χ = the source distribution, a column matrix operator.

This equation can be rearranged as

$$D\phi = [J + L + U + S + T + \frac{1}{k_{eff}}\chi F]\phi. \qquad (25)$$

Assuming that fluxes from two outer iterations are approximately equal, Eq. 25 can be changed to

$$\phi_{n+1} = D^{-1}[J + L + U + S + T + \frac{1}{k_n}\chi F]\phi_n, \qquad (26)$$

which is the equation that the outer iteration flux calculations are based on. Each outer iteration recalculates each point flux by sweeping through the energy groups starting from the highest energy group. After each iteration, a new k_{eff} value is calculated from

$$k_n = \frac{P_n}{L_n} \tag{27}$$

where

P_n = total neutron production rate

and L_n = sum of neutron absorption rate and surface leakage rate.

This process continues until a convergence on k_{eff} is met:

$$\frac{k_n - k_{n-1}}{k_0 - k_n} < 0.05 \tag{28}$$

where

k_0 = initial guess for multiplication factor or 1.0.

The data for CONTROL1 and DVENTR were included after the JCL within the same file, as with the BOLD VENTURE IV processor runs. In the CONTROL1 data, IP1 was increased to 240000 because a larger memory allocation was needed with a 46 × 36 × 46 three-dimensional mesh geometry. IP7 and IP12 were both set to 1 so that the data from both the separate file and the JCL file would be read. The numbers 2 and 7 were specified for the IM array to have DVENTR and then VENTURE executed. The character string "GRUPXS" was specified in the fourth line because the input cross section file was in a group ordered format.

As with other modules, the initialization "DVENTR" was placed in the line immediately following the "END" for CONTROL1. DVENTR, like DCRSPR, requires that its input be in a column-dependent format. The input is also divided into sections which have section numbers right justified in columns 1 - 3 of the first line (card 1) of each section. In card 2 of section 1, the time between each writing of the restart I/O data file RSTRTR (RXX3) was set at 4 min. The value used for the power level in watts (RXX4) was dependent on the case being modeled (see Table 4). The ratio of thermal energy to the sum of the fission and capture energies (RXX5) was kept at the default value of 1.0. The fraction of the reactor considered for the problem was set to 1.0 since the entire system was modeled for versatility in control rod positioning. In card 3 of section 1, the convergence criterion on integral quantities on outer iterations (RXX11) was set to 1.0×10^{-4} and the convergence criterion on local, point quantities (RXX12) was set to 1.0×10^{-3}. Since the buckling is determined by the code for a three-dimensional calculation, 0.0 was specified for the buckling variable (RXX13). In card 5 of section 1, the value 1 was specified to have VENTURE perform a standard diffusion theory solution. ICX2 was assigned 0 so that the multiplication factor would be determined. ICX6 was specified as 4 so that data for multiple planes would be stored. The maximum number of outer iterations (ICX12) was set to 201. A large number was desired for ICX12 so that the problems would converge. In card 6 of section 1, IXE15 was set to 1 so that a total flux interface file (RTFLUX) would either be created or replace the previously existing one. Section 2 contains various control options for which the default values

were desirable for this project, therefore the section was omitted from the data. In card 2 of section 3, IGOM was assigned 14 to specify a three-dimensional rectilinear coordinate system. The value 2 was assigned to IMBL, IMBR, JMBT, JMBB, KMBF, and KMBR to specify extrapolated boundaries for every face of the system. The number of black absorbing zones (NZWBB) was set to 1, although it ultimately was not used in the model. The third line (card 6) of section 3 requires an identifier for the absorbing zone. Since there was no absorbing zone, the value given was greater than the number of materials by 1.

The geometric mesh description was given in section 4. The dimensions of each region and the corresponding number of intervals were specified in all three directions. The format of these lines is such that each region is specified by a number of intervals right justified in a field of three and is followed by its dimension in a field of nine. First, the dimensions from left to right are specified, then from top to bottom, and then from front to back. The specifications for one direction can take as many lines as needed, but a new direction must start on a new line. When the specifications for one direction completely fills its last line, the following line must be left blank. The dimensions given for the left-to-right and front-to-back directions match the dimensions of the water regions and the assemblies (see Fig. 1). The number of intervals within the assemblies was set to 4 so that each fuel rod and its immediately surrounding water would be divided into two intervals. The dimensions given for the top-to-bottom direction correspond to lengths of fuel rod sections and heights of structural and water regions (see Fig. 2). The mesh spacing for all these regions was set as high as possible while keeping the memory requirements and the execution

time reasonable. The ranges used were from 0.25 to 0.52 intervals / cm, depending on the region's material. Section 5 assigns a material to each region specified in section 4 using numbers that are assigned to the material names in section 20. The material names used for this work correspond to the names given in Table 2 with the appropriate beginnings of "LT", "HT", "LP", or "FP". The materials are specified in blocks of data with no blank lines separating them. The number of blocks is equal to the number of regions from front to back and each specifies the materials for a vertical plane. The number of lines in a block is equal to the number of vertical regions and specifies materials from top to bottom. The number of entries in a line is equal to the number of regions from left to right and specifies materials in that direction. Each entry has three columns. For every model of this project, there are nine regions from left to right, eight vertical regions, and eleven regions from front to back. Therefore, section 5 has eleven blocks of data with eight lines and nine entries per line. Section 6 specifies materials for individual mesh elements and overrides the specifications of section 5. This was used to specify the location of the water filled elements and the various types of control rods since they occupy less space than one assembly, which is the standard region size within the core. Using section 6 in this manner allowed the water filled elements to be removed and the control rod positions to be changed without altering section 5. Each material that is to specified in section 6 is labeled with its material number in columns 1 – 4 in a line by itself. The mesh specifications for that material then follow on subsequent lines. Each specification consists of six mesh numbers, each with fields of four. The six numbers represent

beginning and ending mesh number pairs in each of the three directions. The first two represent the limits from left to right, the next two represent the limits from top to bottom, and the last two are the limits from front to back. A maximum of three of these sets can fit on one line. When the last line for one material only has one or two sets of specifications, the last set is followed by a 0. However, if the last line has three sets, the 0 follows in the next line. The specifications for the last material are followed by another 0 in column 4 of a separate line. The lengths of the vertical zones used to match the lengths of the fuel rods and structural regions do not match the section lengths of the control rods. Therefore the lengths of most of the control rod sections are approximate and plugs that separate different sections of the rods were neglected, although the approximations used are as close as the intervals dividing the regions would allow.

In card 2 of section 12, the number of subzones (NSZ) was set to 0 since no subzones were used for this project. In card 3, M1 was set to 1 since the material numbers began at 1. M2 was set to the number of materials, which was dependent on the model. The nuclide set reference number (NS) and the zone classification number (NC) are categorization variables used in cases involving more complex models such as those requiring microscopic cross sections to create macroscopic cross sections for each zone. For more simple models requiring only that the locations of pre-generated macroscopic cross sections be specified, such as with this work, both NS and NC are set to 1. The volume fraction associated with zone concentrations was set to 1.0 since the materials that the cross sections refer to occupy entire zones. A 0 was placed in column 3 of the next line to terminate card 3. In card 2 of section 13, the

maximum number of nuclides in any set (NNS) was set to the number of materials for the model. In card 3, the number of nuclides in the set (NDXS) was set to the same value as NNS. A list of all the six-character material names was given in card 4 to associate the material names with the identification numbers used in sections 5 and 6. They were listed consecutively with twelve entries per line and no spaces separating them since each name has the same number of characters (six) as the field width. In section 20 cards 2 and 3 were repeated for every material. The sequence in section 20 and card 4 of section 13 is the same. Card 2 was given the material number right justified in columns 1 – 3 and card 3 was given the material name in columns 1 – 6 and concentrations of 1.0 in columns 7 – 18. The concentrations were set to 1.0 because macroscopic material cross sections do not need concentration corrections. The last entry was followed by a 0 in column 3 of the next line to terminate the data from section 20. "END" was placed in columns 1 – 3 of the last line to terminate the data.

RESULTS

The first significant results obtained were from the NITAWL-S and XSDRNPM-S executions of the U-$ZrH_{1.6}$-Er fuel cell model at 300 W. XSDRNPM-S is capable of producing an infinite multiplication factor (k_∞) for such a model, which can give some indication of the capabilities of the fuel rod. For the reactor to be capable of operating, the k_∞ for the fuel rod cell needs to be greater than 1.0, and the value obtained is 1.248. For comparison, a similar fuel cell model was created as input to EXTERMINATOR-2, a two-dimensional diffusion code, using the macroscopic material cross sections produced by General Atomic.[22] The k_∞ produced by this model is 1.256, which is different from 1.248 by approximately 0.64 %, which is considered acceptable agreement. Since some of the values used in the input to NITAWL-S were determined from various assumptions and approximations, a sensitivity study was performed for some of them using the fuel cell model at 1 MW, which has a k_∞ of 1.229. Those studied included the DCF and the material temperatures. The extreme values of 1.0 and 0.0 were tested for the DCF. The resulting k_∞ values determined are 1.241 and 1.228, respectively, with corresponding changes of approximately 0.98 % and 0.081 %. This indicates that the DCF does not have a significant effect on the results. An approximation that was made regarding the temperature is that the cladding and water temperatures are equal. This approximation was tested by dropping the water temperature to 280 K. Therefore the oxygen temperature was set to 280 K and the hydrogen temperature, determined from the weighted average

of the hydrogen temperatures in the fuel and in the water, was set to 450 K. These temperature changes had no effect on k_{∞}., thus indicating that small variances in isotopic temperatures do not have a significant effect on the results.

When modeling the U-$ZrH_{1.6}$-Er core, the goal was to show that the method used to model the core was sufficient to model the core with the BeO-UO_2-Er fuel. The k_{eff} values determined from the VENTURE executions with the control rods both in and out of the core and the control rod worths calculated from them were used to verify this method. Also used were the three-dimensional fluxes produced from the VENTURE runs with the shim safety and regulating rods half-way in the core. These runs were used to simulate critical operation since it would have taken several runs of VENTURE to iterate towards a k_{eff} of 1.000.

The k_{eff} values determined for both the 300 W and 1 MW core models with the control rods in all three positions are presented in Table 8. For the case with the control rods at the "half-way" position, it should be noted that this does not include the transient rod, which is out during operation. This column is only presented to show how close the k_{eff} values are to the true operation value of 1.000. The value at 300 W with the control rods out can be compared with the results from previous executions of EXTERMINATOR-2 and BOLD VENTURE IV.[4] The EXTERMINATOR-2 model is a horizontal plane through the core. The control rod positions were filled with water, making it comparable to a control rods out case. The macroscopic cross sections used for both the EXTERMINATOR-2 and BOLD VENTURE IV models were provided by General Atomic at 296 K for 300 W operation.[23]

Table 8. Multiplication Factors for 300 W and 1 MW U-$ZrH_{1.6}$-Er Core Models with Different Control Rod Positions

	Control Rod Position		
Power	Out	Half-Way	In
300 W	1.073	1.041	0.977
1 MW	1.064	1.030	0.964

The k_{eff} obtained for this model is 1.066, which is approximately 0.65 % different from the k_{eff} of 1.073 seen in Table 8. The BOLD VENTURE IV model is a half-core model with a horizontal plane of symmetry at the midpoint of the fuel rods. The control rod positions were filled with water because cross sections for the control rods were not provided. The k_{eff} determined for this model is 1.080, which is also approximately 0.65 % different from the value in Table 8. These differences are considered acceptable. The fluxes from the previous EXTERMINATOR-2 and BOLD VENTURE IV runs are not comparable with the fluxes generated for this work since, for the previous runs, the control rods were out of the system and also because a power level of 1 MW was used with cross sections generated for 300 W operation. However, the power level given to these codes has no effect on the k_{eff} produced. It can be seen in Table 8 that the k_{eff} values at 1 MW are consistently lower than the values at 300 W. This trend is due to the negative temperature coefficient of reactivity inherent in the U-$ZrH_{1.6}$-Er fuel. The reactivity worth in dollars of all the control rods together was determined from the data in Table 8 at 300 W. The reactivity for two of the cases at this power (the control rods in and the control rod out of the system) was determined from

$$\rho = \frac{k_{eff} - 1}{k_{eff}}. \tag{29}$$

The result from each case was then used in

$$\rho_{worth} = \frac{\rho_{out} - \rho_{in}}{\beta} \tag{30}$$

where

ρ_{worth} = reactivity worth of all control rods together in dollars,

ρ_{out} = reactivity of the reactor with the control rods out,

ρ_{in} = reactivity of the reactor with the control rods in,

and β = fraction of neutrons produced in fission that are delayed (0.00699).

The reactivity worth of all the control rods in the U-$ZrH_{1.6}$-Er core at 300 W obtained from Eqs. 29 – 30 is \$13.10. According to measurements, the mathematical sum of the worths of the individual control rods in the current core is \$15.75. One reason that the calculated total worth should not match the mathematical sum of the measured individual worths is that the worth of a control rod decreases with the number of control rods already in the core, as can be seen in the standard integral and differential rod worth curves.[17] Another reason not to expect a perfect match when comparing these numbers is that the model is for a fresh core while the measurements are for a core that has been in operation for a number of years. Whether the burnup effect would increase or decrease the worth of the control rods depends on the relative burnup experienced by the control rods and the fuel. Considering these two reasons for lack of an accurate comparison, \$13.10 is an acceptable value for total rod worth.

The other results used for comparison of the results of the U-$ZrH_{1.6}$-Er core model are the three-dimensional thermal fluxes produced for the cases with the shim safety and regulating rods half-way in the core. As mentioned previously, each run of VENTURE produces a binary file that includes the flux in each energy group at every node in the model. For the cases simulating operation, these files were converted to a card-image format with the module FPRINT.

format of the flux file for the BeO-UO_2-Er core at 2 MW was obtained. Since the resulting card-image file can be rather large (over 106,000 lines for this model), a program was written that reads all flux values over a specified energy group range at every node along a specified direction and sums the fluxes at each node over the specified energy groups. This program (RFLUX.FOR) made it possible to obtain simple thermal flux vs. distance curves with two of the three dimensions fixed. The output from RFLUX.FOR was written in a format that PICSURE, a graphics package on the College of Engineering's VAX 8650, can read. It was only necessary to transfer the output from the IBM to the VAX. For this work, groups 4 – 7 were used in each curve because the upper bound of group 4 (1.130 eV) is close to the upper bound of the thermal range (3.05 eV) in the 27 group library read by NITAWL-S when compared to the upper bound of group 3 (3.000×10^3 eV). The first flux curve is presented in Fig. 3. The format used for this curve is the same format used for all flux curves in this document. The horizontal axis is labeled with the appropriate direction through the core. The fixed positions are given in the figure name. The mesh numbers associated with the notations "Column", "Plane", and "Row" and the NSCR grid labels can be seen in Fig. 1. Also in these figures are the dimensions represented along the horizontal axes of the curves.

Fig. 3 shows the horizontal thermal flux profile at 1 MW along column 7 and row 22 form the north to south end of the model along the west side of the core. The otherwise natural cosine-shaped flux curve has two peaks near the top due to the presence of the water filled elements at B4 and B6. This curve presents the best

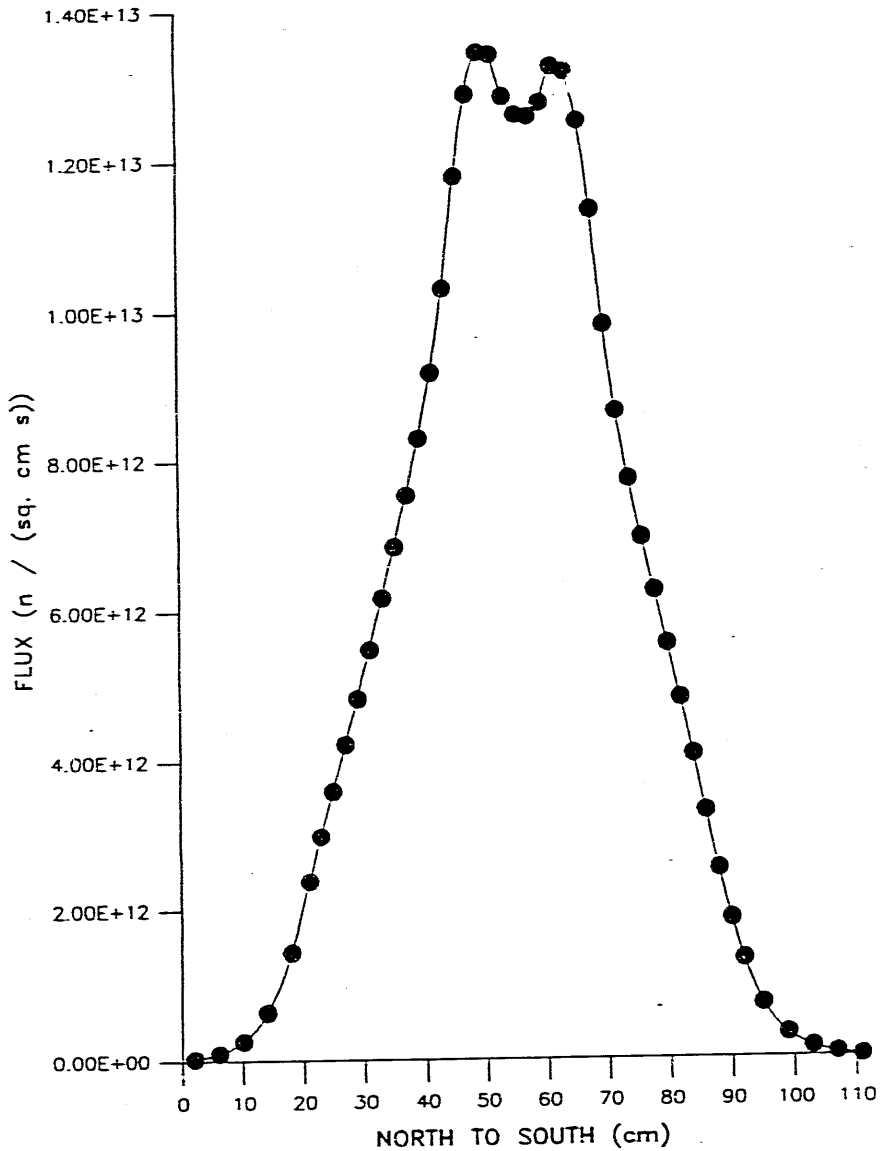

Fig. 3. Thermal Flux for 1 MW U-$ZrH_{1.6}$-Er Core Along Column 7 and Row 22

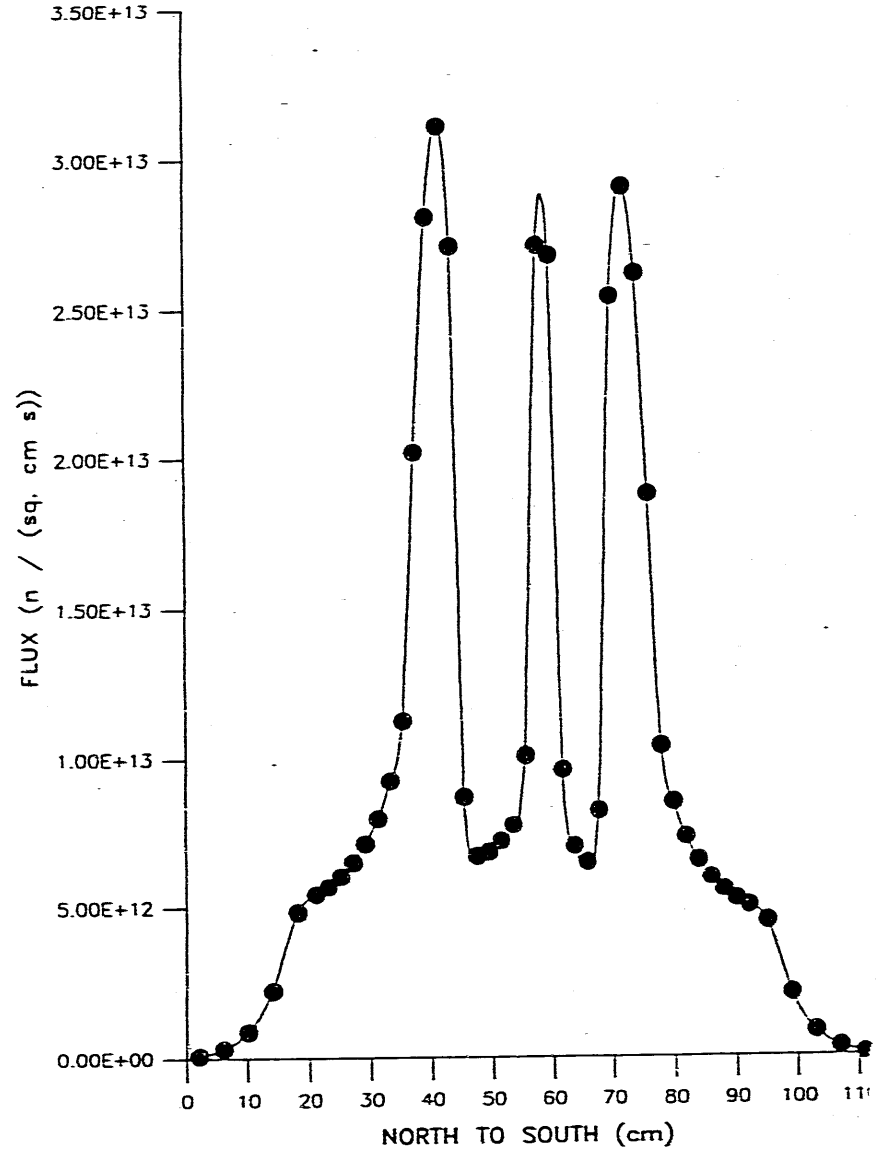

Fig. 4. Thermal Flux for 1 MW U-$ZrH_{1.5}$-Er Core Along Column 18 and Row 22

possibility of comparison with measured fluxes since most of the NSCR's flux measurements are at 1 MW at locations along this direction. The measured flux adjacent to the water filled elements at B6 is 1.0×10^{13} n /(cm^2 · s) and the corresponding calculated value is about 1.4×10^{13} n /(cm^2 · s). These values are quite close considering that the model is for fresh fuel and the current fuel has several years of burnup accumulated. Another source of discrepancy is the approximate methods involved in using SCALE-2 and BOLD VENTURE IV to determine the flux distribution.

Fig. 4 shows the flux profile along column 18 and row 22 through the water notches and the transient rod's channel. Row 22, as can be seen in Fig. 2, specifies a vertical position at the midpoint of the fuel and is used for all horizontal profiles. The center peak of Fig. 4 corresponds to the transient rod's channel and the two surrounding peaks correspond to the water notches. The depressions between the peaks are due to the fuel. The curved sections from 0 to 20 cm and from 90 cm to 110 cm represent the flux through the water regions. The curved sections from 20 cm to 35 cm and from 80 cm to 95 cm represent the flux through the graphite blocks. Fig. 5 shows the horizontal flux profile along column 26 and row 22 from the north to the south end including the regulating rod position. The first peak in this figure is due to the northern graphite block. The second peak corresponds to fuel elements. The spike represents the flux in water directly underneath the regulating rod, which is extended downward to row 21. The last peak is due to the southern graphite block.

The flux curve in Fig. 6 represents the thermal flux along column 18 and plane 21, or from the top of the model to the bottom through a fuel rod at NSCR grid

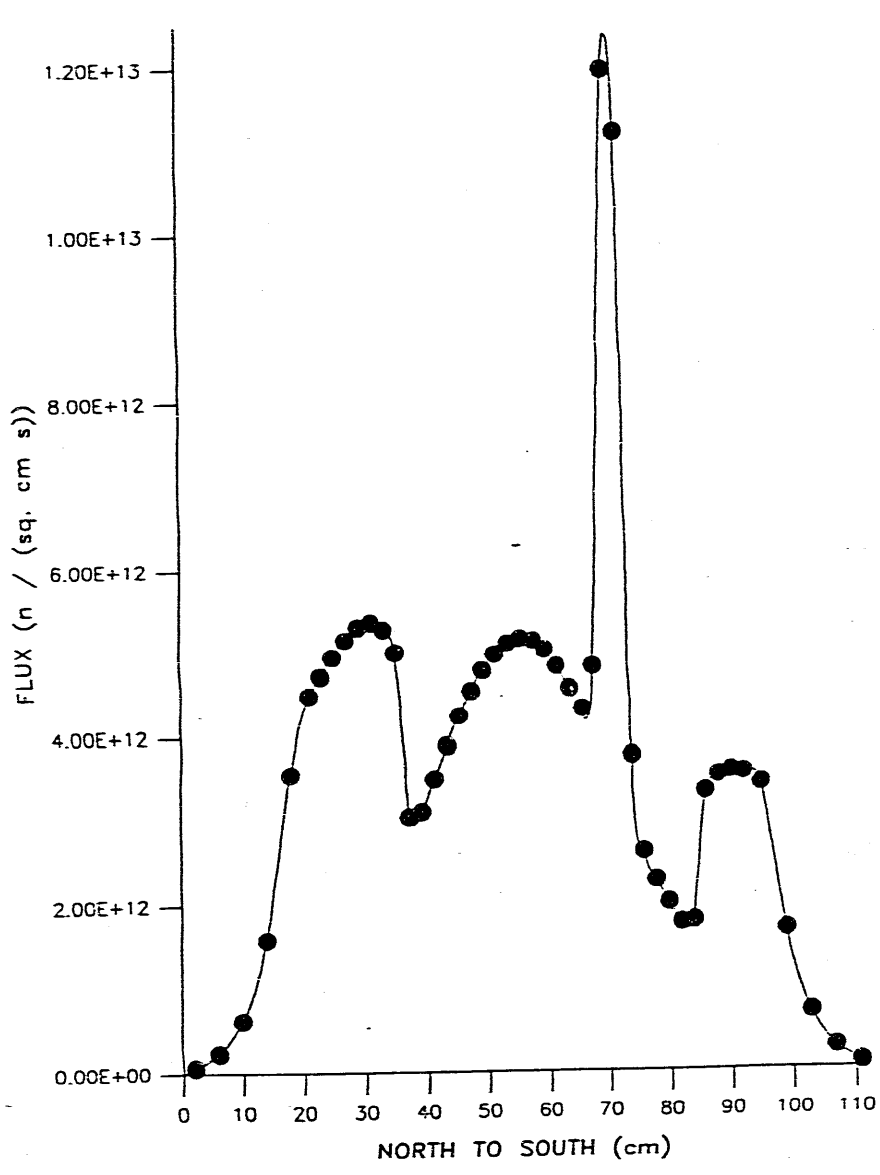

Fig. 5. Thermal Flux for 1 MW U-$ZrH_{1.6}$-Er Core Along Column 26 and Row 22

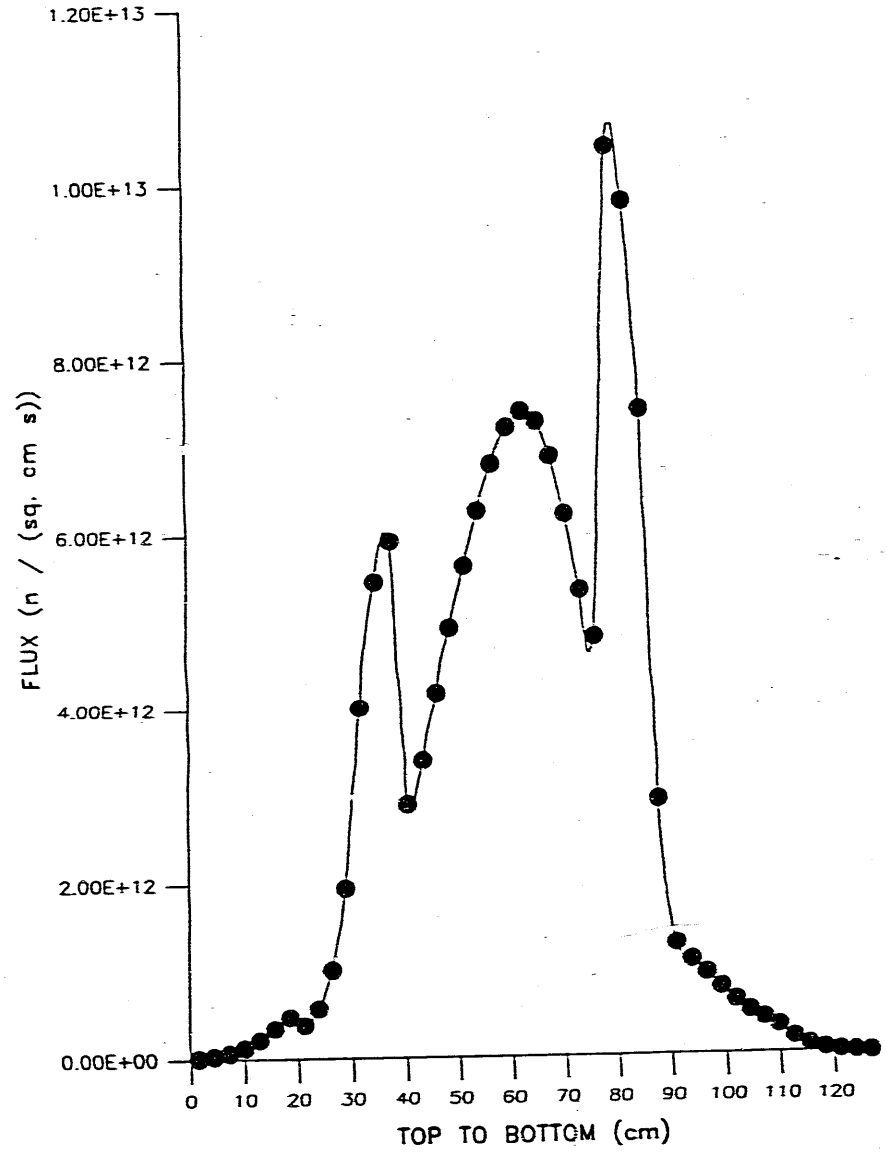

Fig. 6. Thermal Flux for 1 MW U-$ZrH_{1.6}$-Er Core Along Column 18 and Plane 21

location D6. The center peak represents the cosine flux shape through the fuel that is due to leakage from the ends of the fuel region. The surrounding peaks represent the thermal flux increase in the graphite sections of the fuel rod due to thermalization of the high energy neutrons in the graphite. The upper graphite section has a lower peak because of the presence of the borated graphite sections of the shim safety rods at that depth. The lowest portions of the curve represent the flux in the water and homogeneous water and structural regions. The flux in these regions is low due to the graphite separating them from the fuel.

The curve presented in Fig. 7 shows the flux distribution down the water notch at D3, or column 18 and plane 32. This curve shows the characteristic cosine shape of the flux in water. The curve in Fig. 8 shows the flux down column 18 and plane 25, or the transient rod channel, which is all water when the rod is out. The curve is similar to the one seen in Fig. 7 for the water notch except that it has inflections corresponding to the vertical positions of the graphite sections of the fuel rods. Its peak is also slightly higher since it is surrounded on all sides by fuel. Fig. 9 shows the flux profile down column 22 and plane 21, or the shim safety rod at E6. The slight peak at 20 cm corresponds to the boundary between the air tube of the rod and the borated graphite section. The flux through the borated graphite section is represented by the region between that peak and the fuel peak at 58 cm. The flux in this region increases towards the fuel because of the flux being produced by the fuel. The depression in the curve shown before the peak at 58 cm is only a fault in the curve fitting performed by PICSURE. The location of the peak at 58 cm is due both to the

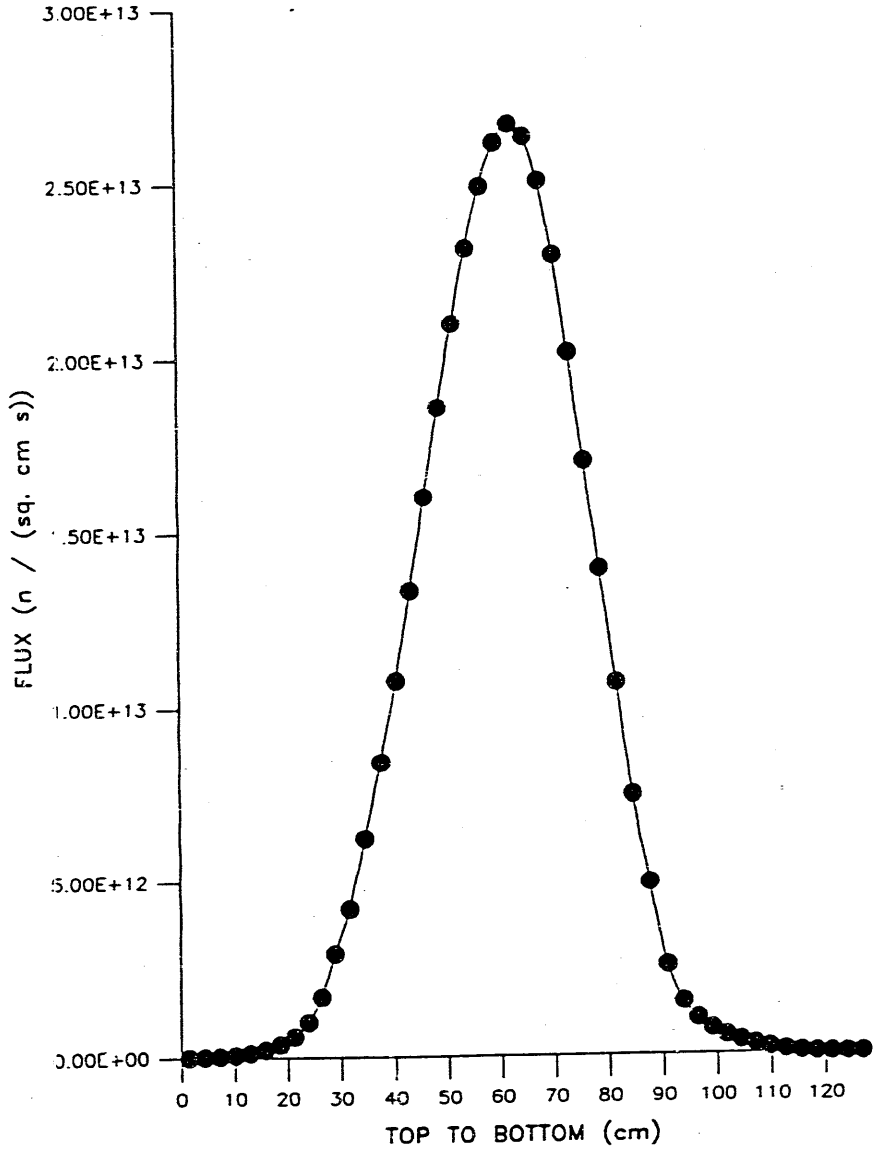

Fig. 7. Thermal Flux for 1 MW U-$ZrH_{1.6}$-Er Core Along Column 18 and Plane 32

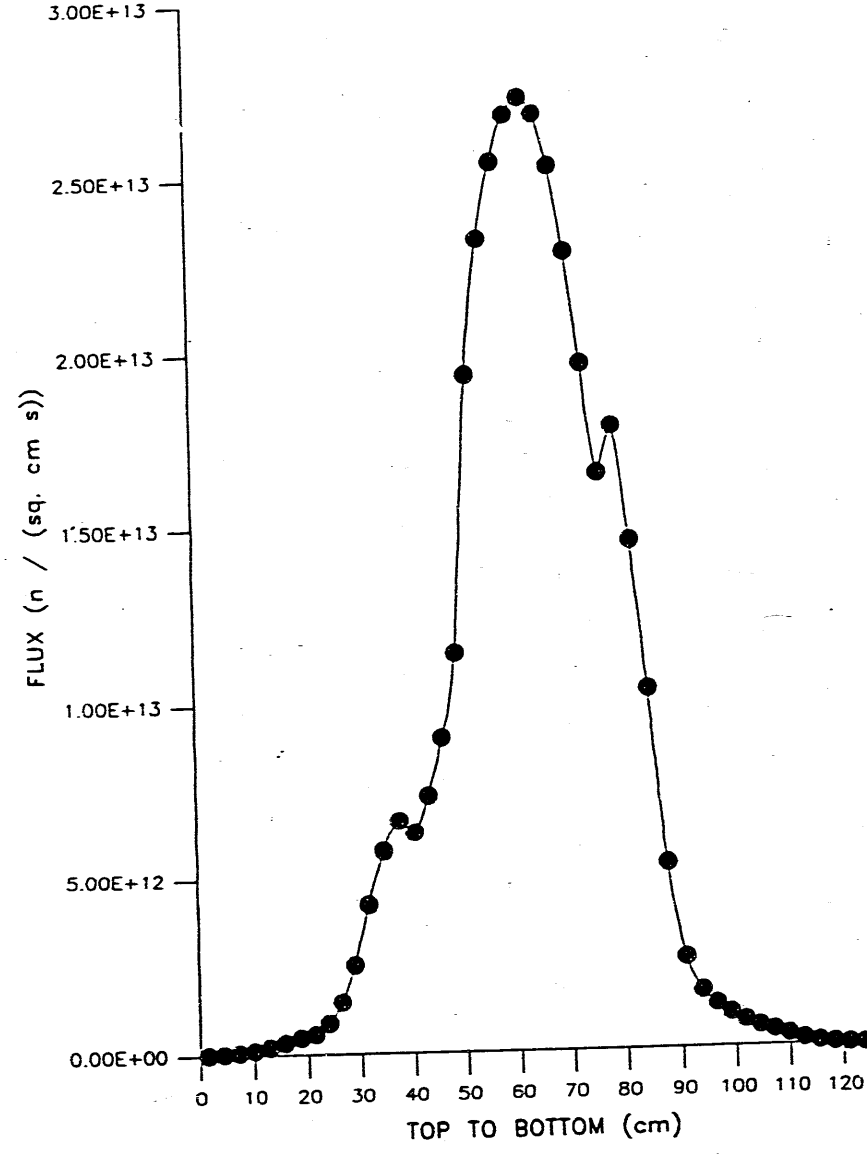

Fig. 8. Thermal Flux for 1 MW U-$ZrH_{1.6}$-Er Core Along Column 18 and Plane 25

end of the borated graphite sections and to the peak at the center of the fuel sections of the surrounding fuel rods. The inflection seen at approximately 80 cm is due to the flux increase in the graphite sections of the surrounding fuel rods. The inflection seen at about 95 cm corresponds to the boundary between the fuel and air sections of the shim safety rod. Fig. 10 shows the vertical flux profile through column 18 and plane 10, or through the northern graphite block at D8. The cosine shape of the curve is due to the influence of the fuel. The lower flux regions around the peak represent the flux in the water and homogeneous water and structural regions.

Fig. 11 shows the horizontal flux profile from the west to east sides of the core through the water notch at D7 along row 22 and plane 15. This curve is a good example of a thermal flux curve that shows the thermal flux increase in water due to thermalization of the high energy neutrons in the water. This effect is seen both in the peaks at the sides of the core and in the peak at the water notch. The flux in the fuel increases towards the water notch. Fig. 12 is the flux along row 22 and plane 31 through the water notch at D3 and the regulating rod's channel. This curve is similar to the one in Fig. 11 except for the additional peak due to the water under the regulating rod. Fig. 13 shows the flux along row 22 and plane 21, or through the shim safety rods rods at C6 and E6. The two peaks are at the boundaries of fuel and water on the sides of the core. Since the division between the borated graphite and fuel sections of the shim safety rods is between rows 21 and 22, this curve does not represent flux in the borated graphite, but its effect on the flux in the fuel region can be seen in the fact that there is some distortion in the cosine shape of the curve.

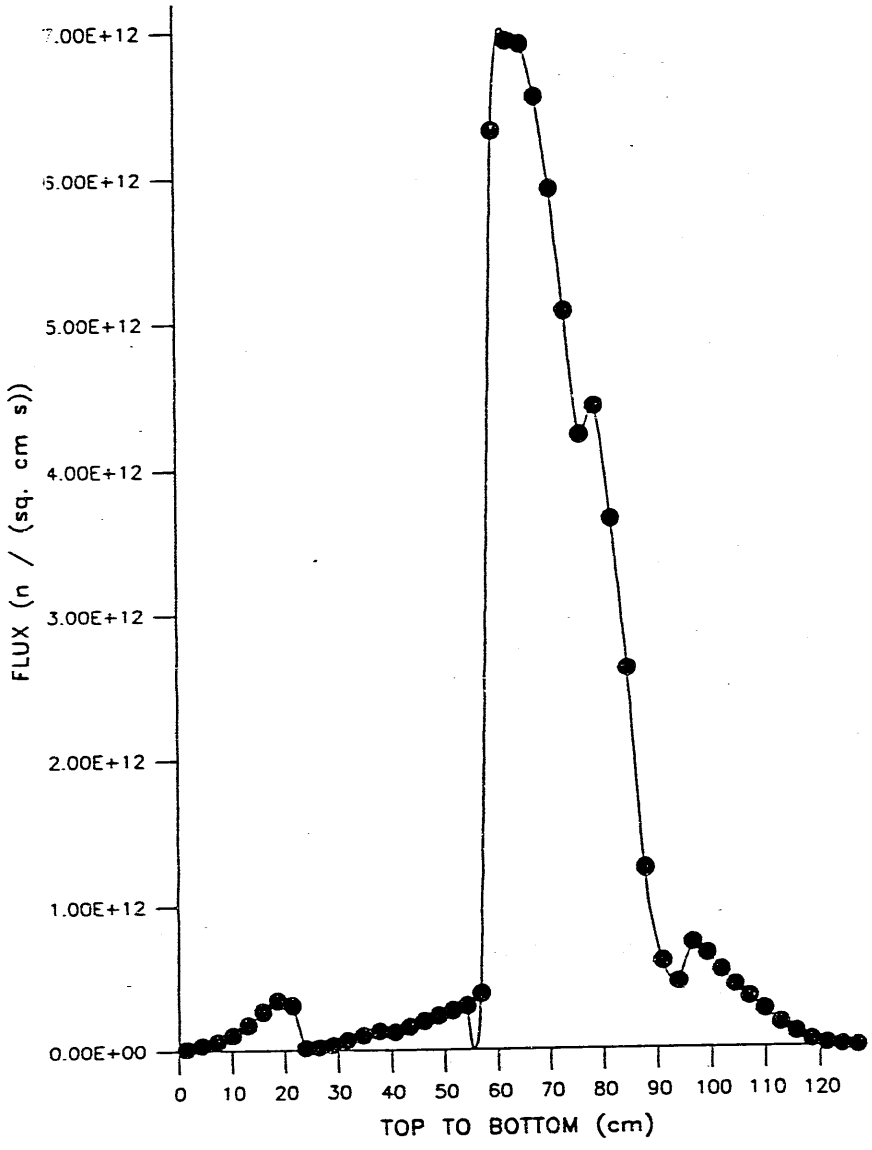

Fig. 9. Thermal Flux for 1 MW U-$ZrH_{1.6}$-Er Core Along Column 22 and Plane 21

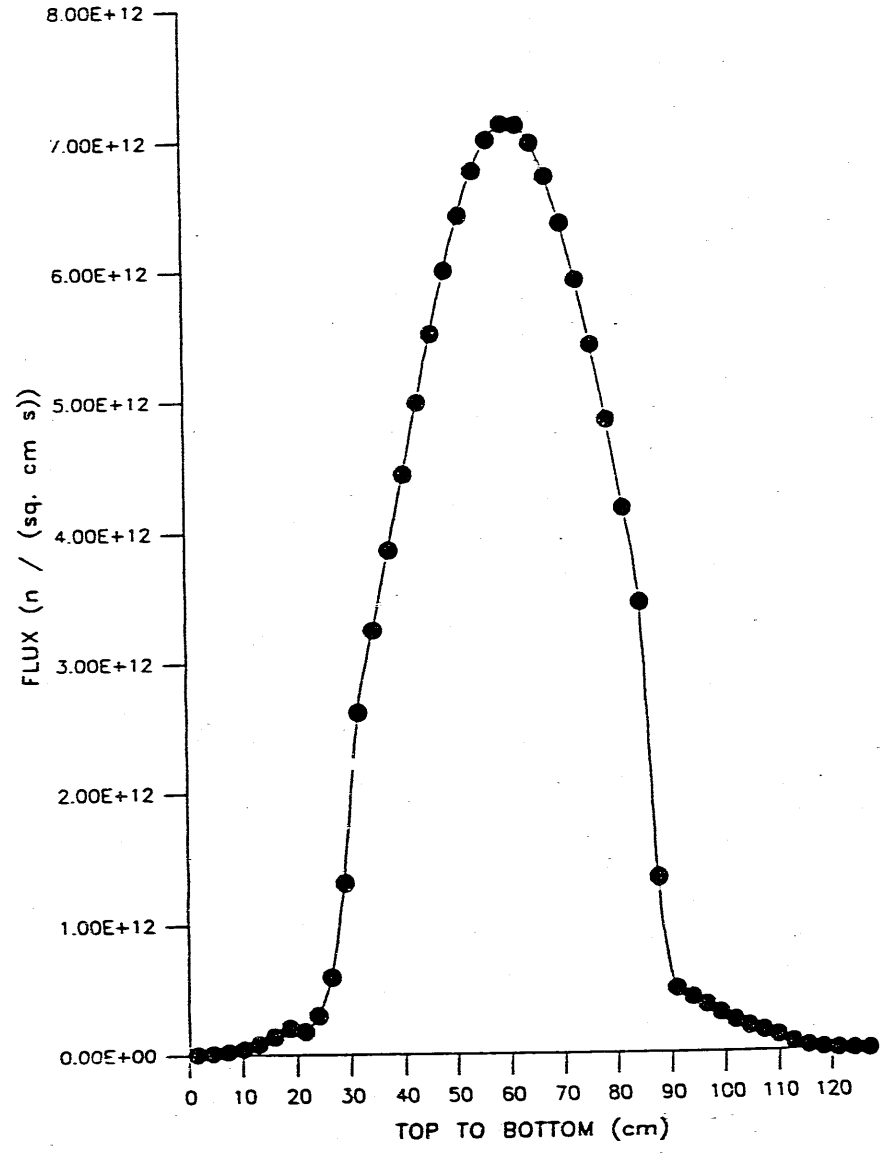

Fig. 10. Thermal Flux for 1 MW U-$ZrH_{1.6}$-Er Core Along Column 18 and Plane 10

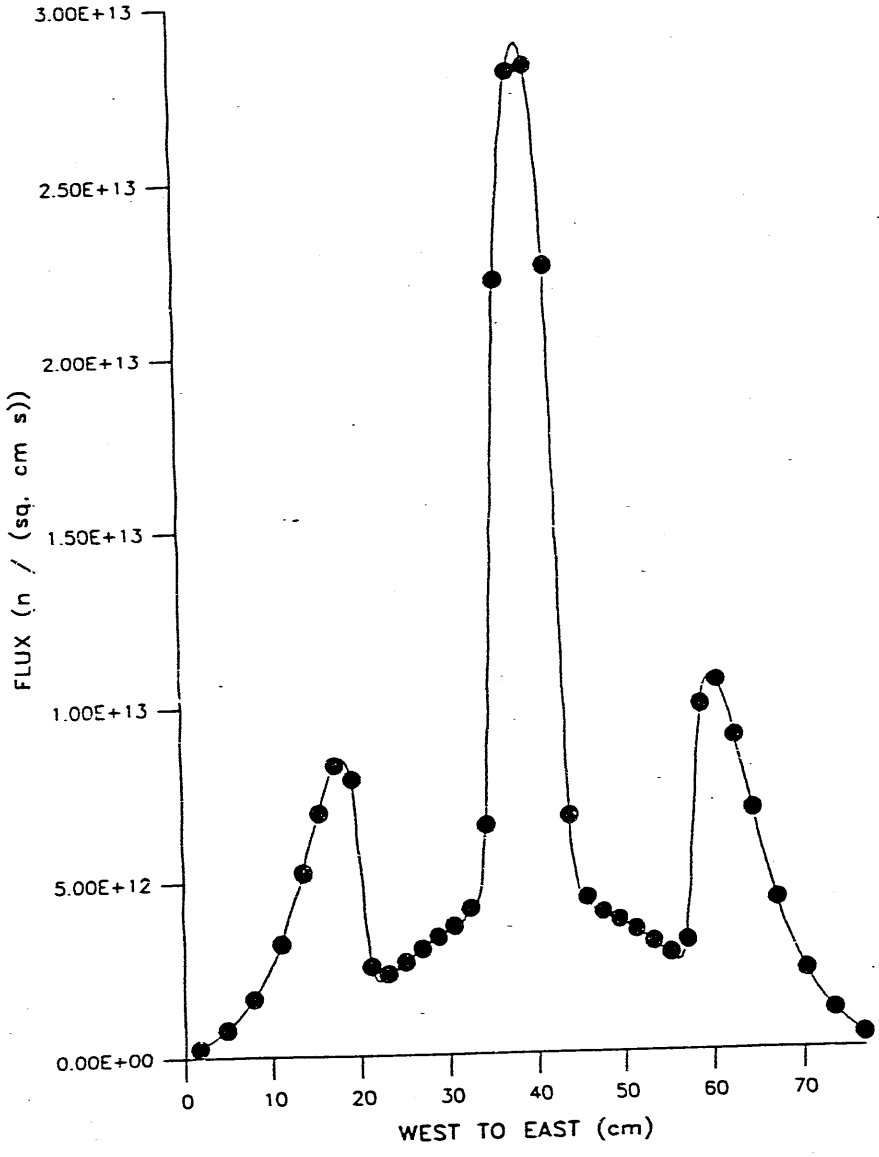

Fig. 11. Thermal Flux for 1 MW U-$ZrH_{1.6}$-Er Core Along Row 22 and Plane 15

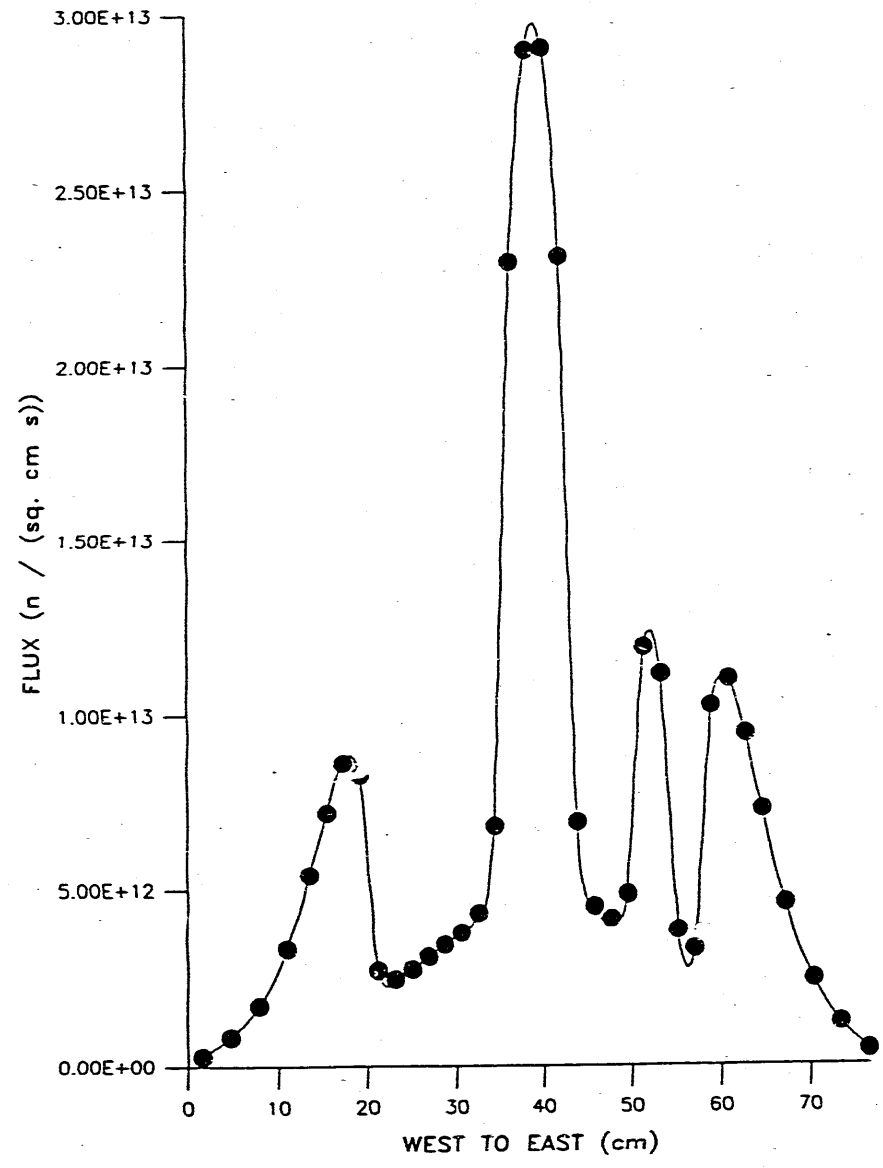

Fig. 12. Thermal Flux for 1 MW U-$ZrH_{1.6}$-Er Core Along Row 22 and Plane 31

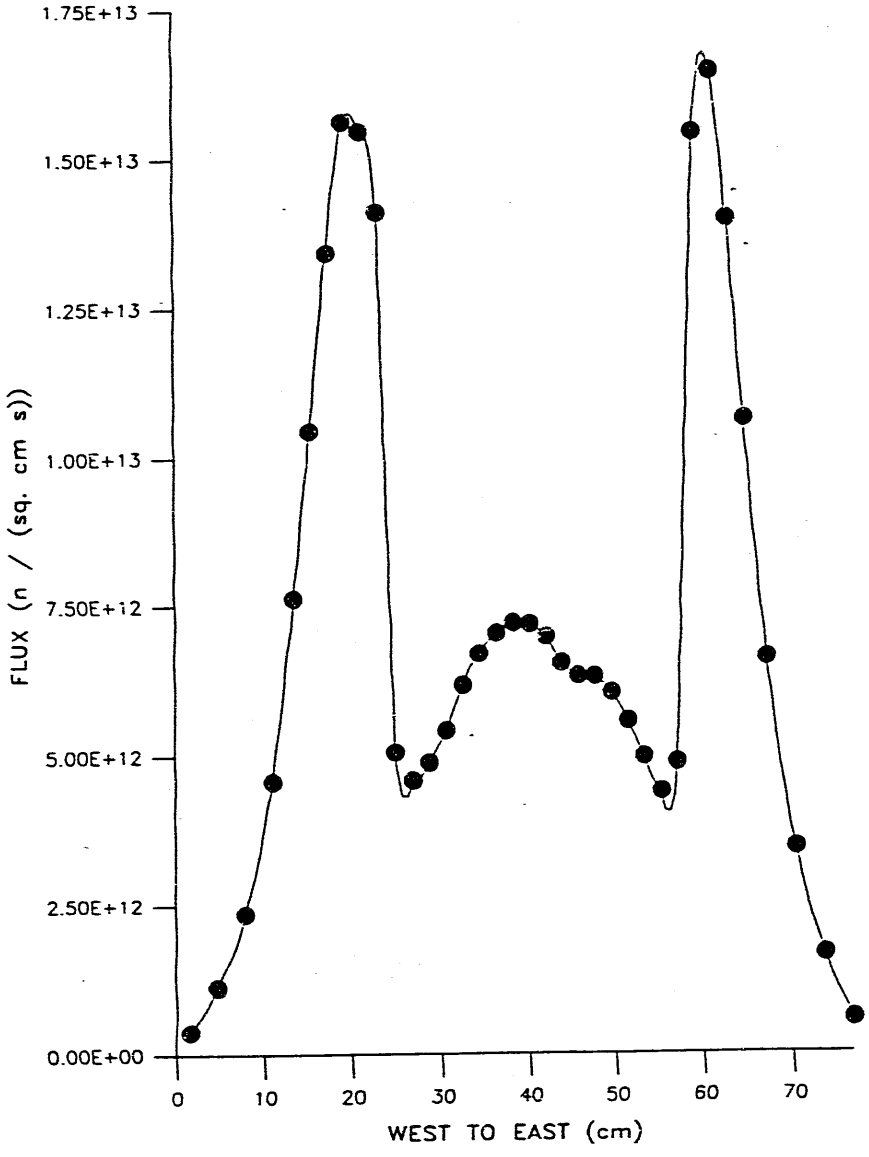

Fig. 13. Thermal Flux for 1 MW U-$ZrH_{1.6}$-Er Core Along Row 22 and Plane 21

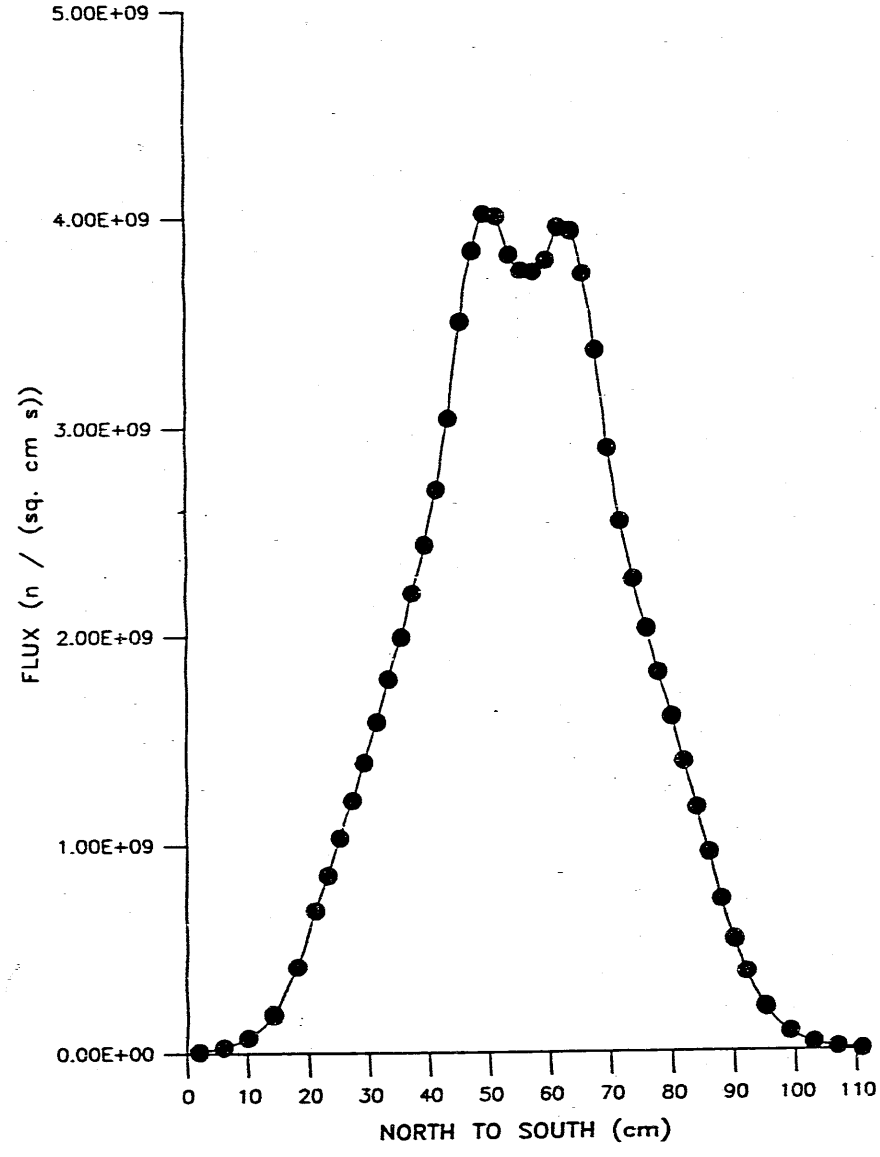

Fig. 14. Thermal Flux for 300 W U-$ZrH_{1.6}$-Er Core Along Column 7 an Row 22

The flux shapes for the U-$ZrH_{1.6}$-Er core at 300 W, seen in Figs. 14 – 24, are the same as the shapes at 1 MW. The magnitude of the flux for the 1 MW operation is uniformly greater than the magnitude of the flux for the 300 W operation by a factor of $1 \times 10^6/300$, or 3.333×10^3. The only discrepancies are slight and are due only to various inaccuracies introduced by the solution.

The results obtained for the U-$ZrH_{1.6}$-Er core were determined to be accurate enough to use the same method to model the reactor with the proposed BeO-UO_2-Er fuel. The primary concern with this fuel was whether it would be possible to have enough ^{235}U in the fuel with the imposed enrichment limit of 20 atomic percent. Since it was not anticipated that the fuel loading would be sufficient if the graphite sections of the fuel rods were retained, the graphite sections were replaced with fuel from the beginning of the analysis. During the process of making several trial loadings, the water filled elements at B4 and B6 were replaced with fuel rods to further increase the amount of ^{235}U. The water filled elements were deemed expendable. An additional increase in the total ^{235}U loading was achieved by increasing the percentage of UO_2 in the fuel. The ACRR core has 236 fuel rods with fuel that is 21.5 mass percent UO_2 and an enrichment of 35 atomic percent.[24] That mass percentage of UO_2 is not high enough for the NSCR because the enrichment is limited to 20 atomic percent and there are only 90 fuel rods when the water filled elements are replaced. Several trial runs were performed to determine the appropriate percentage of UO_2, each with increases in the value. The concern at the time was loss of structural integrity at higher temperatures if the percentage of UO_2 was too high. Although it has been

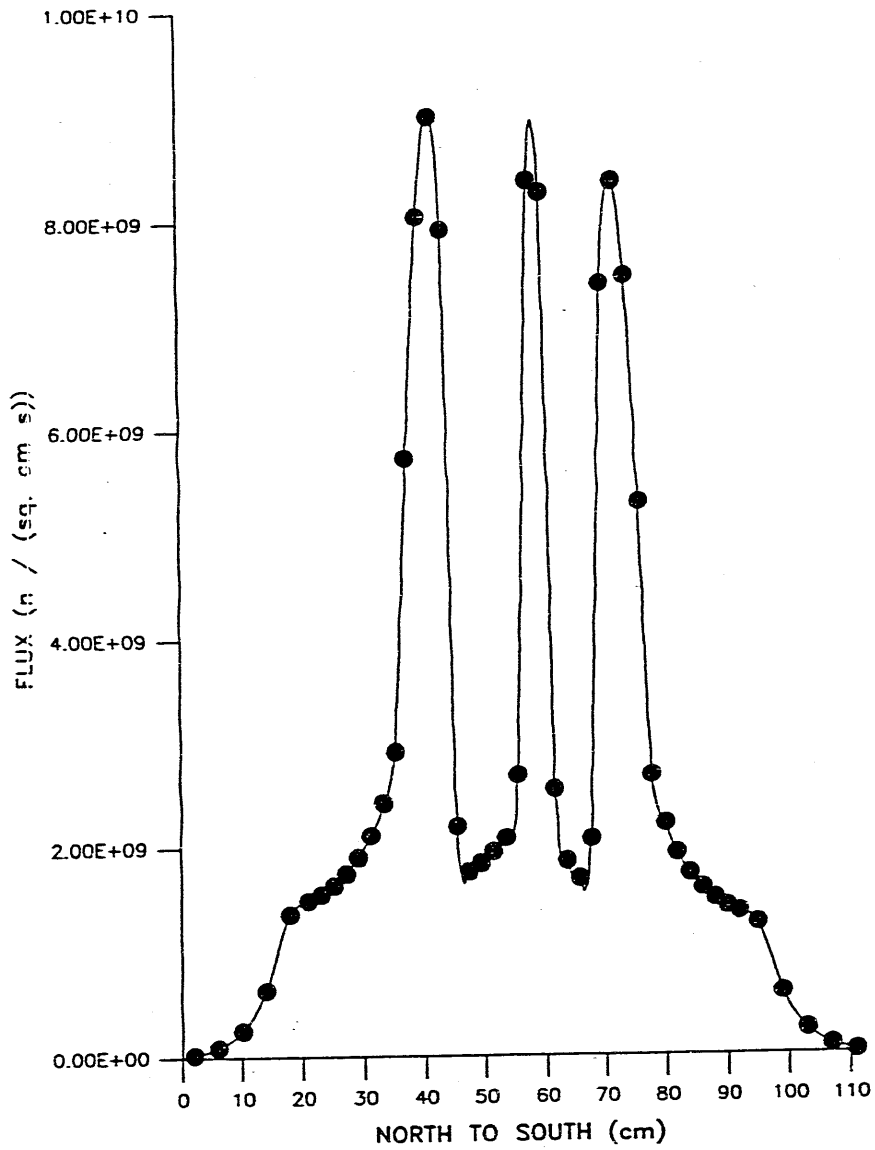

Fig. 15. Thermal Flux for 300 W U-$ZrH_{1.6}$-Er Core Along Column 18 and Row 22

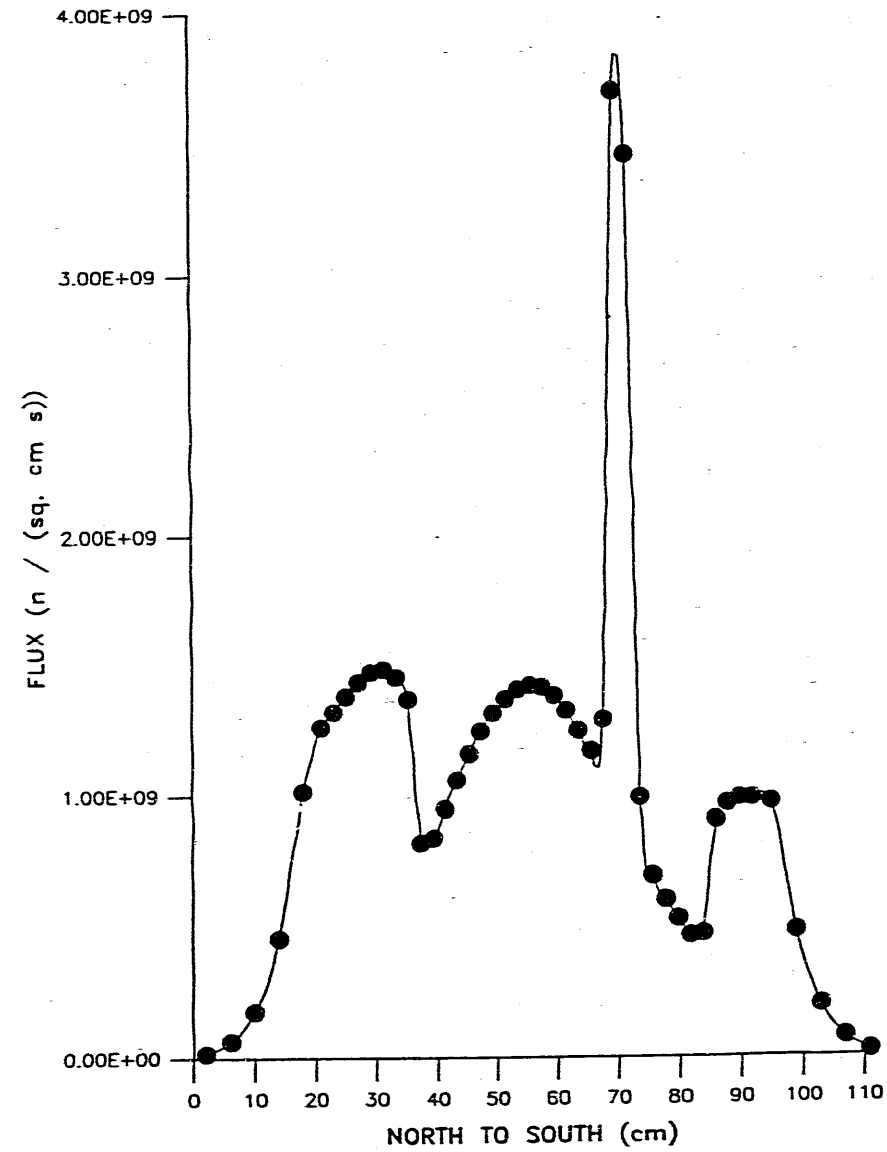

Fig. 16. Thermal Flux for 300 W U-$ZrH_{1.6}$-Er Core Along Column 26 and Row 22

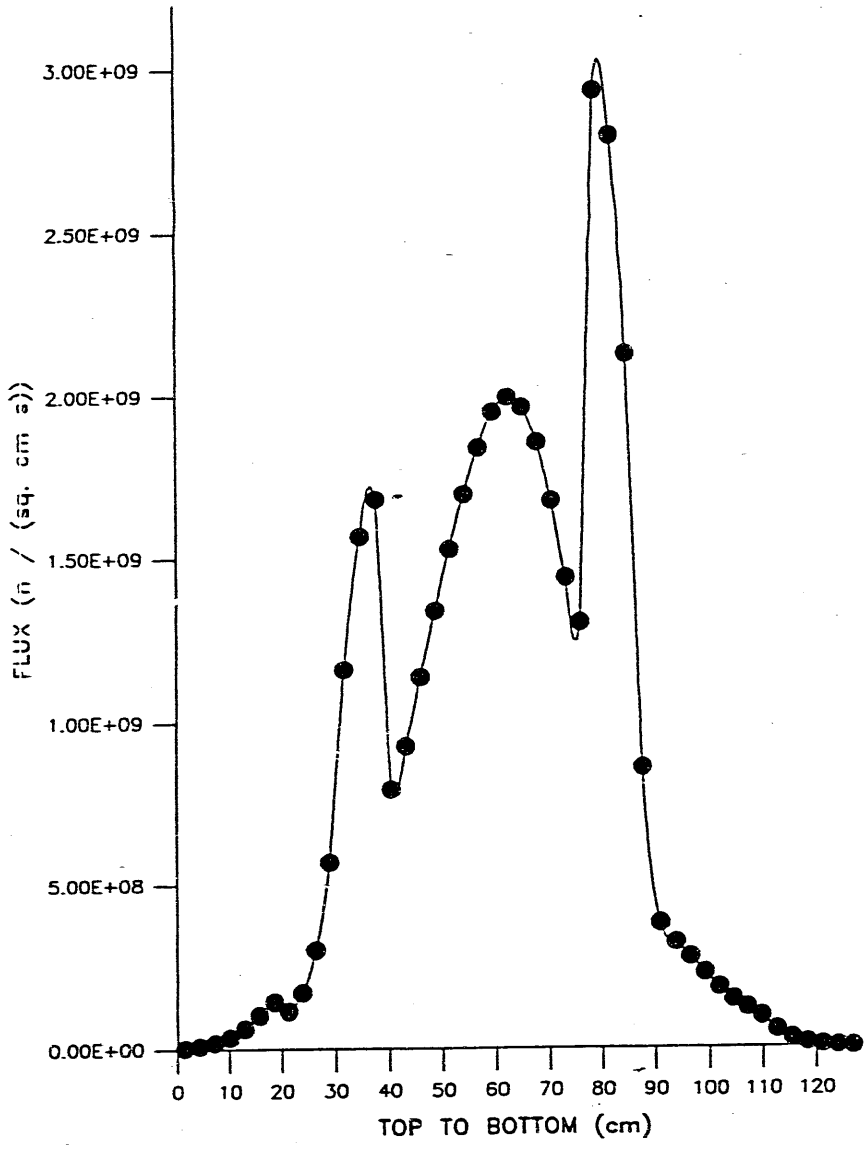

Fig. 17. Thermal Flux for 300 W U-$ZrH_{1.6}$-Er Core Along Column 18 and Plane 21

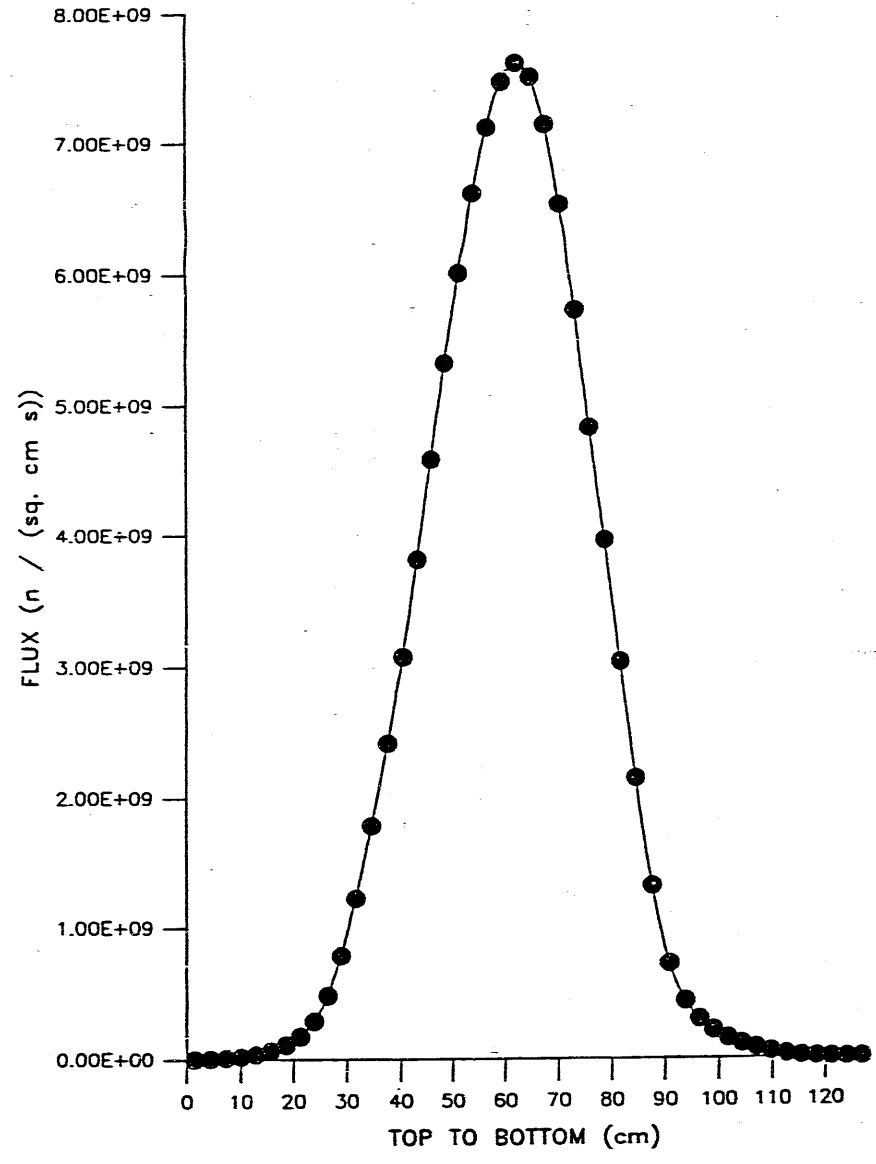

Fig. 18. Thermal Flux for 300 W U-$ZrH_{1.6}$-Er Core Along Column 18 and Plane 32

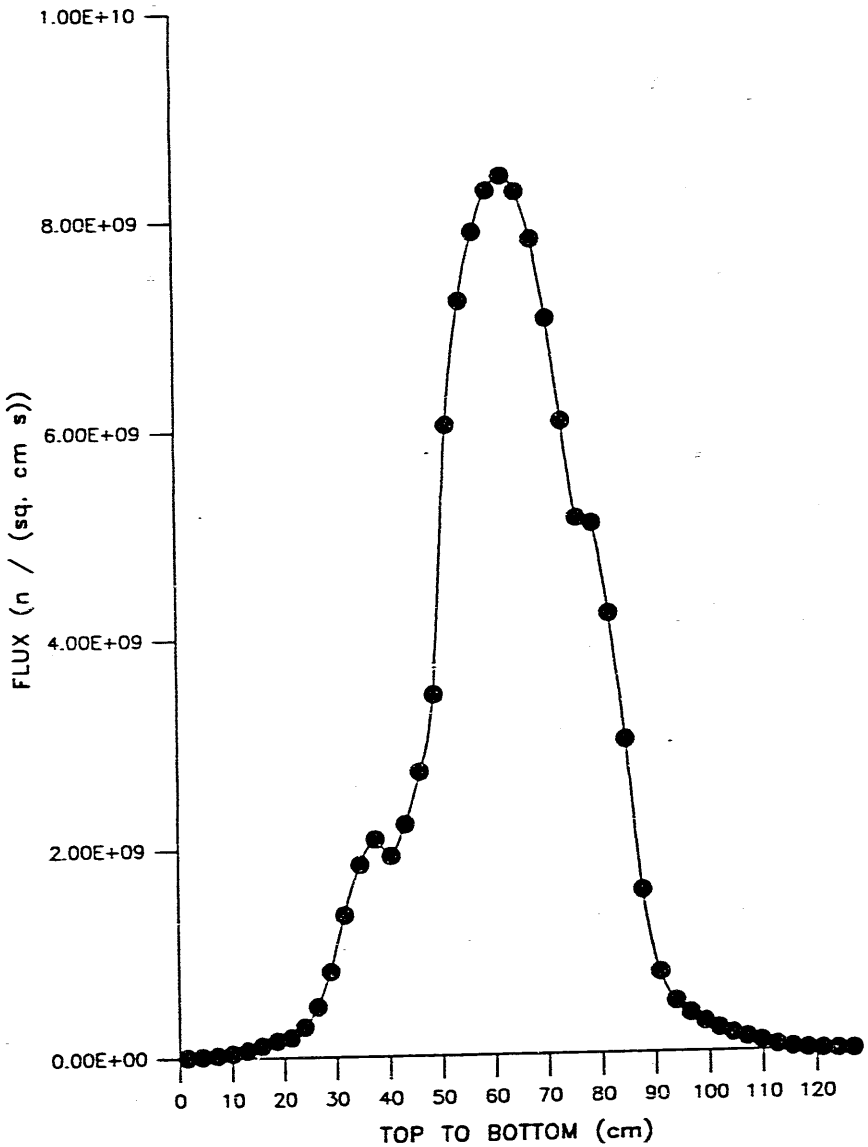

Fig. 19. Thermal Flux for 300 W U-$ZrH_{1.6}$-Er Core Along Column 18 and Plane 25

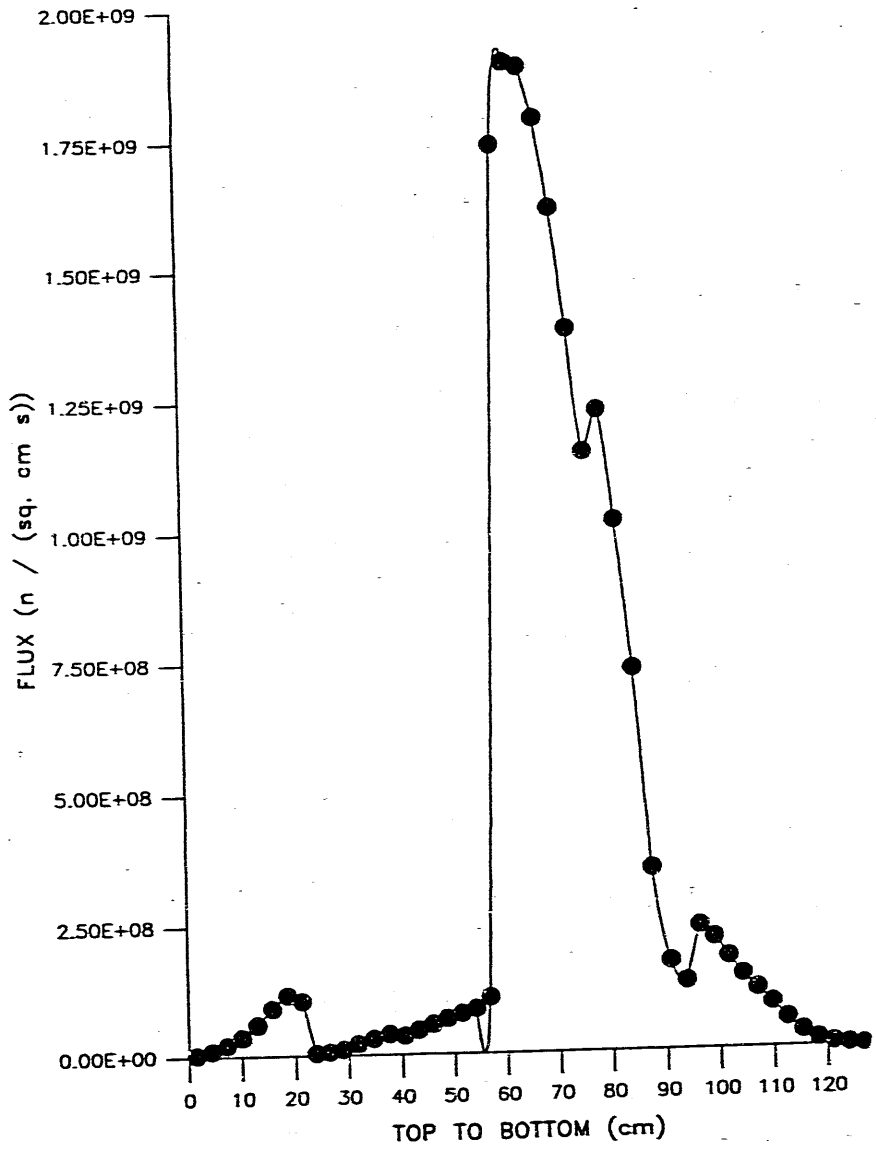

Fig. 20. Thermal Flux for 300 W U-$ZrH_{1.6}$-Er Core Along Column 22 Plane 21

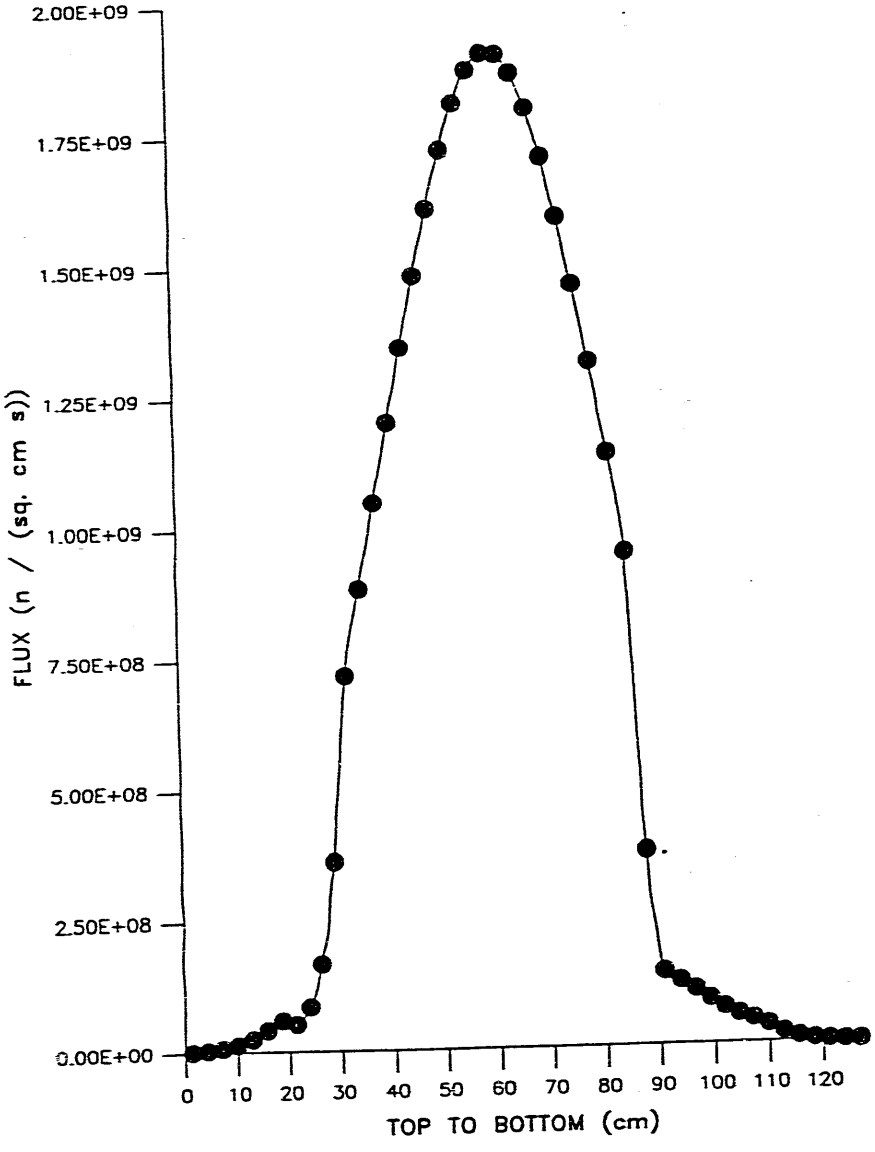

Fig. 21. Thermal Flux for 300 W U-$ZrH_{1.6}$-Er Core Along Column 18 and Plane 10

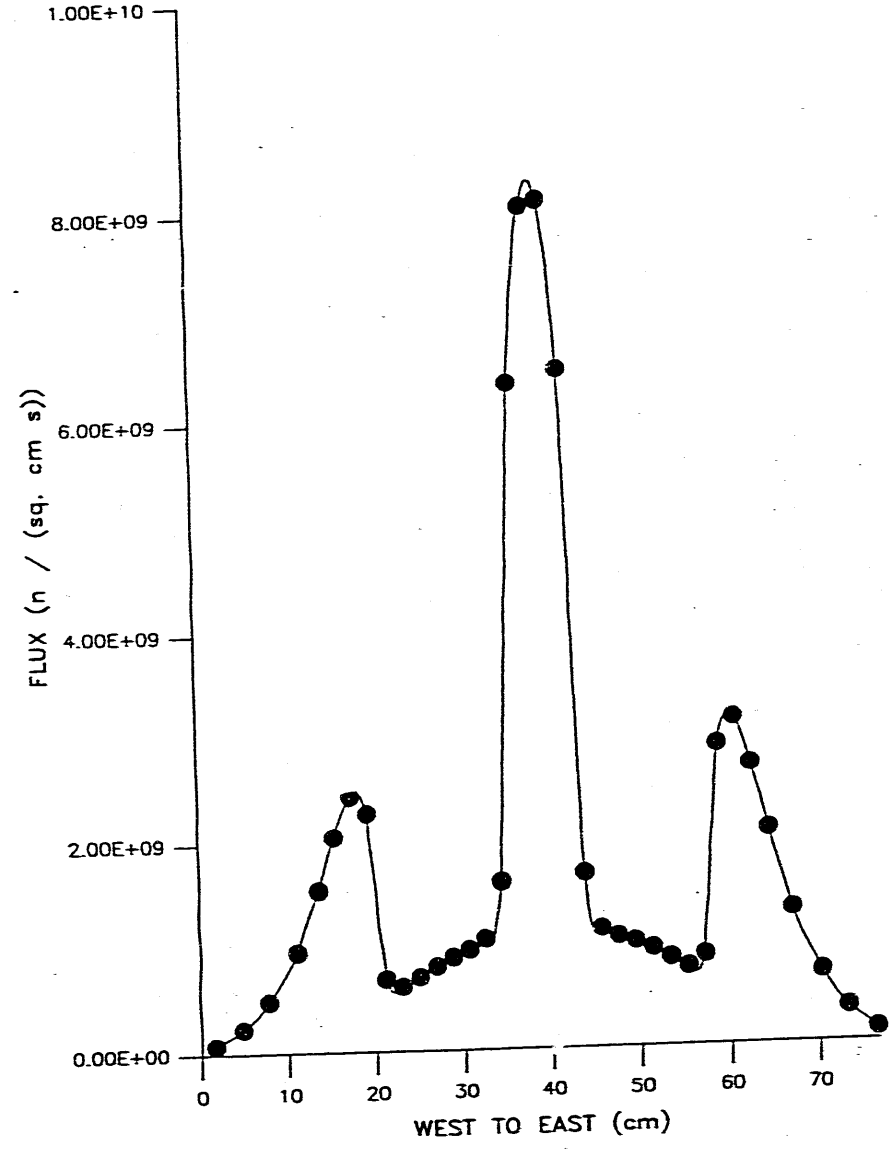

Fig. 22. Thermal Flux for 300 W U-$ZrH_{1.6}$-Er Core Along Row 22 and Plane 15

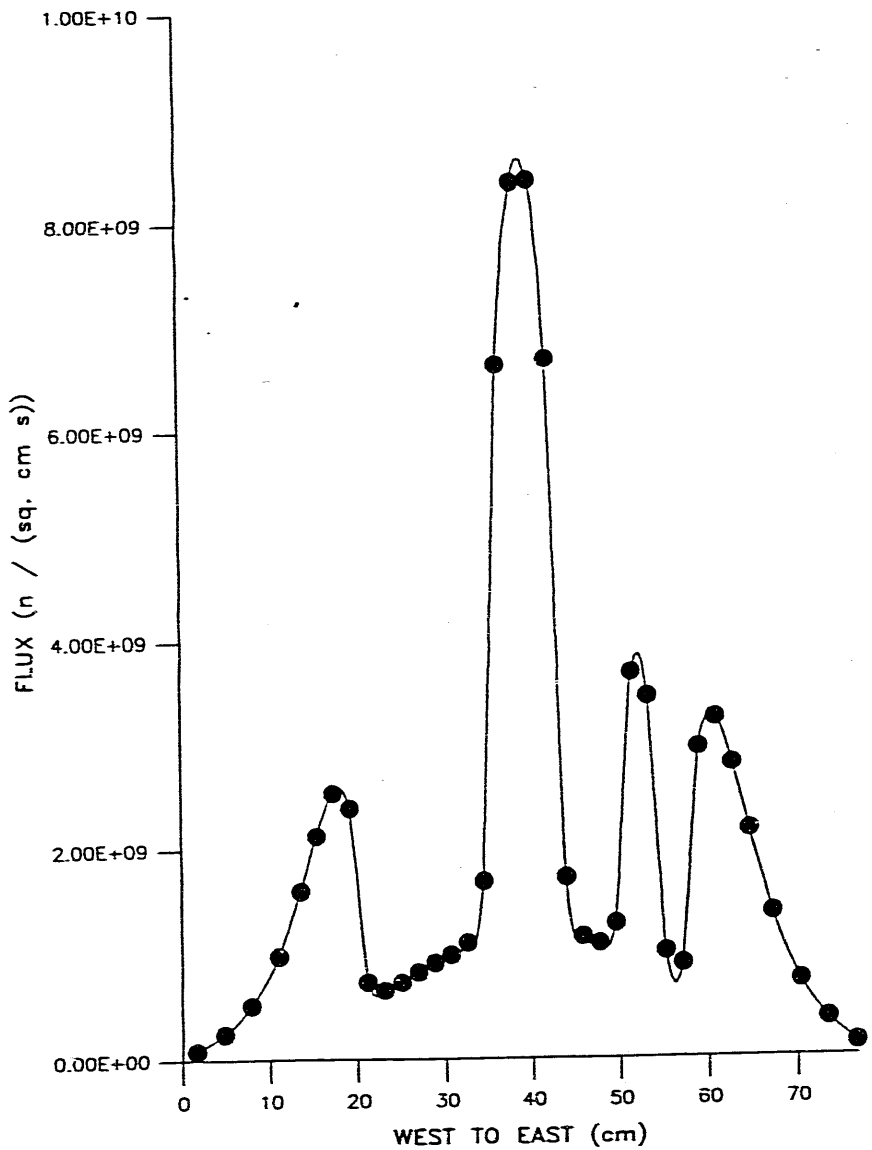

Fig. 23. Thermal Flux for 300 W U-$ZrH_{1.6}$-Er Core Along Row 22 and Plane 31

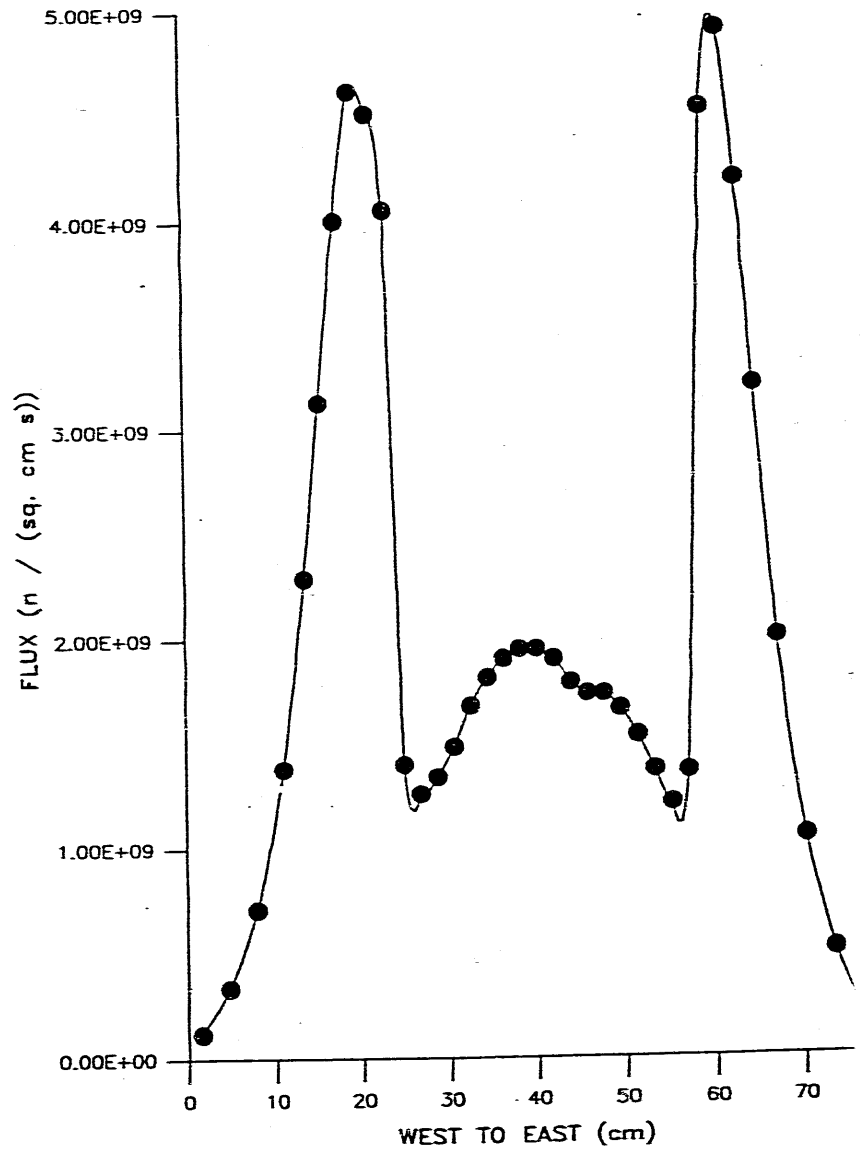

Fig. 24. Thermal Flux for 300 W U-$ZrH_{1.6}$-Er Core Along Row 22 and Plane 2

learned since these runs that as much as 80 mass percent (52.35 volume percent) of UO_2 within the BeO-UO_2 is possible, 55.32 mass percent (25.38 volume percent) of UO_2 within the BeO-UO_2 was determined to be sufficient for operation.[28] The k_{eff} values at both 300 W and 2 MW for this model are presented in Table 9. These k_{eff} values are lower than those for the U-$ZrH_{1.6}$-Er core, meaning that the excess reactivity would be lower and the fuel lifetime would be shorter. Increasing the percentage of UO_2 in the fuel closer to the 80 mass percent figure would improve the fuel lifetime.

To be sure that the BeO-UO_2-Er fuel would give a desirable flux profile, a set of flux curves for each power level was produced using the same directions through the core as the U-$ZrH_{1.6}$-Er flux curves. The shapes of the curves through the same locations are similar to those for the U-$ZrH_{1.6}$-Er fuel. Fig. 25, the profile along the west side of the 2 MW BeO-UO_2-Er core, shows the smooth cosine-shaped flux that would be obtained after removing the water filled elements from B4 and B6. The curve shown in Fig. 3 has separate peaks for each pair of water filled elements. The mid fuel height horizontal flux profile across the water notches and the transient rod's channel presented in Fig. 26 matches the flux profile shown in Fig. 4 except for the heights of the peaks. There is also a resemblance between Figs. 27 and 5, the north to south profiles that pass through the regulating rod.

Fig. 28, which shows a vertical profile through a fuel rod cell in a 2 MW core, is quite similar to Fig. 6 except for a few differences that are due mostly to the replacement of the graphite sections by more fuel. The cosine shaped curve is wider in

Table 9. Multiplication Factors for 300 W and 2 MW BeO-UO_2-Er Core Models with Different Control Rod Positions

	Control Rod Position		
Power	Out	Half-Way	In
300 W	1.045	1.002	0.911
2 MW	1.040	0.998	0.907

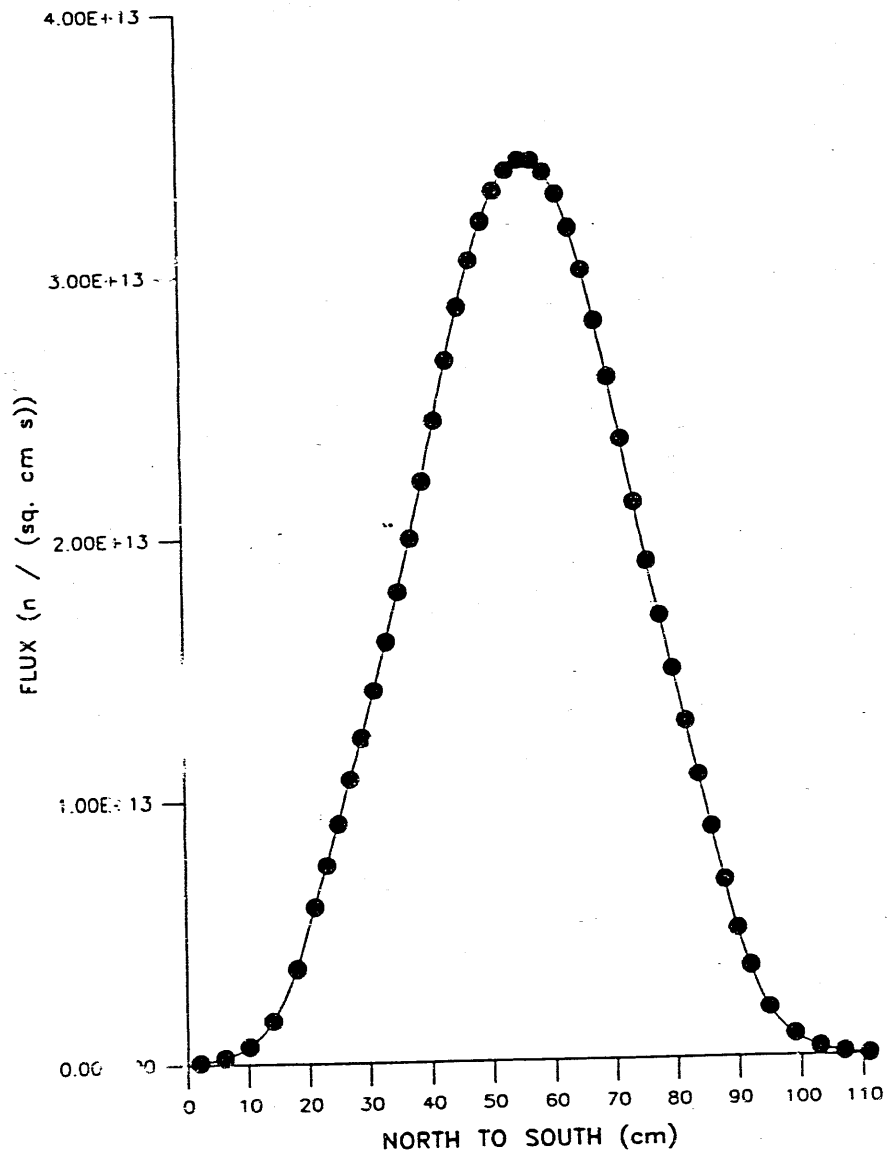

Fig. 25. Thermal Flux for 2 MW BeO-UO_2-Er Core Along Column 7 and Row 22

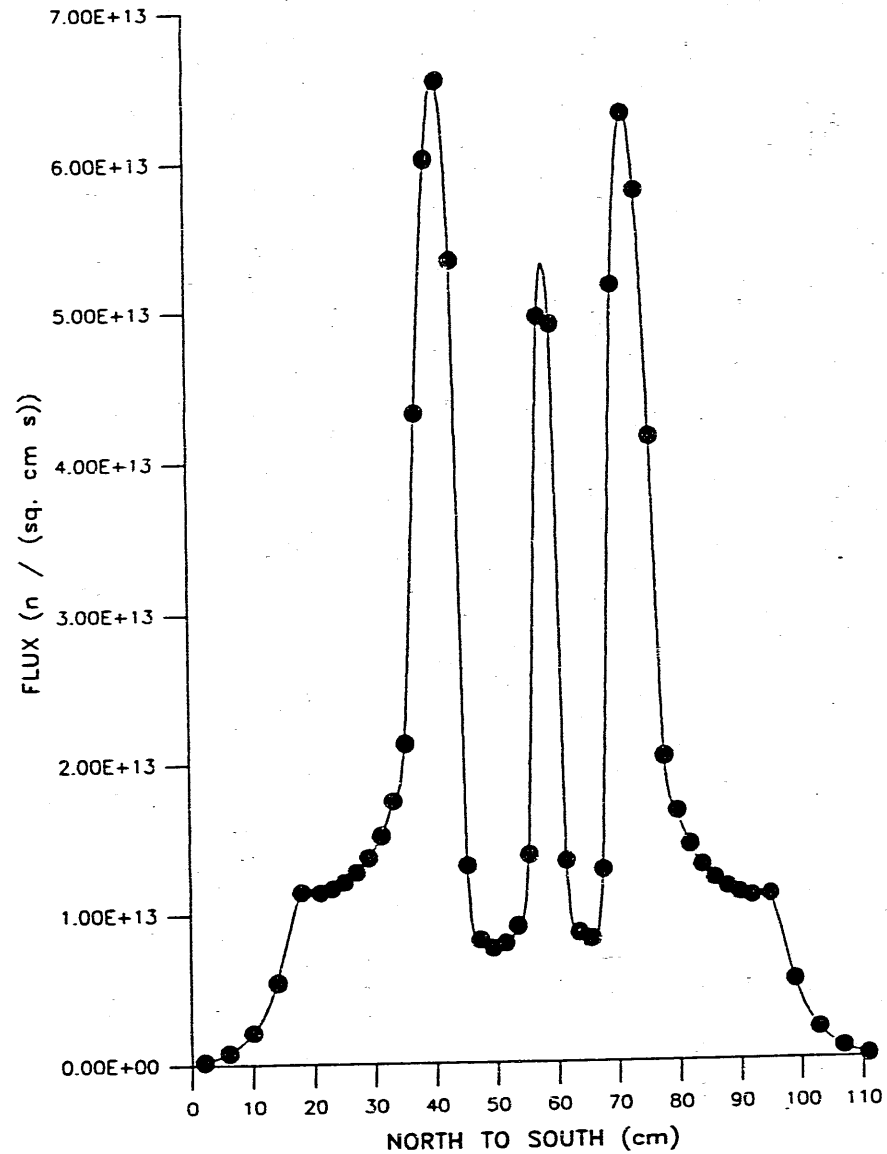

Fig. 26. Thermal Flux for 2 MW BeO-UO_2-Er Core Along Column 18 and Row 22

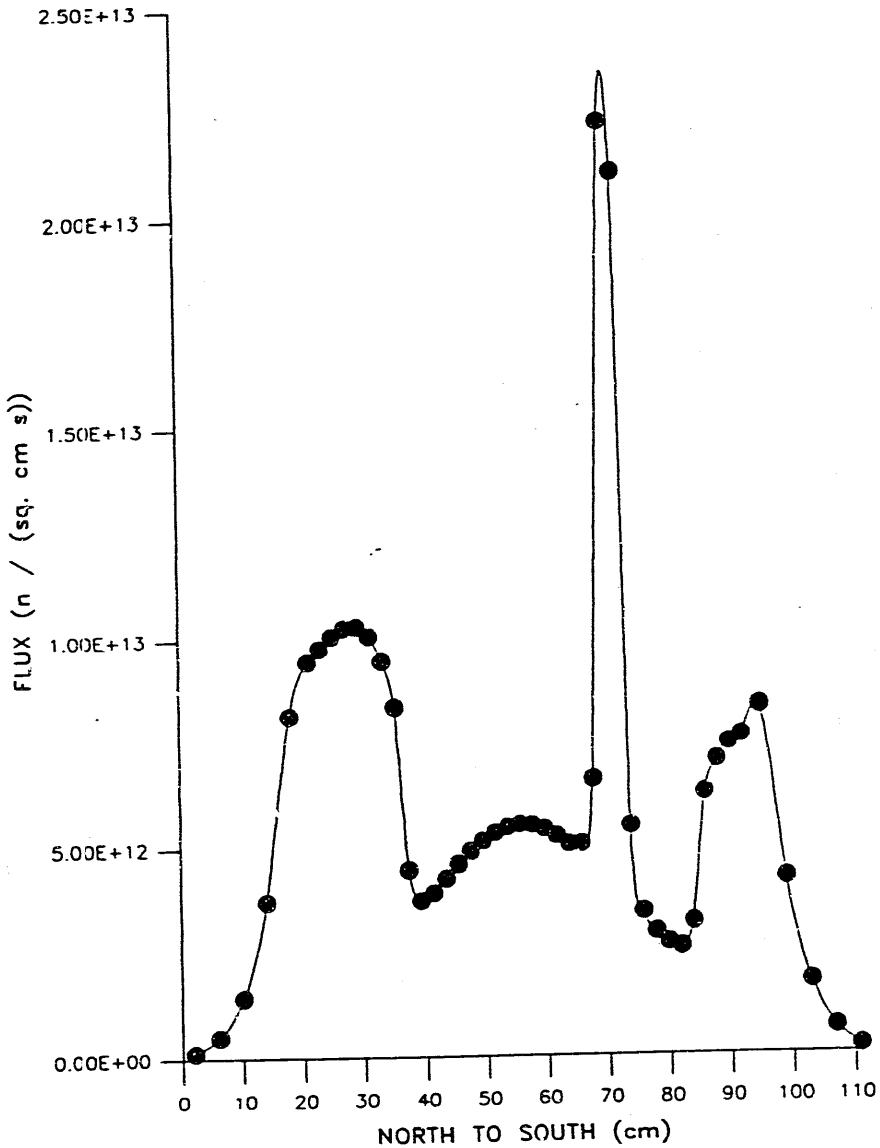

Fig. 27. Thermal Flux for 2 MW BeO-UO_2-Er Core Along Column 26 and Row 22

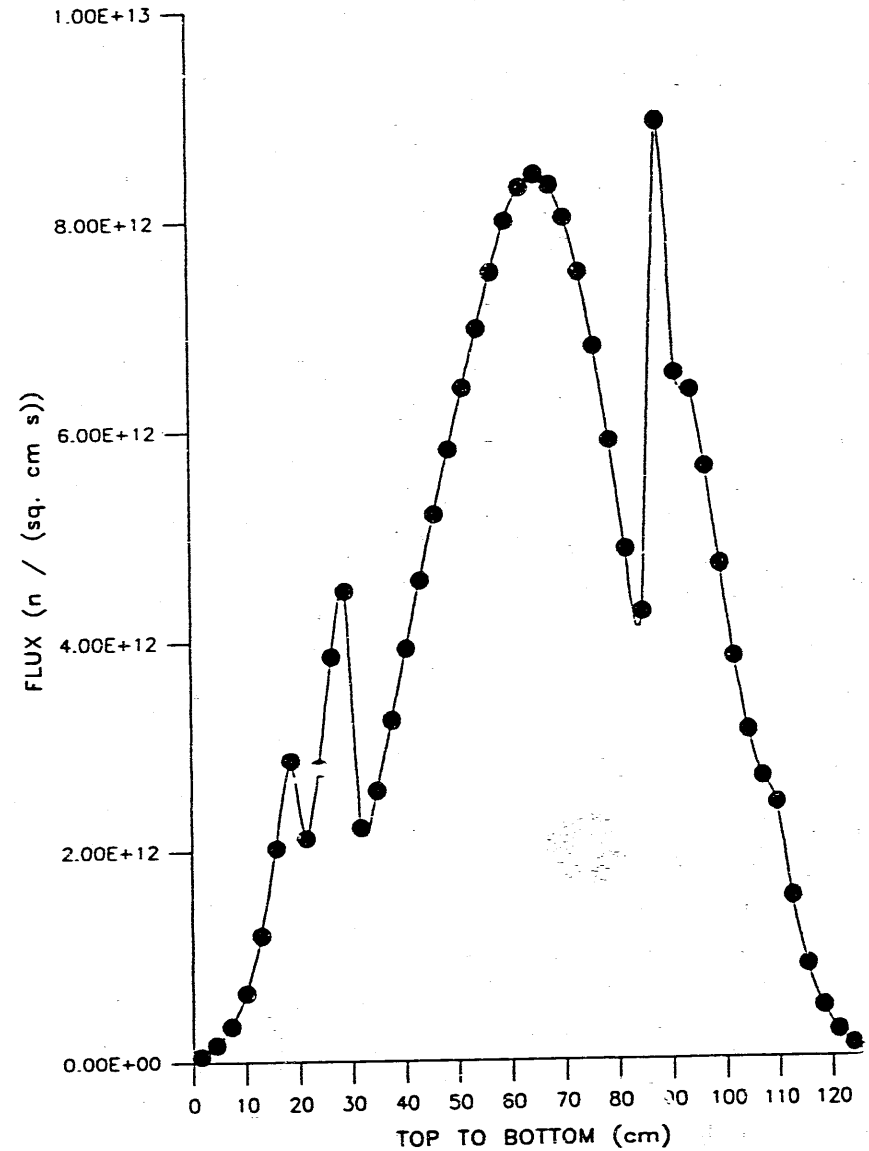

Fig. 28. Thermal Flux for 2 MW BeO-UO_2-Er Core Along Column 18 ar Plane 21

Fig. 28 since there is more fuel. The immediately surrounding peaks represent thermal flux increases in homogeneous water and structural regions rather than graphite. The flux increase in the water region at the top of the core is more pronounced due to the lack of the graphite as a reflector. The inflections below the core at the boundaries of the various water and structural regions are also more pronounced. The shape of the flux profile though the water notch at D3 shown in Fig. 29 matches that shown in Fig. 7. The inflections shown in the transient rod's channel in Fig. 30 are at the upper boundary between the water and the structural region and the lower boundary between the fuel and the structural region in nearby fuel rod cells. Fig. 31 shows the flux profile through the shim safety rod cell at E6. The first peak seen at approximately 5 cm represents the boundary above the borated graphite section of the shim safety rod. The dominant peak is similar to the one seen in Fig. 9. The peak at approximately 86 cm is due to lower boundary of the fuel sections of the fuel rods. The peak at 114 cm is due to the lower boundary of the fuel section of the shim safety rod. The shape of the flux curve shown in Fig. 32 is essentially the same at that shown in Fig. 10, both of which represent vertical flux profiles through the northern graphite block. The inflections in the curve represent boundaries between water, structural, and fuel regions.

Fig. 33, which shows the flux profile from east to west through the northern water notch at mid fuel height, has the same basic shape shown in Fig. 11. Only the flux magnitudes are different. In Fig. 34, which shows the flux profile through the other water notch and under the regulating rod, the same peaks exhibited in Fig. 12

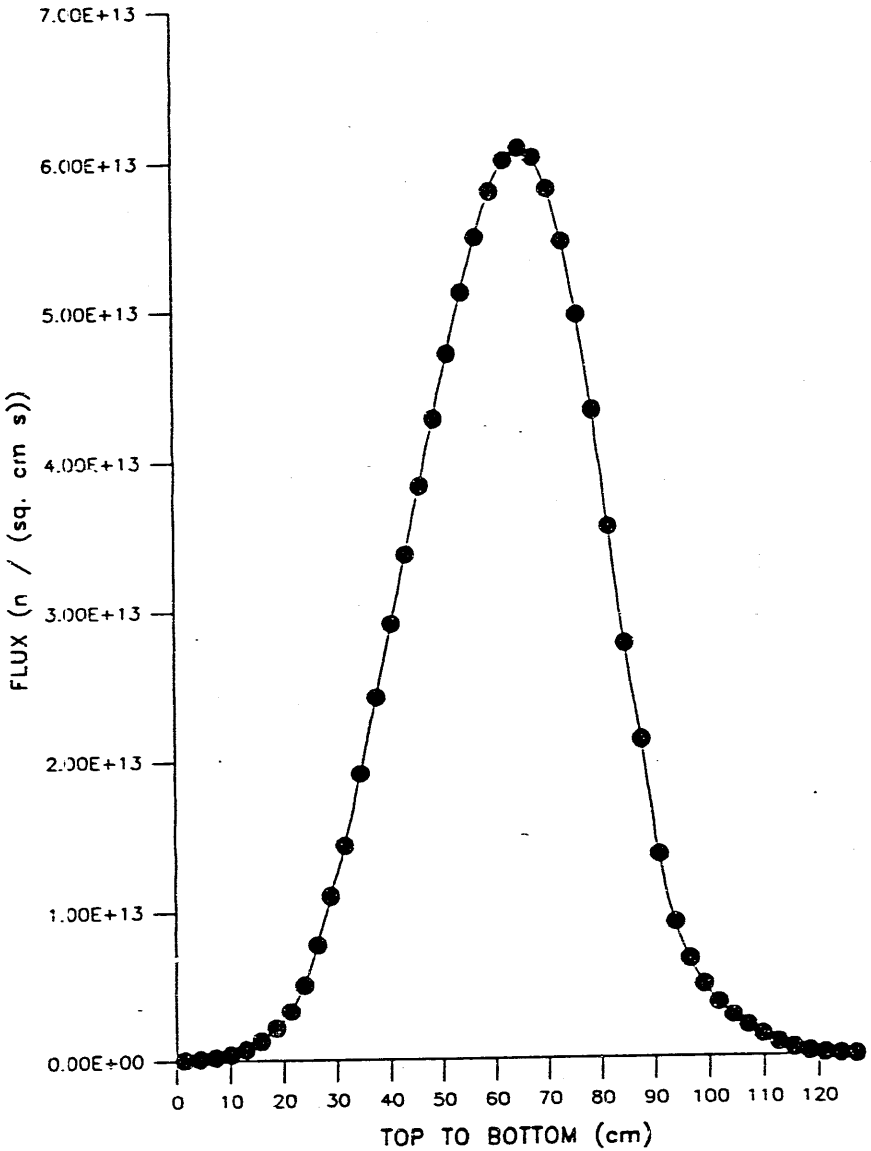

Fig. 29. Thermal Flux for 2 MW BeO-UO_2-Er Core Along Column 18 and Plane 32

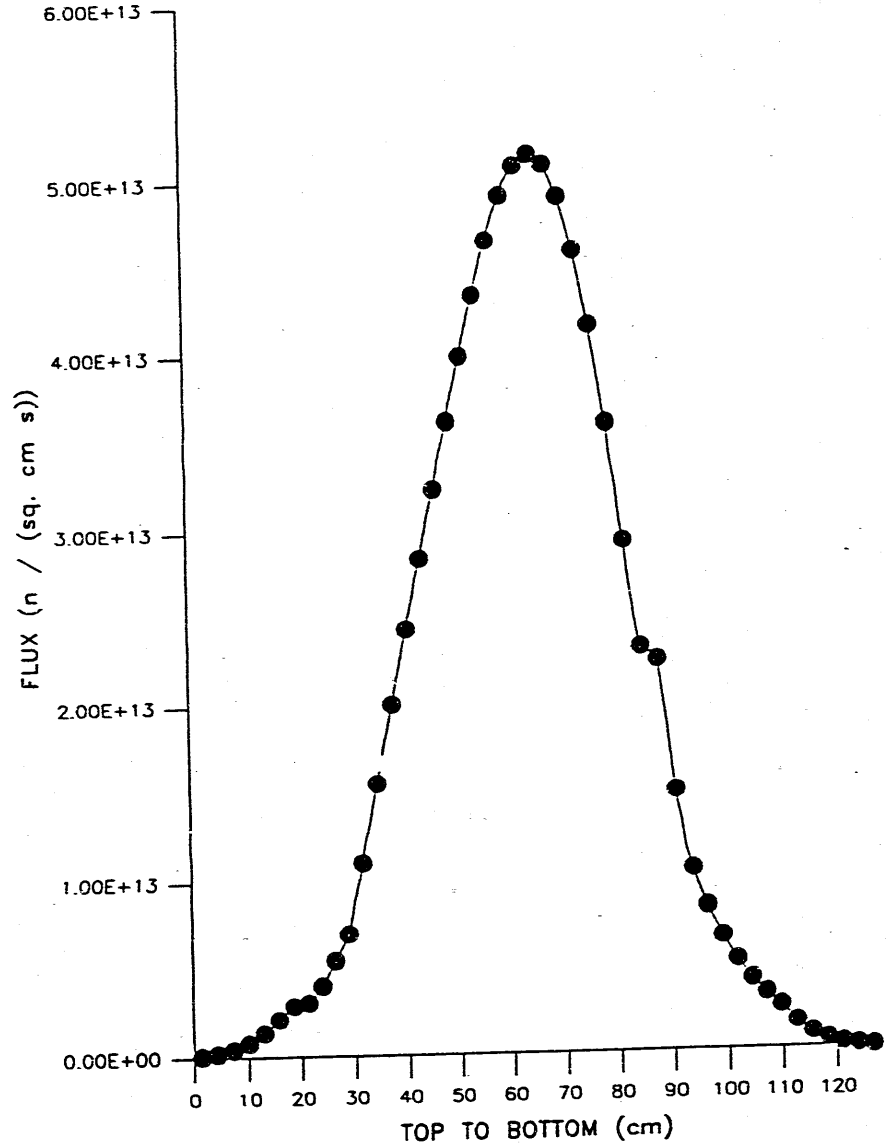

Fig. 30. Thermal Flux for 2 MW BeO-UO_2-Er Core Along Column 18 and Plane 25

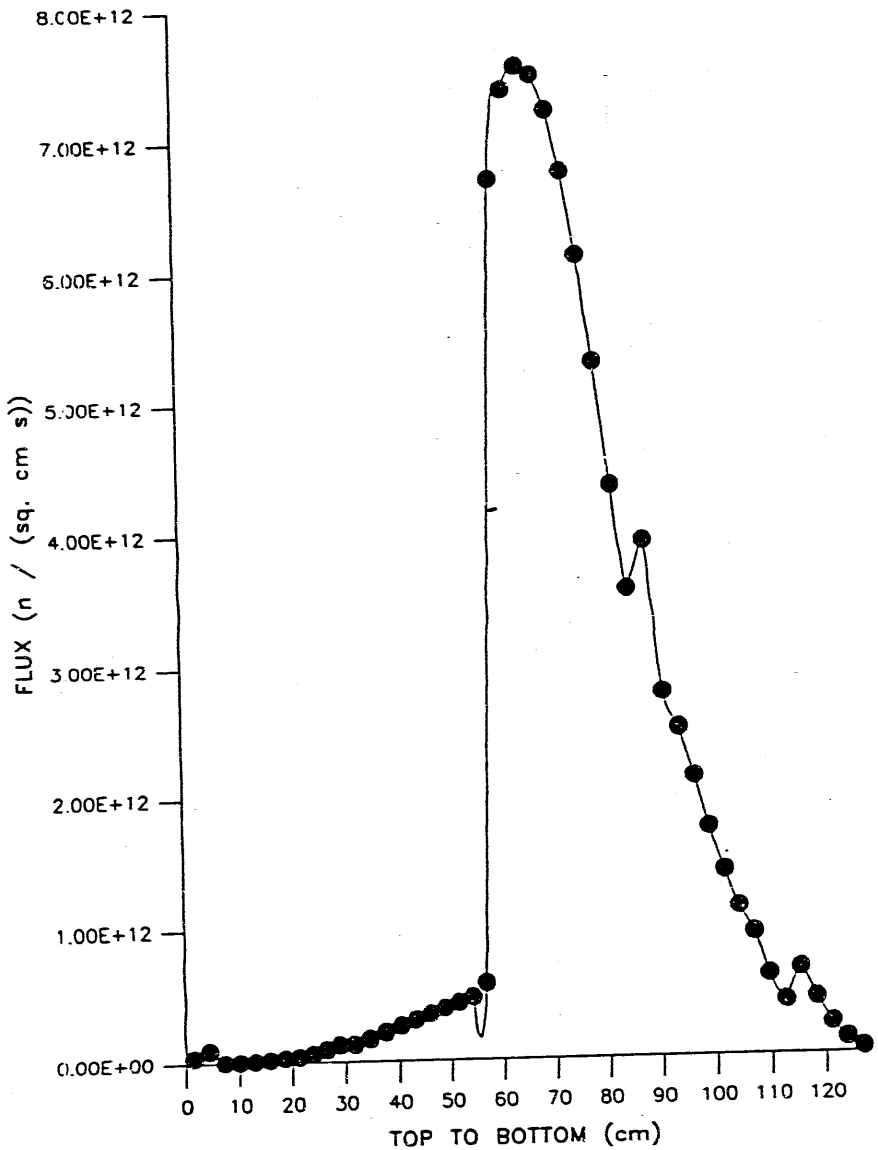

Fig. 31. Thermal Flux for 2 MW BeO-UO_2-Er Core Along Column 22 and Plane 21

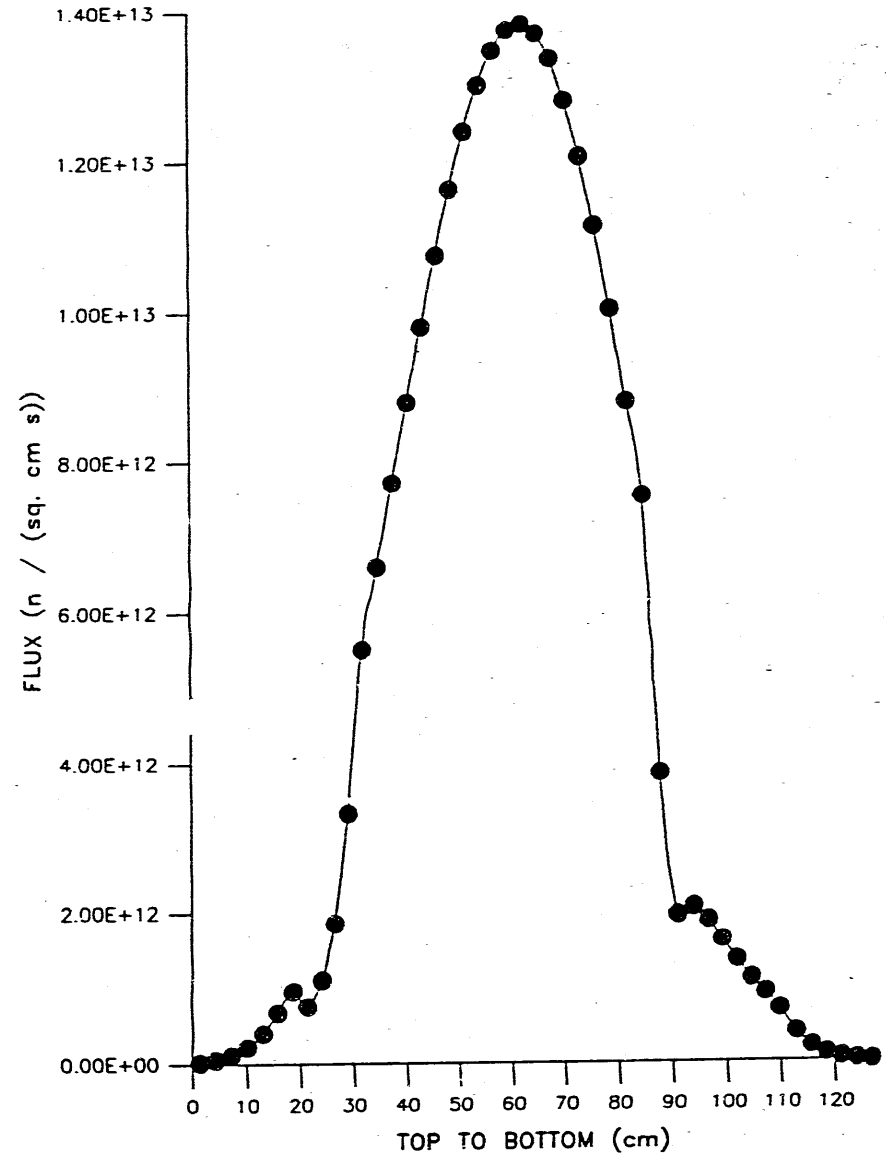

Fig. 32. Thermal Flux for 2 MW BeO-UO_2-Er Core Along Column 18 and Plane 10

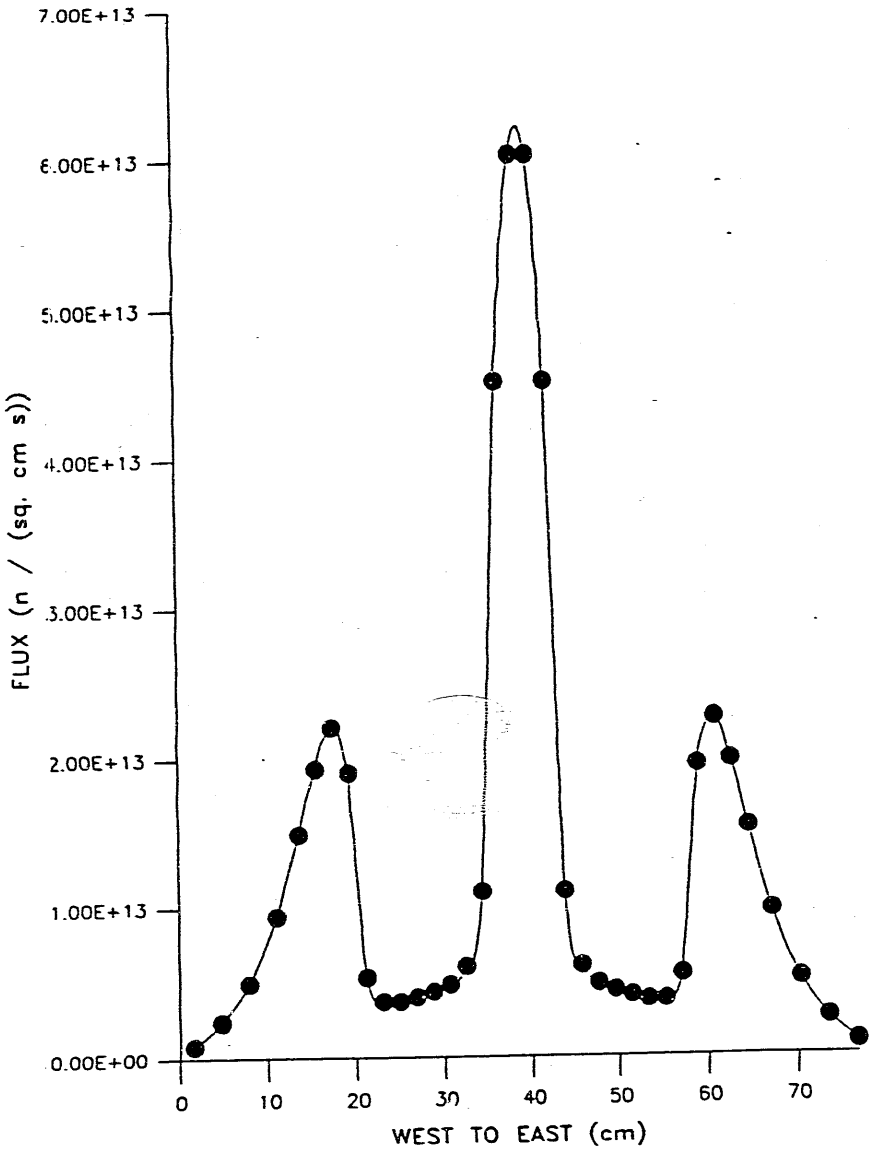

Fig. 33. Thermal Flux for 2 MW BeO-UO_2-Er Core Along Row 22 and Plane 15

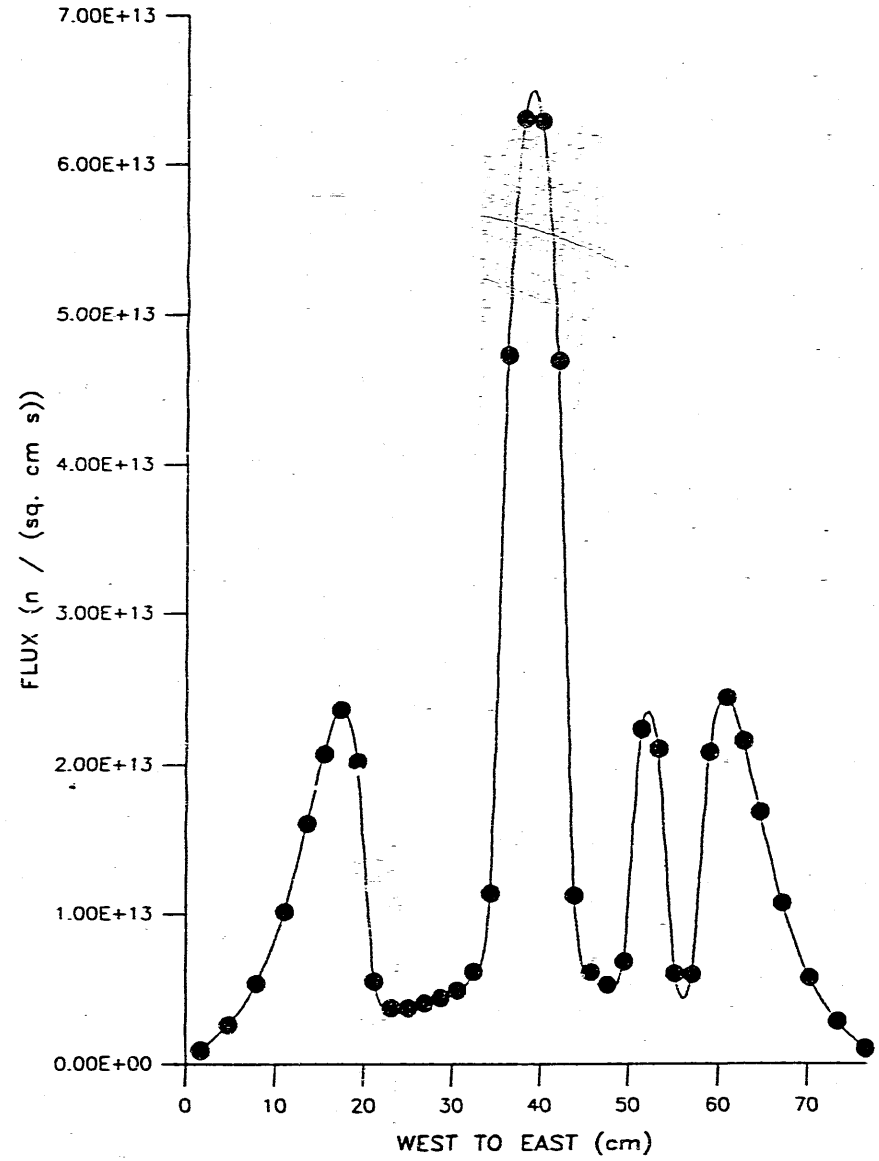

Fig. 34. Thermal Flux for 2 MW BeO-UO_2-Er Core Along Row 22 and Plane 31

are shown. The west-to-east profile through the shim safety rods at C6 and E6 shown in Fig. 35 resembles the profile shown in Fig. 13.

The flux profiles shown in Figs. 36 – 46 match the shapes of the profiles shown in Figs. 25 – 35. The only difference is the magnitudes, which are higher for the 2 MW core by a factor of $2 \times 10^6/300$ or 6.667×10^3. A comparison of these curves with Figs. 14 – 24 shows that thermal fluxes in water regions are usually higher for the BeO-UO_2-Er core at 300 W than for the U-$ZrH_{1.6}$-Er core at the same power level.

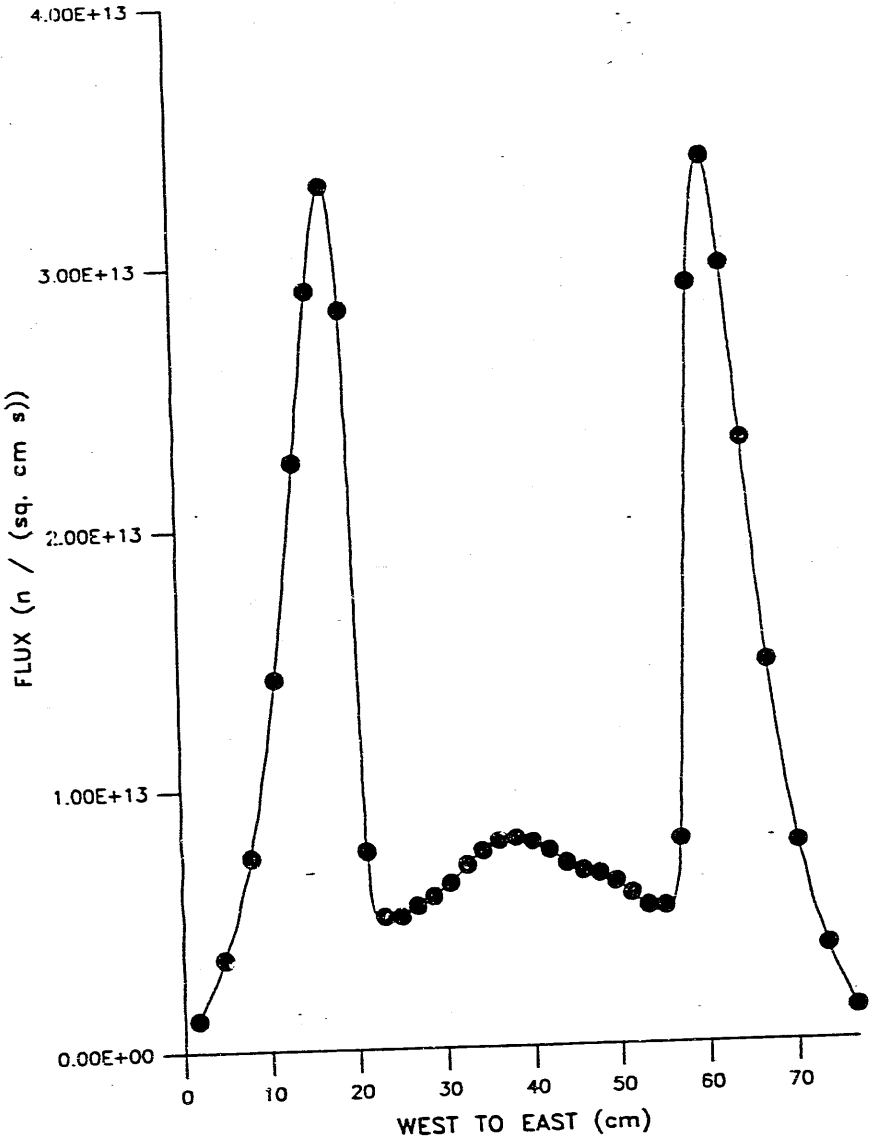

Fig. 35. Thermal Flux for 2 MW BeO-UO_2-Er Core Along Row 22 and Plane 21

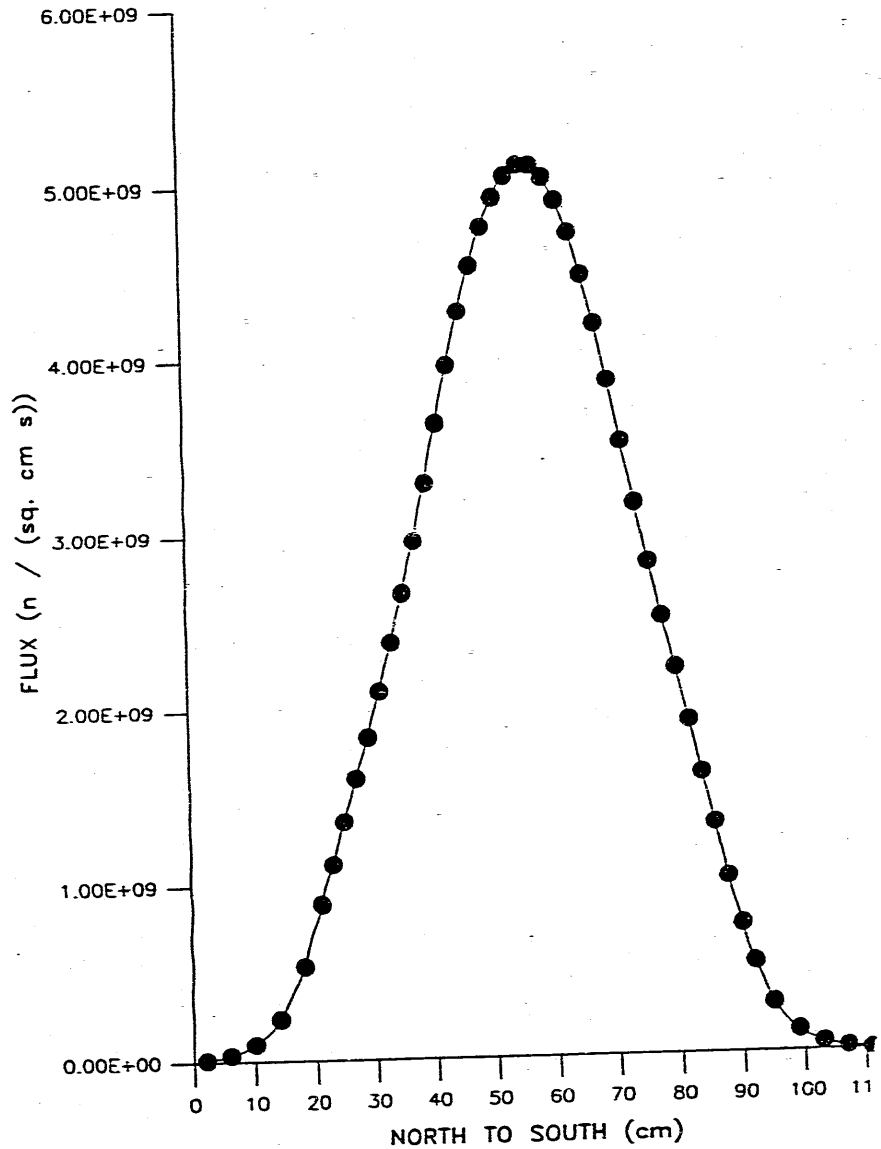

Fig. 36. Thermal Flux for 300 W BeO-UO_2-Er Core Along Column 7 and Row 22

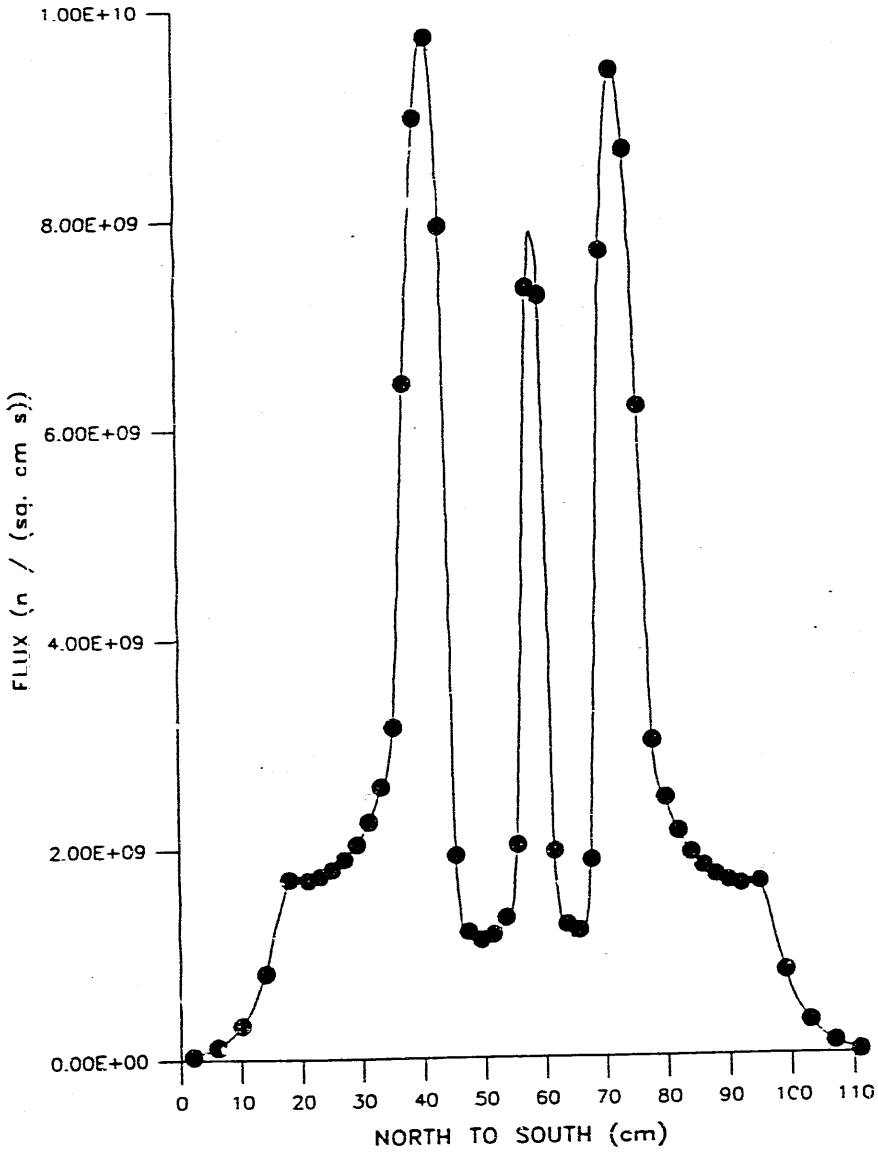

Fig. 37. Thermal Flux for 300 W BeO-UO_2-Er Core Along Column 18 and Row 22

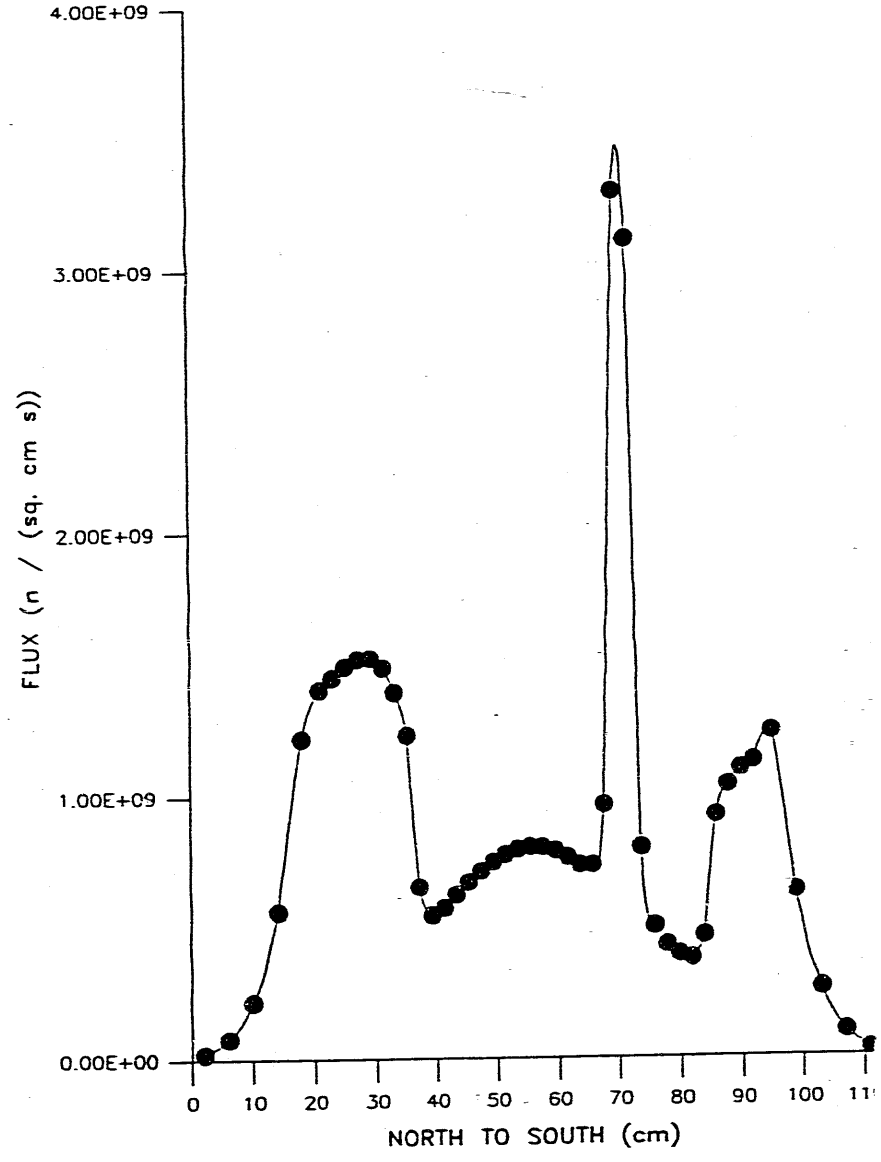

Fig. 38. Thermal Flux for 300 W BeO-UO_2-Er Core Along Column 26 and Row 22

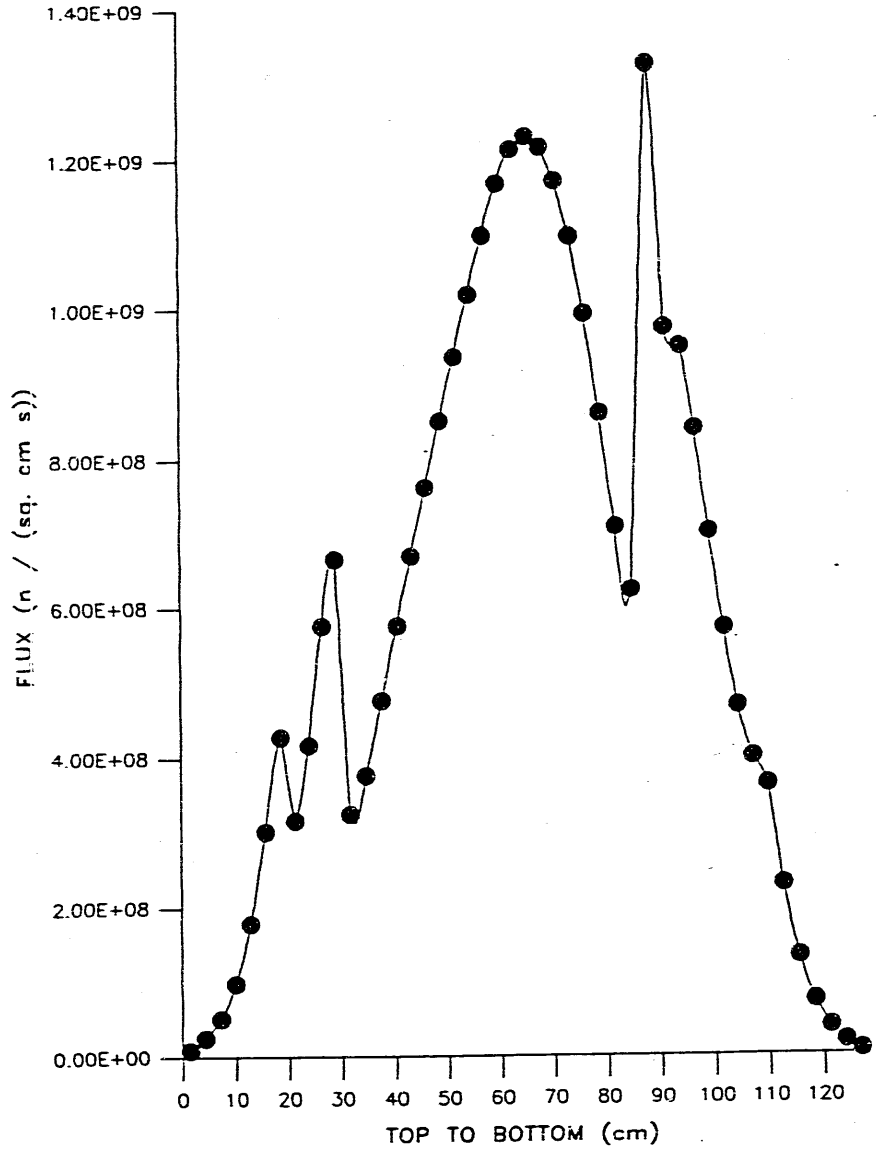

Fig. 39. Thermal Flux for 300 W BeO-UO_2-Er Core Along Column 18 and Plane 21

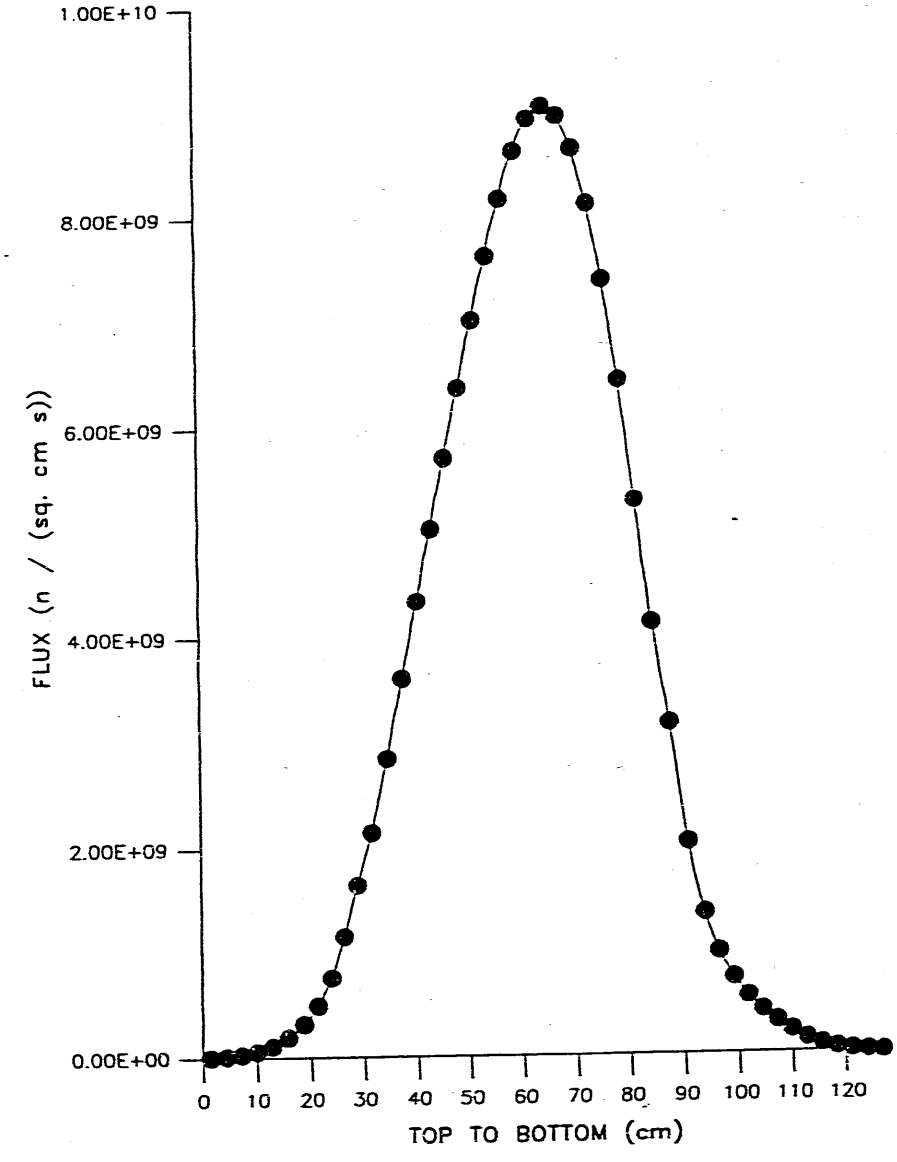

Fig. 40. Thermal Flux for 300 W BeO-UO_2-Er Core Along Column 18 and Plane 32

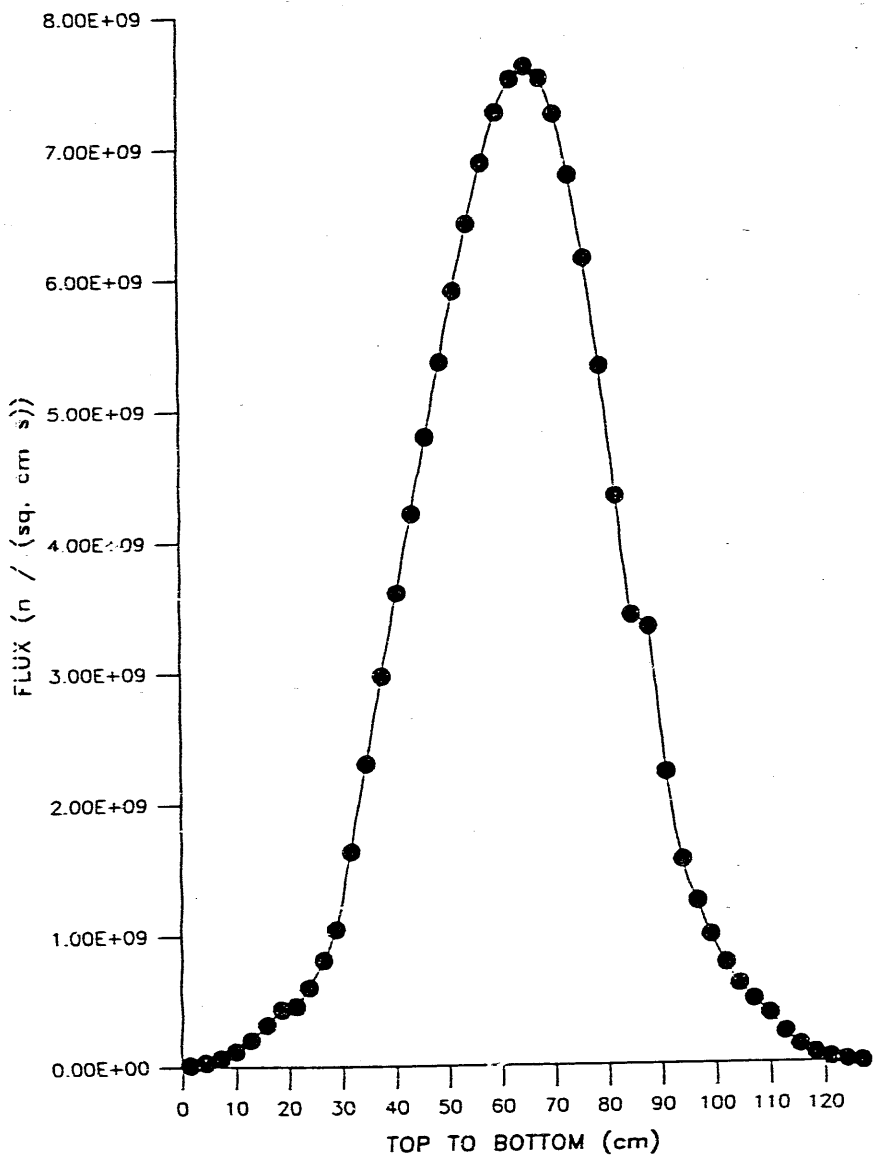

Fig. 41. Thermal Flux for 300 W BeO-UO_2-Er Core Along Column 18 and Plane 25

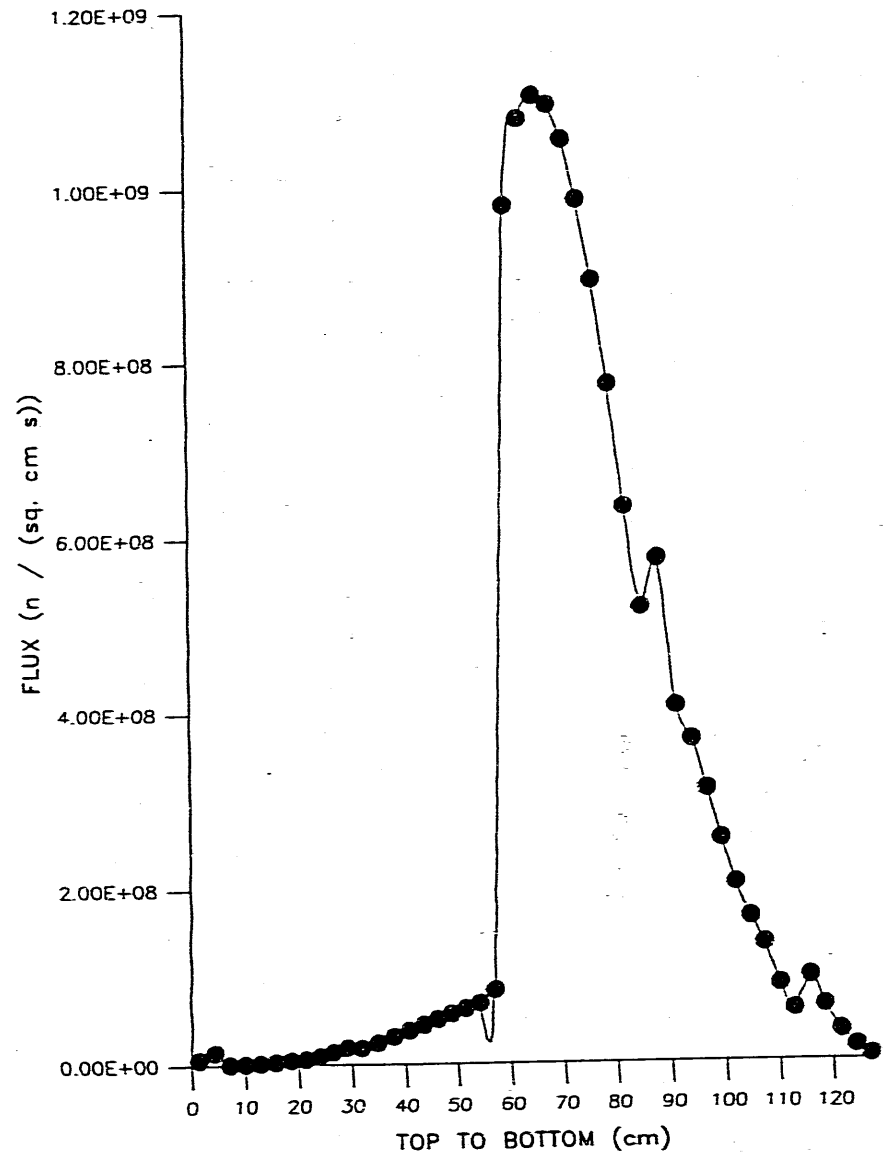

Fig. 42. Thermal Flux for 300 W BeO-UO_2-Er Core Along Column 22 and Plane 21

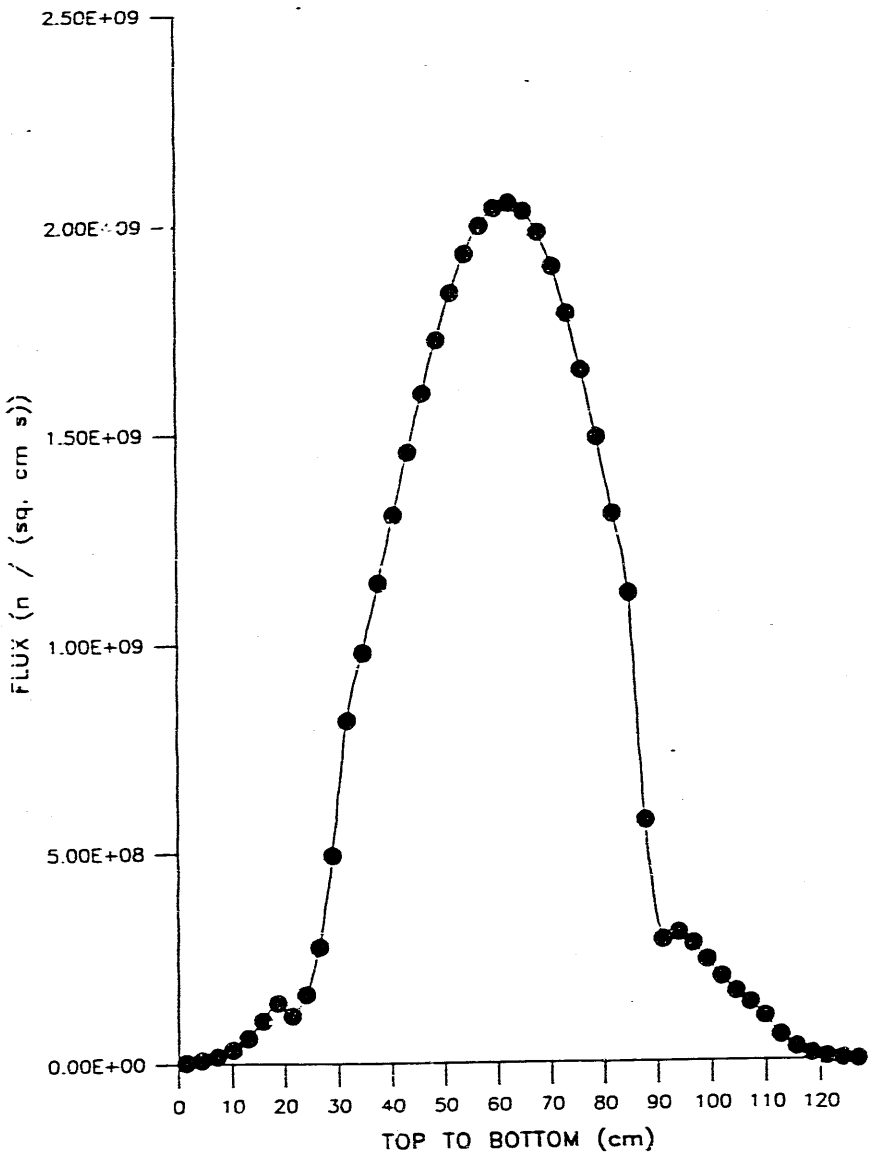

Fig. 43. Thermal Flux for 300 W BeO-UO_2-Er Core Along Column 18 and Plane 10

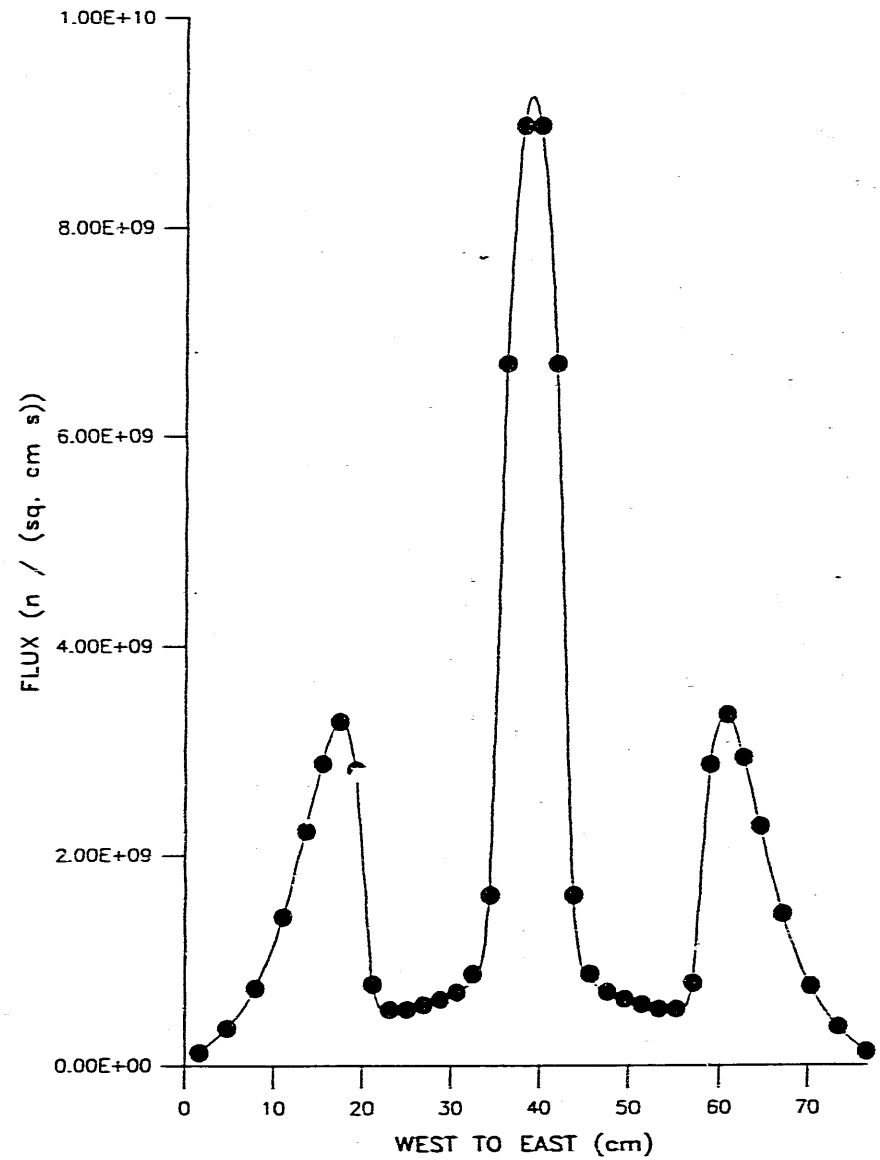

Fig. 44. Thermal Flux for 300 W BeO-UO_2-Er Core Along Row 22 and Plane 15

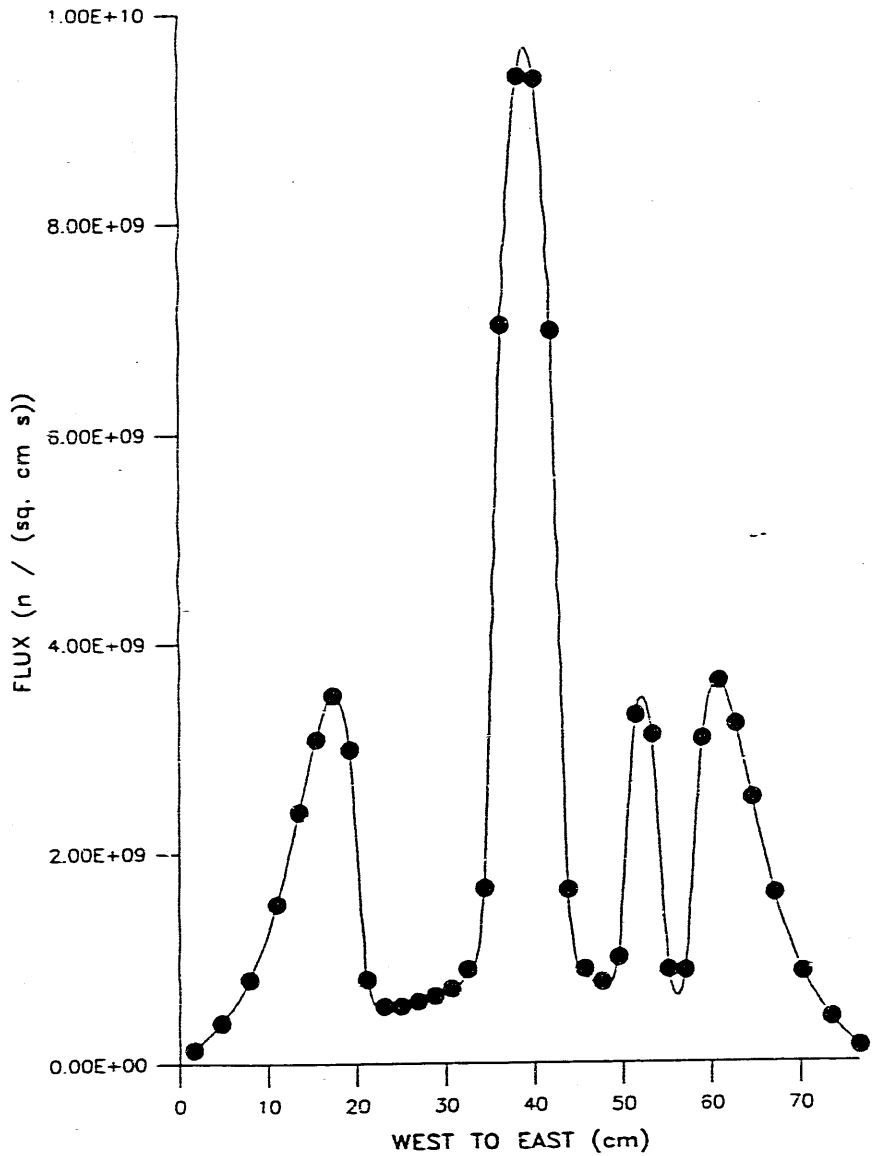

Fig. 45. Thermal Flux for 300 W BeO-UO_2-Er Core Along Row 22 and Plane 31

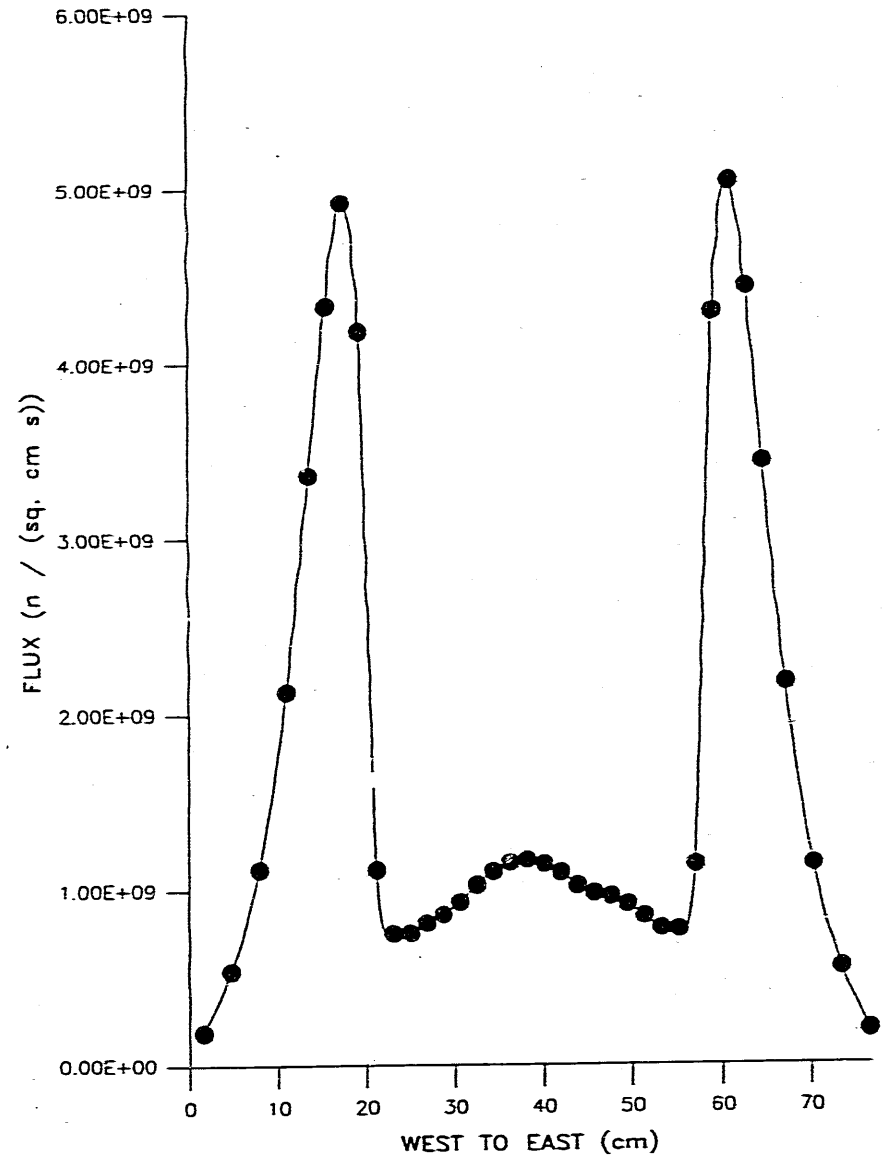

Fig. 46. Thermal Flux for 300 W BeO-UO_2-Er Core Along Row 22 and Plane 21

CONCLUSIONS AND RECOMMENDATIONS

The k_{eff} results obtained for the U-$ZrH_{1.6}$-Er core compare well with anticipated trends and previous calculations for a fresh core. The flux profiles obtained for the core compare fairly well to measured fluxes for the current core. The two factors that must be taken into consideration when comparing these calculated flux results with measured values are that the calculations were performed by codes that approximate solutions to various equations and also that the calculations were performed for a fresh core, when the measured values are for a core with several years of burnup. With all these factors considered, the method of modeling the NSCR reactor used in this work, from AIM to VENTURE, appears to be valid and is therefore repeatable for another fuel.

The results obtained from modeling the NSCR reactor with the proposed BeO-UO_2-Er fuel show no unanticipated or undesirable trends. The trends match those seen for the U-$ZrH_{1.6}$-Er core where physical features are similar. Since it is possible to make k_{eff} large enough with this fuel and since the flux profiles are high enough with no unwanted spikes that would cause an early burnup, it is believed that the U-$ZrH_{1.6}$-Er fuel rods can be replaced with BeO-UO_2-Er fuel rods that are similar in design to those modeled for this core. It is also believed that this fuel will allow 2 MW operation.

Before the fuel is to be constructed, more work should be performed to determine the optimum mass fraction of UO_2 in the fuel. This would include both changing

the appropriate values used as input for this work and also implementing a code that has the capability of performing burnup calculations. A code that models transients would make an analysis of pulses possible. Also to be considered are the results of the thermal-hydraulic and material studies being performed. A comparison with the results of the analysis being performed with the General Atomic 20 percent enriched fuel must also be made.

Another concern is the continued operability of SCALE, BOLD VENTURE, and any other code that may be used for this project. As updates on the IBM 3090-200E are made, SCALE-2 and BOLD VENTURE IV become outdated. They both have ASSEMBLY routines that cease to execute after certain hardware and software changes are made. For SCALE-2, this has involved the use of an emulator for the IBM 3350 disks that runs on the IBM 3380 disks. It is not known how much longer that emulator will be available. The continued use of SCALE-2 has also depended on the replacement of some of the ASSEMBLY routines by FORTRAN-77 routines from a copy of SCALIAS-3.1, an incomplete revision of SCALE. Another difficulty is that the FORTRAN in SCALE is FORTRAN-H, making it impossible to recompile any of these modules, should it become necessary, without converting them to FORTRAN-66, which is currently available on the IBM. The best solution for some time is likely to be the compilation of SCALE-4, an all FORTRAN-77 version that is not yet complete. For BOLD VENTURE IV, it has also been necessary to substitute ASSEMBLY routines with FORTRAN-77 routines from SCALIAS-3.1. However, this capability is not likely to continue since not many ASSEMBLY routines between SCALE-2 and BOLD VENTURE IV are in common. Eventually, BOLD VENTURE V, an all FORTRAN-77 version, should become available.

REFERENCES

1. "Nuclear Regulatory Commission Rules and Regulations", Title 10, Chapter 1, Part 50.64, Nuclear Regulatory Commission (February 1986).

2. "SCALE-2, A Modular Code System for Performing Standardized Computer Analyses for Licensing Evaluation," NUREG/CR-0200 (ORNL/NUREG/CSD-2), Oak Ridge National Laboratory (1983).

3. "BOLD VENTURE IV, A Reactor Analysis Code System, Version IV," Oak Ridge National Laboratory (1984).

4. Ricardo Yupari, "Three Dimensional Neutronics Calculations for the TAMU Nuclear Science Center TRIGA Reactor Using BOLD VENTURE," Master of Science Thesis, Texas A&M University (December 1985).

5. Anand Gangadharan, Department of Nuclear Engineering, Texas A&M University, Research in Progress.

6. John Vukovics, Department of Nuclear Engineering, Texas A&M University, Thesis Research in Progress.

7. "SCALIAS-3.1, A Modular Code System for Performing Standardized Computer Analyses for Licensing Evaluation," NUREG/CR-0200 (ORNL/NUREG-/CSD-2), Oak Ridge National Laboratory (1986).

8. W. C. Jordan, "SCALE Cross-Section Libraries," draft SCALE documentation, Oak Ridge National Laboratory.

9. S. Pearlstein, R. Kinsey, and C. Dunford, "Characteristics of ENDF/B-V," BNL-NCS-24113, Brookhaven National Laboratory.

10. "Safety Analysis Report for Nuclear Science Center Reactor, Texas A&M University," Texas A&M University (June 1979).

11. W. E. Ford, III, "Workshop Demonstration of Methods for Generating and Using Multigroup Cross Sections," Computational Methods in Nuclear Reactor Analysis, Tennessee Industries Week Course NE-2, University of Tennessee, August 15-19, 1988.

12. K. R. Boldt, T. R. Schmidt, B. F. Estes, and J. A. Reuscher, "Sandia Annular Core Research Reactor (ACRR) Safety Analysis Report," SAND-77-0208, Sandia National Laboratory (April 1978).

13. "Research Reactor Core Conversion from the Use of Highly Enriched Uranium to the Use of Low Enriched Uranium Fuel Guidebook," IAEA-TECDOC-233, International Atomic Energy Agency (1980).

14. Rajalakshmi Parthasarathy, Department of Nuclear Engineering, Texas A&M University, Thesis Research in Progress.

15. W. E. Ford, III, R. M. Westfall, C. C. Webster, "A 218-Neutron-Group Master Cross-Section Library for Criticality Safety Studies," Transactions of the American Nuclear Society, Vol. 22, American Nuclear Society (1975).

16. W. E. Ford, III, C. C. Webster, R. M. Westfall, "A 218-Group Neutron Cross-Section Library in the AMPX Master Interface Format for Criticality Safety Studies," ORNL/CSD/TM-4, Oak Ridge National Laboratory (July 1976).

17. "AMPX-II Modular Code System for Generating Coupled Multigroup Neutron-Gamma-Ray Cross-Section Libraries from Data in ENDF Format," ORNL/TM-3706, Oak Ridge National Laboratory (December 1978).

18. "Reactor Physics Constants", ANL-5800, Argonne National Laboratory (July 1963).

19. John R. Lamarsh, Introduction to Nuclear Reactor Theory, Reading, Mass.: Addison-Wesley Publishing Company (1966).

20. J. W. Davis, "Two-Dimensional Neutronics Analysis of the TAMU Nuclear Science Center Reactor Using Transport and Diffusion Theory Based Codes," Master of Science Thesis, Texas A&M University (December 1988).

21. James J. Dunderstadt and Louis J. Hamilton, Nuclear Reactor Analysis, New York: John Wiley & Sons (1976).

22. "Neutron Cross Sections, Resonance Parameters," BNL-325, Vol. II, Brookhaven National Laboratory (June 1973).

23. "Neutron Cross Sections, Curves," BNL-325, Vol. II, Brookhaven National Laboratory (January 1976).

24. Rod O'Connor, Fundamentals of Chemistry, Minneapolis: Burgess Publishing Company (1981).

25. R. T. Primm, Oak Ridge National Laboratory, Private Communication (March 1988).

26. J. W. Davis, Texas A&M University, Private Communication, (February 1988).

27. Computer macroscopic cross section data provided by General Atomic Corporation for the Texas A&M Nuclear Science Center Reactor (1974).

28. K. D. Reeve, "Fabrication and Structure of BeO Based Fuels," Beryllia Based Dispersion Fuels - Fabrication, Structure, Properties, Irradiation Behavior, Journal of Nuclear Materials, Vol. 14 (1964).

END

DATE FILMED

06/20/91